Fisheries
and Environment
Canada

MANUSCRIPT REPORT SERIES No. 3

TIDAL PROPAGATION IN CHESTERFIELD INLET, N.W.T.

W.P. BUDGELL

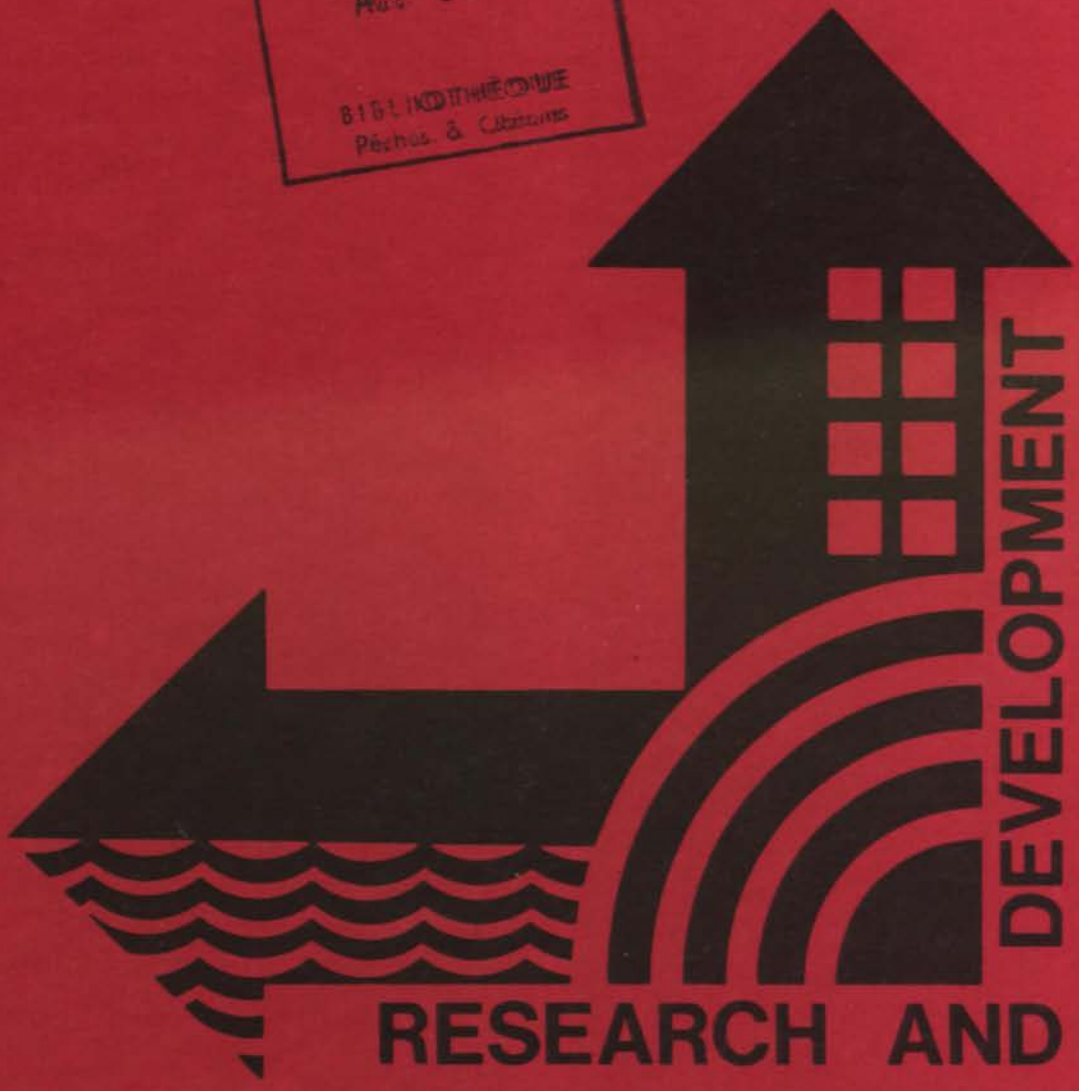

OCEAN AND AQUATIC SCIENCES
CENTRAL REGION

CANADA CENTRE FOR INLAND WATERS
BURLINGTON, ONTARIO

TIDAL PROPAGATION

IN

CHESTERFIELD INLET, N.W.T.

by

W.P. BUDGELL

MANUSCRIPT REPORT SERIES NO. 3

1976
OCEAN & AQUATIC SCIENCES
CENTRAL REGION

ABSTRACT

Chesterfield Inlet drains an area of 290,000 km^2 of predominantly continuous permafrost terrain between Great Slave Lake and northern Hudson Bay. The 220-kilometre-long inlet may be used as an important navigation link to Baker Lake and potential pipeline sites. The inlet forms a complex network and is characterized by strong tidal forcing.

A one-dimensional numerical model, using a weighted, implicit, finite difference scheme, was modified for application to the network. Sparse matrix techniques were incorporated into the model to speed Gaussian Elimination in the solution of the equations.

Tidal constituents, derived from admittance calculations, were used to predict water levels at eight tide gauge locations. Tidal predictions at Sandpiper Island were used as the downstream boundary condition for the numerical model, while tidal predictions at the other gauge locations were used in the model calibration.

The observed and model-computed water levels are in good agreement over the lower half of the inlet. Appreciable differences between the observed and computed values were encountered in the upper reaches. Although some of these discrepancies are attributable to errors in the upstream boundary condition and schematization of the model, there is evidence to suggest that time and range errors may exist in some of the recorded tidal data.

The variation in the phase and amplitude of the tide throughout the inlet is determined through an examination of the tidal constituents and the model results. Power spectra of the observed and model-predicted water levels reveal that nonlinear interactions of the major tidal constituents take place in the upper portion of the inlet.

ACKNOWLEDGMENTS

The author wishes to express his thanks to Mr. L.R. Muir of Ocean and Aquatic Sciences, Central Region, Environment Canada, and Dr. W. James of McMaster University for critically reviewing the manuscript and providing many helpful comments; to Messrs. B. Wright and M. Casey of the Canadian Hydrographic Service for relating their field observations; to the Tides and Water Levels Section of the Canadian Hydrographic Service for providing water level information ; to the Water Survey of Canada for supplying water level and discharge data; to Mrs. C. Kennedy for typing the manuscript; and to Mr. M. Donnelly and Mr. J. Elliot for performing the drafting.

TABLE OF CONTENTS

LIST OF FIGURES

LIST OF TABLES

LIST OF SYMBOLS

b	- Topwidth of conveyance section.
b_s	- Topwidth of storage section.
e	- Base of natural logarithms (2.718 . . . .)
g	- Acceleration due to gravity.
h	- Depth of channel invert below datum.
h^*	- Hydraulic mean depth.
i	- Imaginary unit, $\sqrt{-1}$, in Chapter 3.
j	- Index.
k	- Friction coefficient.
m	- Index.
n	- Manning's friction coefficient.
n	- In Chapter 4, an index.
q	- Lateral inflow.
t	- Time.
u	- Average velocity at a cross-section.
x	- Distance.
z	- Water level above datum.
z_o	- Mean water level above datum.
$z_1(t)$, $z_2(t)$	- Time series.
A	- Cross-sectional area.
A	- In Chapter 4, a coefficient matrix.
A_{1j}, A_{2j}	- Amplitude of the jth constituent.
B	- A vector of constants.
C	- Frictionless shallow-water wave celerity in Chapter 3.
C	- Chezy friction coefficient.
$C_{12}(\sigma)$	- Co-spectrum of two time series.
F	- Arbitrary function of space and time.
$G_1(\sigma)$, $G_2(\sigma)$	- Power spectrum.
$H_{12}(\sigma)$	- Admittance function relating two time series.
k_1, k_2	- Constant of Proportionality.
N	- Number of reaches in a river network.
Q	- Volume discharge.

$Q_{12}(\sigma)$ - Quadrature spectrum of two time series.

R - A point in time and space.

X - Solution vector.

α - Weighting factor in equations (4.4) and (4.5).

$\gamma_{12}(\sigma)$ - Coherence between two time series.

Δt - Computational time step.

Δx - Computational distance step.

ζ_i - Contribution to the water level or rectilinear current from i^{th} constituent.

θ - Weighting factor in finite difference equations.

σ - Frequency.

σ_j - Frequency of the jth constituent.

$\phi_{12}(\sigma)$ - Phase difference between two time series.

ϕ_j - Phase of the jth constituent.

CHAPTER 1

1.0 INTRODUCTION

Tidal propagation in Chesterfield Inlet will be studied herein through the examination of field data and the application of numerical modelling techniques. Like most Arctic water bodies, only a minimal amount of field data has been collected at Chesterfield Inlet. Due to the limited quantity and quality of the available data, the major physical quantities involved are described in a general fashion; it is not possible to delineate the physical quantities involved in precise numerical terms. It is hoped that this study will form the basis for further hydrodynamic studies in Chesterfield Inlet and that the results will prove useful in planning future field work there.

1.1 DESCRIPTION OF CHESTERFIELD INLET

Chesterfield Inlet, located as shown in Figure 1, is a long, narrow inlet situated on the northwest coast of Hudson Bay 540 kilometres north of Churchill, Manitoba, at a latitude of 63° 30'. The inlet links Baker Lake to Hudson Bay, a distance of 220 kilometres.

Lying in the Precambrian Shield, Chesterfield Inlet was created by glacial action. The inlet itself is rocky. Outcroppings of gneissic granite and grandolite formations are common. In the western portion, the channel is often bounded by steep, pink, granite cliffs 100 metres in height, while in the central portion, large granite boulders predominate. Near the mouth the channel is defined by continuous walls of granitic gneiss. The bottom is rocky and irregular except near the mouth where silt is found. The mean channel depth varies from 50 metres at the mouth to 6 metres at the entrance to Baker Lake. The inlet follows a tortuous route from Hudson Bay to the Bowell Islands (Figure 2). At its mouth, deep channels separate numerous islands, while at the Bowell Islands, the main channel divides into several narrow passages. Barbour Bay, Cross Bay, and the Quoich River form major embayments, while shoals occur throughout the length of the inlet.

Tidal forcing is quite strong everywhere in the inlet. The tidal range varies from a maximum of 5 metres at Deer Island to a minimum of 1.5

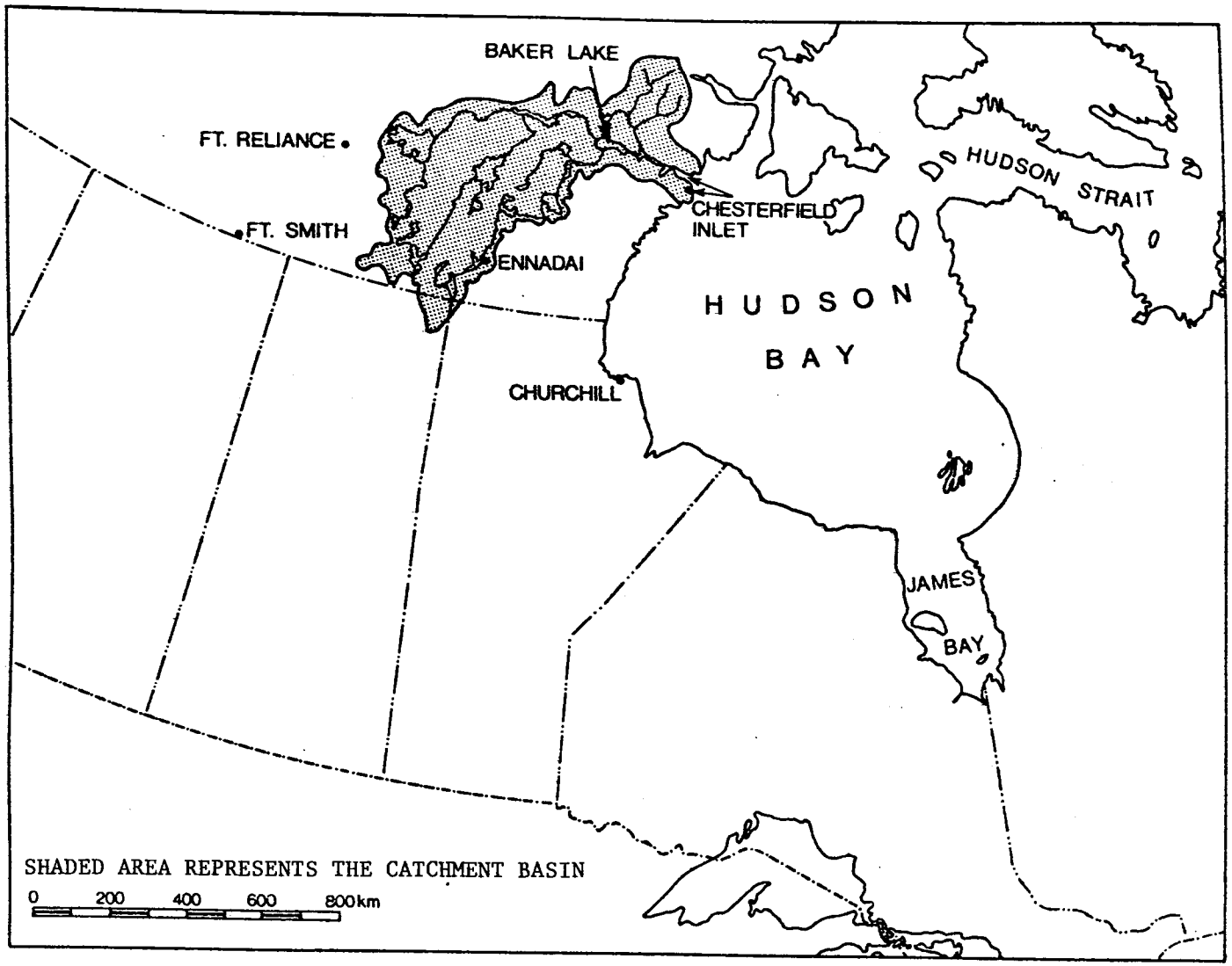

FIGURE 1: Location of Chesterfield Inlet and Its Catchment Basin

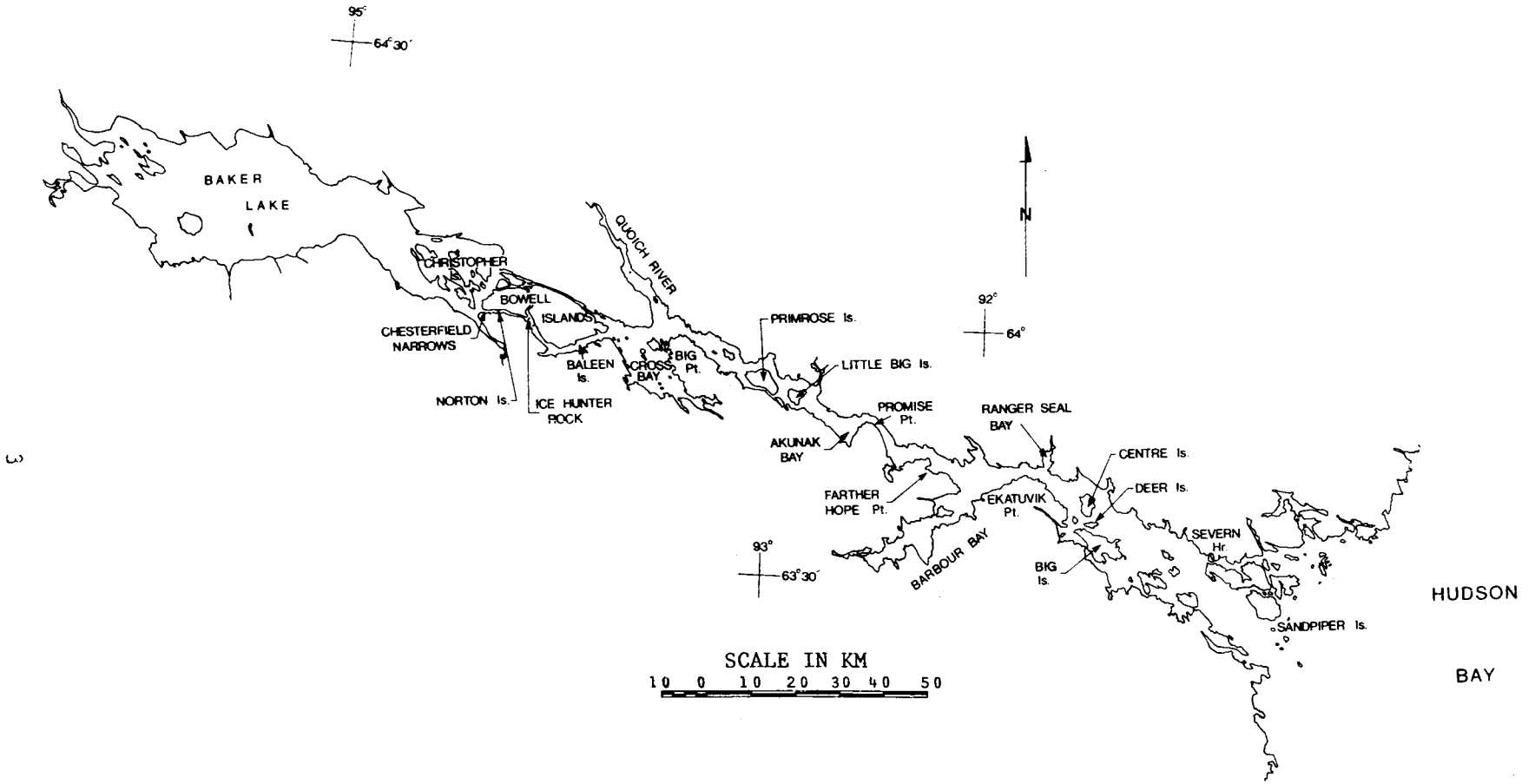

FIGURE 2: Chesterfield Inlet

metres at the entrance to Baker Lake. Tidal action in Baker Lake itself is negligible. The currents in the inlet are tidally driven and current speeds in excess of 4.5 metres per second are observed at Chesterfield Narrows.

1.2 ECONOMIC SIGNIFICANCE OF CHESTERFIELD INLET

At the present time, the major activity along the inlet consists of barges running supplies from the community of Chesterfield Inlet at the mouth to the community of Baker Lake at the western extremity of the lake of the same name. These barges travel the inlet for the two months of the year between breakup and freezeup.

In the future, however, it is possible that Chesterfield Inlet will assume a role of greater significance. The latest proposal for the location of the Eastern Arctic Pipeline has it passing just west of Baker Lake. Should that proposal be accepted, it is very likely that Baker Lake would become a major marshalling point for pipeline construction. Chesterfield Inlet would then be used as a transportation corridor to move large quantities of equipment and supplies to Baker Lake. The only obstacle preventing ocean-going ships from travelling all the way to the community of Baker Lake is a sill rising to within 6 metres of the water surface in the Chesterfield Narrows.

Increased shipping in Chesterfield Inlet raises the problem of water quality. Oil slicks, generated by supply vessels colliding or running aground in areas such as Chesterfield Narrows, would be a very real risk.

Should shipping increase in Chesterfield Inlet, considerably more tide and current data would be required to ensure safe navigation. A thorough understanding of the hydrodynamics of the inlet would also be necessary in order to predict oil slick movement and aid oil spill contingency planning.

1.3 METHOD OF APPROACH

The hydrology of the Chesterfield Inlet basin will be reviewed to determine the magnitude of the mean flow and its variation in time. This is necessary to help establish the datum. The available tidal data will then be examined to provide an overview of tidal propagation within the

inlet.

A one-dimensional numerical model will be applied to the inlet to provide a more complete picture of the hydrodynamics. More specifically, the following aspects of the tidal propagation will be examined:

1) the variation in amplitude and phase of the tide throughout the inlet;
2) the variation of tidal currents throughout the inlet;
3) the effect of stage at Baker Lake upon the tidal propagation;
4) the nonlinear properties of Chesterfield Inlet; and
5) the effect of changes in the section geometry at Chesterfield Narrows.

Finally, the data required to supplement and expand tidal knowledge essential to navigation in the inlet will be specified.

CHAPTER 2

2.0 HYDROLOGY OF CHESTERFIELD INLET

Much of the runoff in the Chesterfield Inlet catchment basin derives from snowmelt which has a diurnal cycle. These cycles could persist throughout the drainage pattern and affect flow in the inlet. In order to ascertain whether these effects influence the tidal analysis, it is necessary to gain some knowledge of the hydrology of the area.

In addition, the flows are used in determining a mean elevation for Baker Lake. The elevation of Baker Lake is the upstream boundary condition for the numerical model of the inlet.

2.1 DESCRIPTION OF CATCHMENT BASIN

One of the most striking features of Chesterfield Inlet is the size of its catchment basin. The catchment area shown in Figure 1 extends from Hudson Bay in the east (longitude 91° W) to 120 kilometres west of Great Slave Lake (longitude 107° W) and from Wager Bay (latitude 66° N) in the north to northern Saskatchewan (latitude 59° N) in the south. The total area of the catchment basin is 287,100 km^2. The major tributaries in the Chesterfield Inlet system are the Thelon, Kazan, and Quoich Rivers with subcatchment areas of 147,200 km^2, 68,100 km^2, and 29,800 km^2, respectively. The subcatchments are delineated in Figure 3.

These territories were referred to as the "Barren Lands" by the early explorers, and justifiably so. For the most part, the drainage basin is treeless, barren ground characterized by low altitude, low to moderate relief, and generally disorganized drainage except for a few large rivers. Considerable water storage occurs in the many lakes and innumerable shallow surface depressions. The vegetation over most of the area consists of non-vascular mosses and lichen with occasional shrubs. Black spruce and tamarack forests exist in the southwest portion of the basin and cover roughly 20 per cent of the total catchment area.

A significant feature of the catchment basin is the temperature structure of the subsurface soils. Continuous permafrost is predominant in the northern portion of Chesterfield Basin while discontinuous permafrost is found in the southern portions of the watershed and in the vicinity of

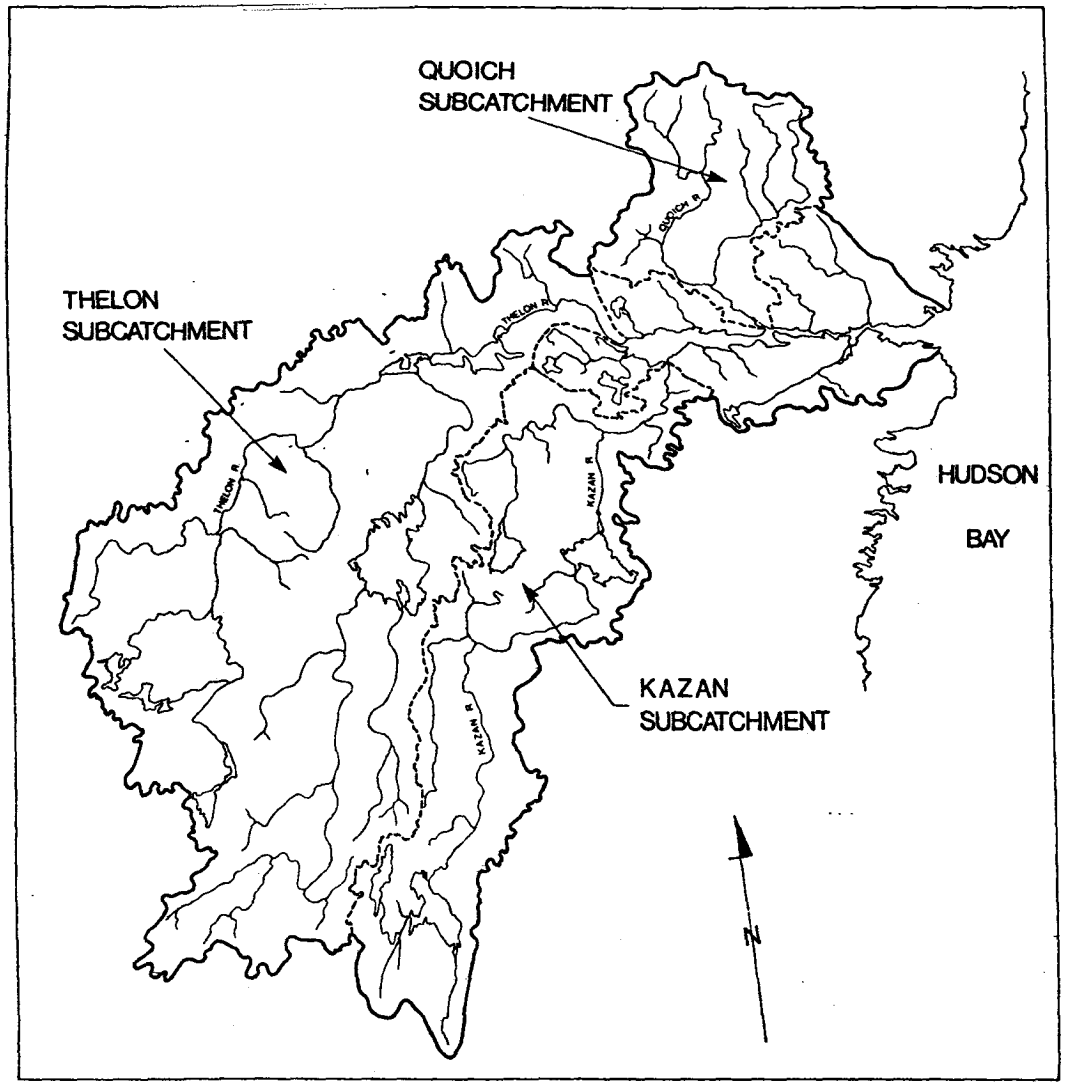

FIGURE 3: Chesterfield Inlet Catchment Area

some of the larger lakes. The continuous permafrost areas have an active (seasonally thawed) layer at the surface which is approximately 1 to 2 metres thick overlying a permafrost layer which is in excess of 100 metres thick.

2.2 WATER BALANCE

An annual water balance for the Chesterfield catchment was computed from contour maps of mean annual precipitation and runoff supplied by the Department of Indian and Northern Affairs. The contours were based on data collected from 1941 to 1970. Weighted means for precipitation and runoff were calculated by planimetry. The mean annual precipitation computed in this manner is 247 mm, and the value for mean annual runoff is 172 mm.

A separate calculation for runoff was performed as a check on the planimetered value. Monthly mean discharges supplied by the Water Survey of Canada for the Thelon, Kazan, and Quoich Rivers were used in determining a mean discharge value for Chesterfield Inlet. The monthly mean discharges are listed in Table 1. Runoff from areas in the Chesterfield catchment not included in the subcatchments of the rivers listed above was calculated by assuming that these areas had the same properties as the Quoich basin. (The mean runoff per unit area determined for the Quoich subcatchment was applied to the otherwise excluded areas.) The total mean annual runoff calculated in this manner was 161 mm. This runoff value agrees to within 7 per cent of the value computed through the use of runoff contours. It should be noted that these values are estimates of total runoff. Insufficient data are available to support calculations of surface runoff. It is probable that during the ablation period total runoff is approximately equal to direct runoff since infiltration and interflow are restricted to the active layer.

If we assume no storage effects in the basin, which should be a valid assumption over the long-term, then the difference between mean annual precipitation and runoff can be attributed to evapotranspiration. Thus, mean annual evapotranspiration should be no more than 75 mm, which is 30 per cent of the mean annual precipitation. A contour map by Church [10] would indicate that the mean annual evaporation from small lake surfaces in

	Thelon (m^3/sec)	Kazan (m^3/sec)	Quoich (m^3/sec)	Other (m^3/sec)	Total (m^3/sec)
January	286	177	4	6	473
Feburary	238	149	3	4	394
March	209	127	3	4	343
April	255	121	6	8	390
May	567	166	42	59	834
June	2480	897	233	328	3938
July	1390	1185	213	300	3088
August	1010	837	224	316	2387
September	921	656	328	462	2367
October	777	523	159	224	1683
November	563	376	54	76	1069
December	361	253	12	17	643

TABLE 1: Monthly Mean Discharges

the Chesterfield watershed is approximately 225 mm. As expected, this value is considerably higher than the mean evapotranspiration over the whole catchment. The lichen and moss ground cover of the Chesterfield Basin appear to be particularly efficient in reducing overall evapotranspiration. Nebiker and Orvig [26] and Dingman [12] have suggested that a low value of evapotranspiration in lichen and moss-covered areas may be due to the fact that these plants transpire to a lesser degree than do vascular plants.

The estimate for evapotranspiration in the Chesterfield Inlet basin is consistent with the findings of Findlay [14], Anderson [4], and Kane and Carlson [23], all of whom studied catchments with a lichen or moss ground cover. Their results are summarized in Table 2.

2.3 RUNOFF REGIME

Although only 40 per cent of the annual precipitation in the Chesterfield Inlet catchment is in the form of snow, the effect of snow storage is the single most important feature in the hydrologic cycle. For seven to eight months of the year, precipitation is stored on the ground in the form of snow; thus, when the snow pack starts melting in mid May, the effect is the same as if seven to eight months of precipitation had fallen over the two-week melting period. This phenomenon is readily observed in the 1973 daily discharge data for the Thelon, Kazan, and Quoich Rivers, as shown in Figure 4. Snowmelt begins about May 15th. In less than three weeks, the discharge of the Thelon increases from 340 m^3/sec (12,000 cfs) to 3,060 m^3/sec (108,000 cfs), the Kazan from 170 m^3/sec (6,000 cfs) to 1,900 m^3/sec (67,000 cfs), and the Quoich from 14 m^3/sec (500 cfs) to 453 m^3/sec (16,000 cfs). In all three cases, the rising limb of the hydrograph is much steeper than the receding limb; this is partially attributable to surface storage in the many lakes and ponds. From Figure 4 we see that the level of Baker Lake peaks approximately 9 days after the maximum discharge of the Thelon River. The rate of storage change is a maximum for Baker Lake during the period from May 25th to June 9th. This rate of storage change is $A\ \partial z/\partial t$; where A is the area in m^2, z is the elevation in metres, and t is time in seconds. In Baker Lake for the period of interest, the average rate of storage change is +977 m^3/sec or 21 per

Watershed	Area Sq.km.	Surface Cover	Precipitation (mm)	Runoff (mm)	Evapotranspiration (mm)	Percent Evapo-transpiration
Knob Lake drainage basin Schefferville Quebec	35	dwarf spruce, birch, lichen and woodland	915	635	280	31
Boot Creek Inuvik N.W.T.	31	spruce, birch lichen heath upland	285	210	75	26
Putuligayak River, Prudhoe Bay, Alaska	568	muskeg and heath tundra	94	75	27 *	29

* From evaporation pan data.

TABLE 2: Evapotranspiration in Catchments similar to that of Chesterfield Inlet

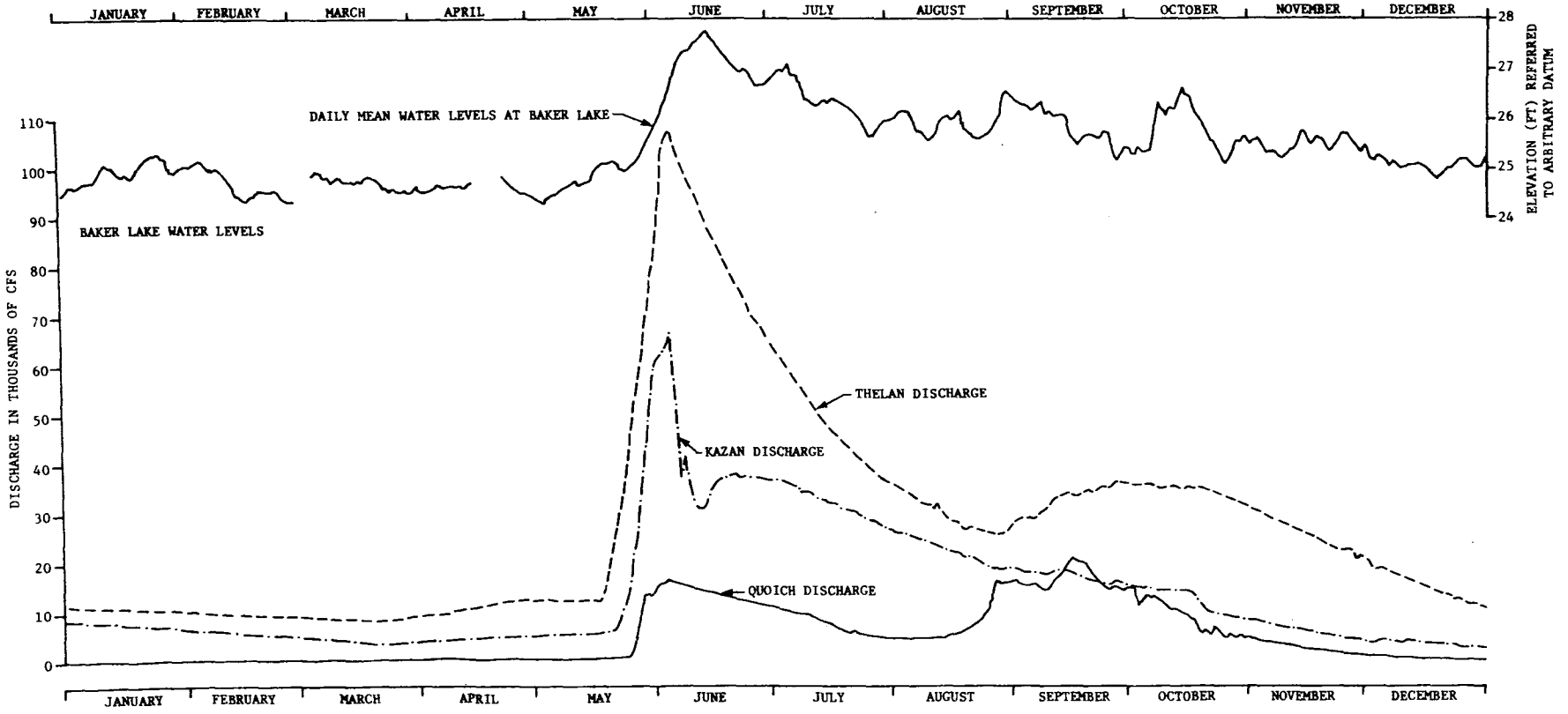

FIGURE 4: Daily Mean Baker Lake Water Levels and Daily Mean Discharges at Thelon, Kazan, and Quoich Rivers for 1973

cent of the rate of inflow into the lake.

The Quoich River has its maximum discharge in mid September, suggesting that snow storage is less important than the late summer rains in this subcatchment, since this lag could not be due to on-channel storage. From Figures 4 and 5 we see that the late summer discharges of the three rivers are roughly related to the rainfall events at the stations located as shown in Figure 1. Anderson [4] has hypothesized that such late summer discharges in permafrost areas are caused by increased base flow. When cooler weather occurs in August, evapotranspiration decreases allowing a greater proportion of rainfall to percolate down to the frost layer and be stored in the soil. The soil moisture thus obtained helps to melt the frost and increases the base flow.

With the lower temperatures of September and October, a greater proportion of the precipitation falls as snow. Freezeup usually occurs by mid October. Hence, runoff declines from September onward with very little flow from the end of November through to April as precipitation accumulates on the surface as snow.

The relative contributions of the major rivers to the Chesterfield Inlet freshwater supply can be seen from the plot of the mean monthly discharges (Figure 6). In calculating the total freshwater discharge, the storage effects of Baker Lake and Chesterfield Inlet have been neglected. The period of record for the discharge measurements used is 2 years for the Thelon River, 9 years for the Kazan River, and 3 years for the Quoich River. The maximum monthly mean freshwater discharge through Chesterfield Inlet, east of the Quoich River, is approximately 3,900 m^3/sec (139,000 cfs) while the base flow is 343 m^3/sec (12,000 cfs).

From Table 1 we see that the Thelon and Kazan Rivers combine to produce 86 per cent of the total peak discharge and 98 per cent of the winter minimum base flow. The nature of the freshwater input to Chesterfield Inlet is such that individual rain storms are relatively unimportant due to the low density, short duration, and infrequency of these events. Snowmelt in mid May has much greater impact and generates rapidly-increasing discharge.

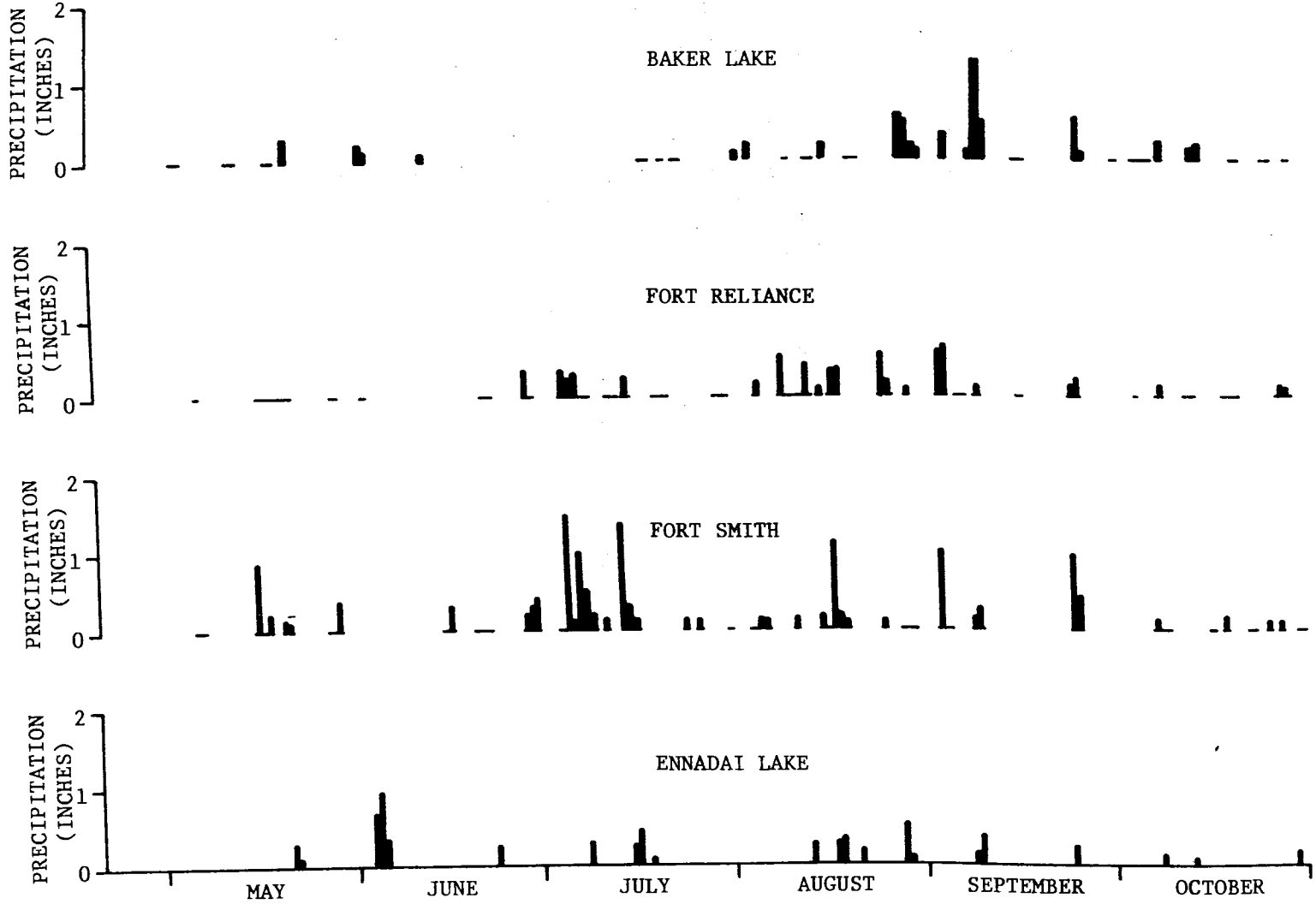

FIGURE 5: Precipitation Recorded at Gauging Stations Near the Chesterfield Inlet Basin from May to October, 1973

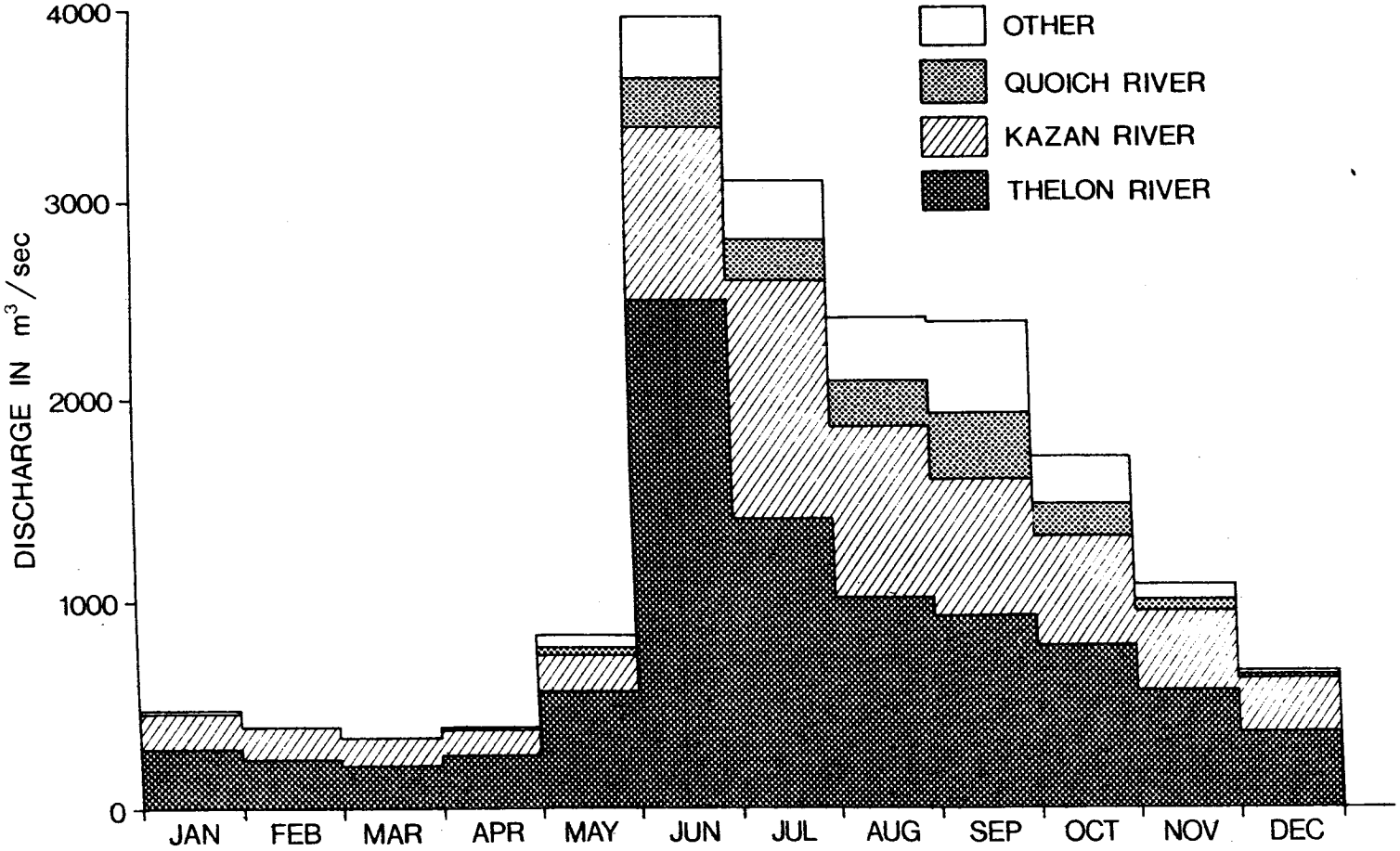

FIGURE 6: Monthly Mean Discharges of Chesterfield Inlet and Its Tributaries

2.4 CLASSIFICATION OF RIVER REGIME

We may gain further insight into the nature of the freshwater supply into Chesterfield Inlet by comparing the runoff regimes for the Thelon, Kazan, and Quoich Rivers to the following regime types for northern rivers as described by Church [10]:

1) Subarctic, nival regime:
   (a) winter dry,
   (b) perennial flow;
2) Arctic, nival regime;
3) Proglacial regime; and
4) Muskeg regime.

The Thelon and Kazan Rivers may be categorized as having a subarctic, nival regime with perennial flow. This type is marked by a snowmelt flood in spring followed by relatively low levels of flow throughout the summer except for occasional rain-storm events. Often, in the larger subarctic rivers, flow persists under the ice cover as seepage continues through the winter. Church suggests that some of this goundwater flow is from unfrozen gravels along the river channels and lake beds. This regime type quite often characterizes northward-flowing rivers, such as the Thelon and Kazan, whose headwaters lie in the discontinuous permafrost zones to the south where some infiltration may be maintained. The large lakes in these two catchments will allow some continuous flow throughout the winter.

The Quoich River is more difficult to classify since it seems to possess some characteristics of both the subarctic nival and the muskeg regimes. The Quoich maintains year-round flow and has a steep rise in its hydrograph due to snowmelt, like the subarctic nival regime with perennial flow. However, the receding limb of the hydrograph has a very gentle slope which could be due to copious surface storage as would be found in moss-covered catchments characteristic of a muskeg flow regime.

2.5 IMPACT OF RUNOFF UPON THE TIDAL REGIME

The amplitude and phase of the tide within the inlet may be influenced by the freshwater discharge. Ages and Woollard [1] have shown that in the Fraser River estuary increased damping of the tide and a delay in the time of high water accompany an increase in the freshwater discharge

due to runoff. In the Chesterfield Inlet system, the elevation of Baker Lake is directly related to the surface runoff from the catchment basin and is used in referencing Baker Lake water levels to mean sea level. Thus, the effect of the freshwater discharge upon the tidal regime may be investigated by varying the elevation of Baker Lake in numerical model computations, as is done in Chapter 5.

If the diurnal variations in runoff due to snowmelt were to persist throughout the drainage pattern, these effects could not easily be distinguished from those of the diurnal tides. Thus, there would be significant errors in the amplitudes and phases of the diurnal tidal constituents determined by a tidal analysis. Because of the great amount of surface depression and on-channel storage present within the drainage basin, however, it is evident that diurnal snowmelt variations have negligible effect upon the tidal computations.

CHAPTER 3

3.0 ANALYSIS OF TIDAL DATA

In order to understand tidal propagation in Chesterfield Inlet, it is first necessary to study the recorded water level data. The results of constituent analyses by the harmonic and admittance methods were used to determine the variation in magnitude and phase of the major constituents as the tide progresses up the inlet. The tidal predictions generated from these constituents are later used as the downstream boundary condition and at other stations for comparisons during the model calibration.

3.1 AVAILABLE DATA

The data used in this study were obtained by the Canadian Hydrographic Service in the summer of 1974. During the course of a bathymetric survey, eight shore-based Ottboro tide gauges were installed along the length of the inlet. The locations of these gauges are shown in Figure 7. Although tidal data were collected near the community of Chesterfield Inlet at the mouth of the inlet during the summer of 1973, these data were not used because Godin et al [20] found progressive time errors in the record.

The 1974 gauges were in place for periods of time varying from four days to seven weeks, as shown in Figure 8. Plots of the digitized hourly water levels for each of the stations are given in Figure 9. The water levels for a given station are referred to a chart datum determined from the lowest low water of the period of record. A chart datum selected in this manner is not in any way related to an established datum such as that of the Geodetic Survey of Canada, nor is it related to any other datum in the inlet

By examining the plots in Figure 9, a few general observations may be made. A pronounced difference between spring and neap tides can be seen in the records up to Promise Point, this difference reaching a maximum near Deer Island. At Primrose Island, the fortnightly modulation is relatively small. The gauges at Baleen Island and Norton Island were not in place long enough to permit an examination of the fortnightly spring-neap cycle, although evidence that it exists is present in the records. At Deer Island, a sudden increase of 2.5 metres in the mean water level is observed beginning August 13th. This shift in the record is evidently an instrument

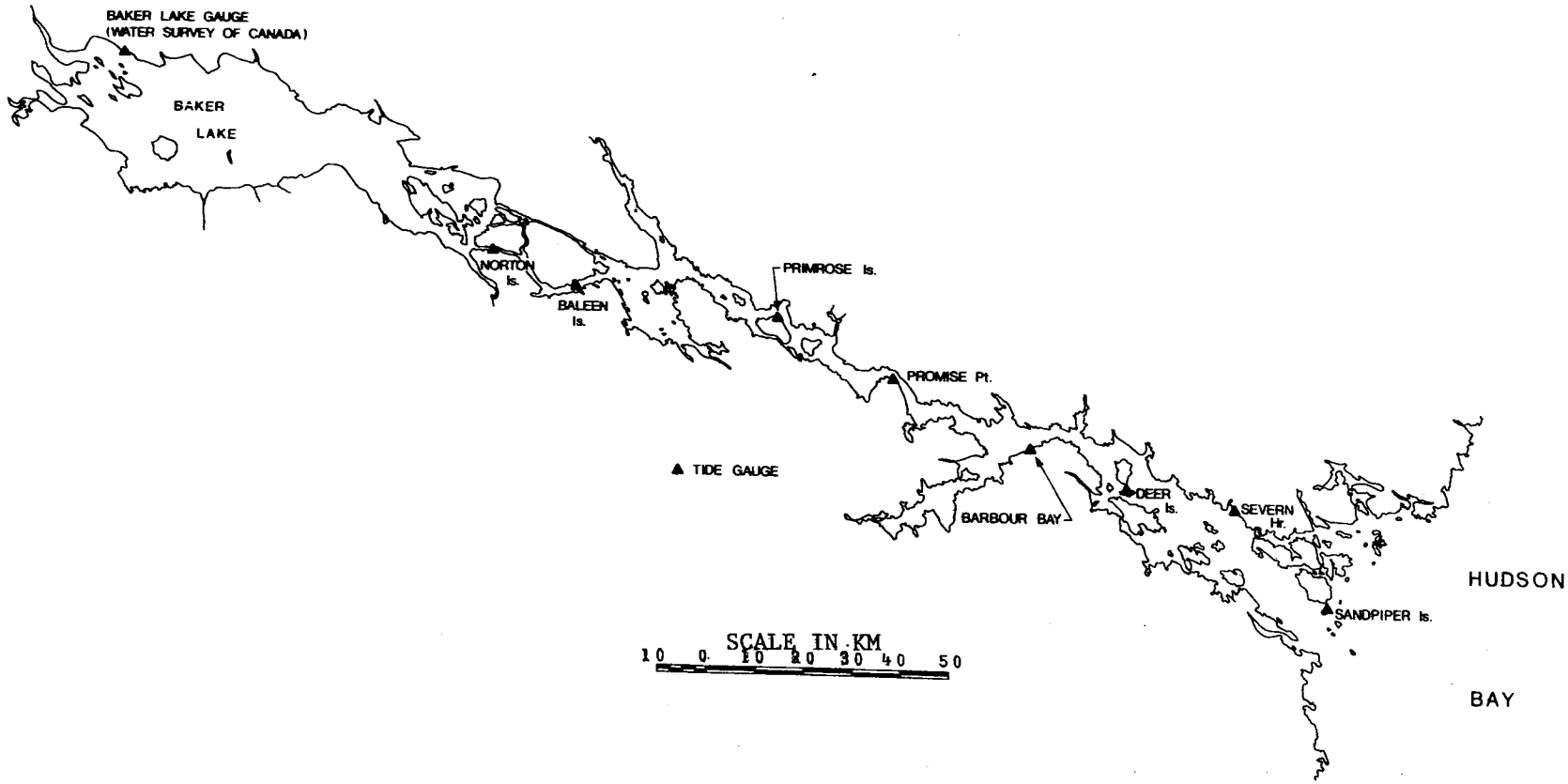

FIGURE 7: Location of Tide Gauge Stations in Chesterfield Inlet

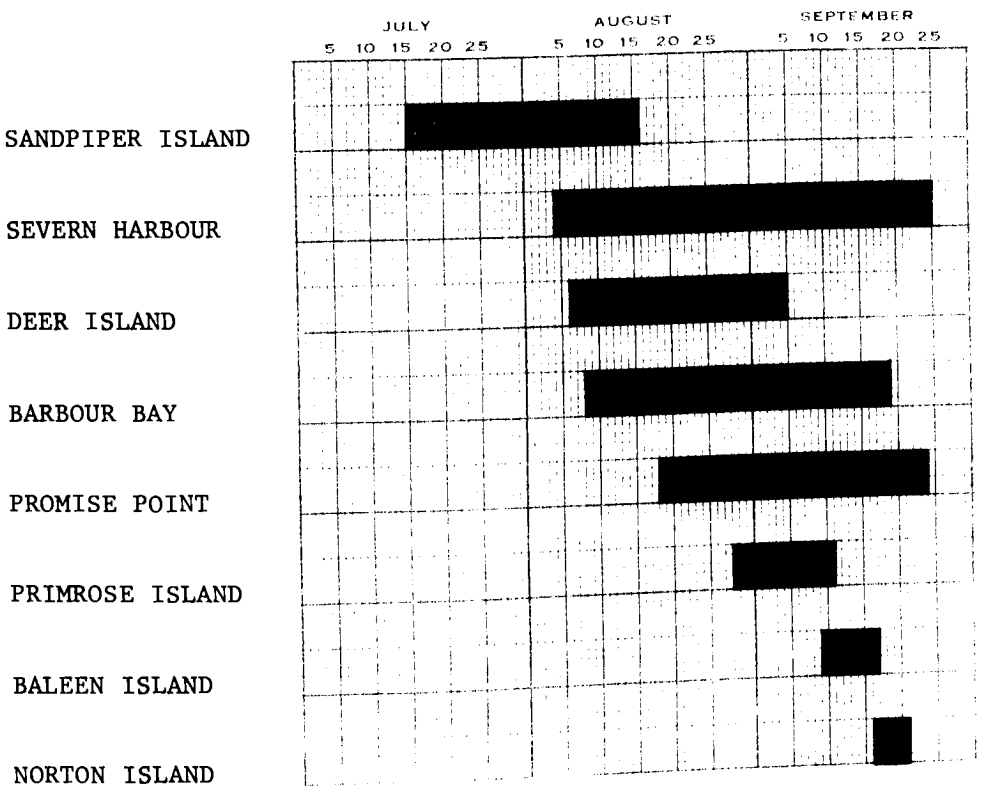

FIGURE 8: Durations of the Records Obtained from Chesterfield Inlet Tide Gauges

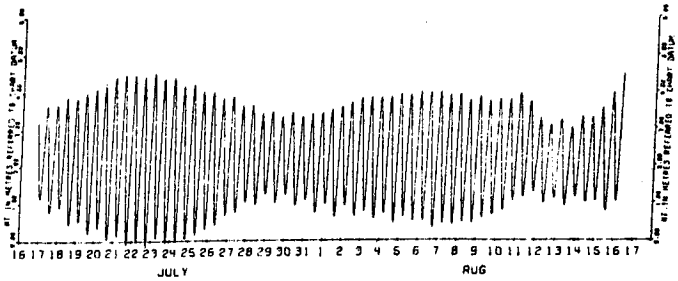

HOURLY WATER LEVELS 02-SANDPIPER ISLAND

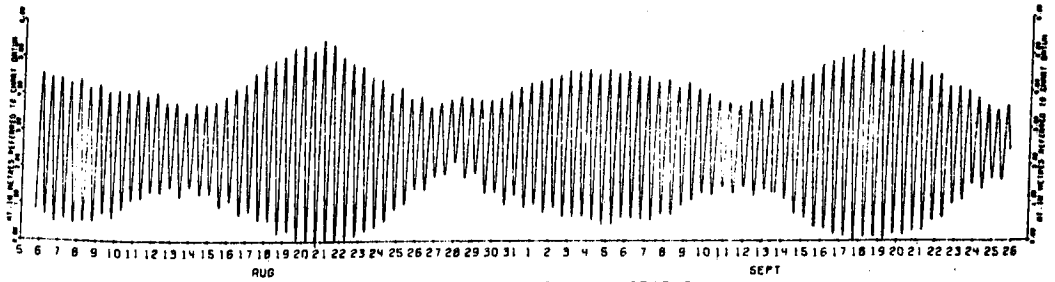

HOURLY WATER LEVELS 03-SEVERN HARBOUR

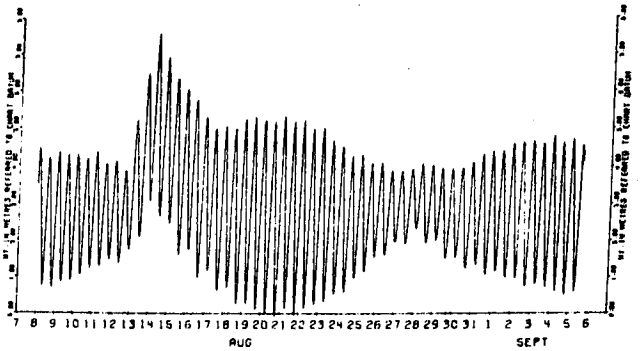

HOURLY WATER LEVELS 04-DEER ISLAND

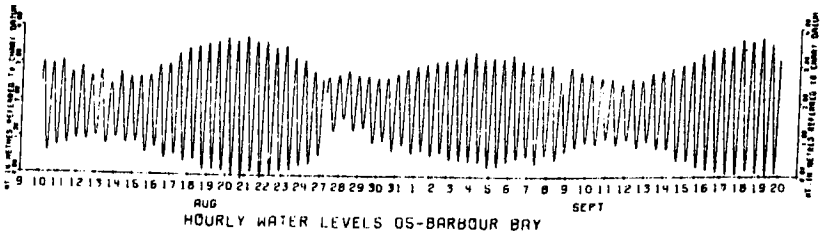

HOURLY WATER LEVELS 05-BARBOUR BAY

FIGURE 9(a): Water Level Records Obtained from Chesterfield Inlet Tide Gauges

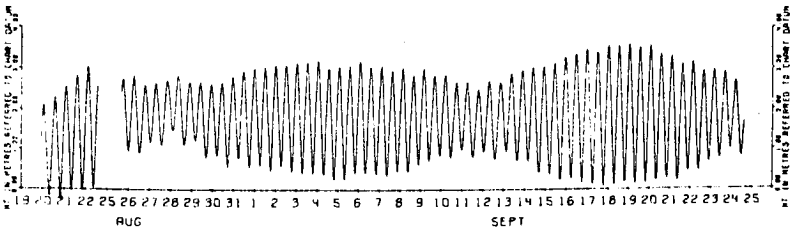

HOURLY WATER LEVELS 06-PROMISE POINT

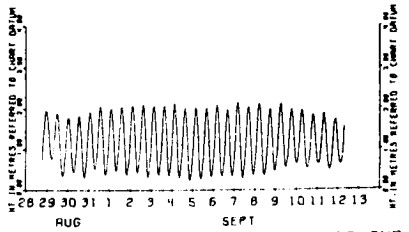

HOURLY WATER LEVELS 07-PRIMROSE ISLAND

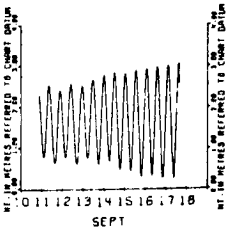

HOURLY WATER LEVELS 09-BALEEN ISLAND

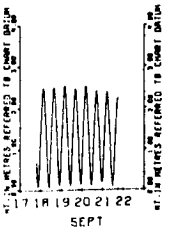

HOURLY WATER LEVELS 08-NORTON ISLAND

FIGURE 9(b): Water Level Records Obtained from Chesterfield Inlet Tide Gauges

malfunction since this anomaly is not present in the records of any of the other gauges.

In addition to the water level data described above, 15-minute water levels at Baker Lake for the month of September, 1974, have been obtained from the Water Survey of Canada. The data from the western extremity of Baker Lake are plotted at an exaggerated scale in Figure 10. The water levels from that station are referred to an arbitrary datum. We see that the water level record at Baker Lake consists of a semi-diurnal oscillation superimposed on a larger fortnightly oscillation.

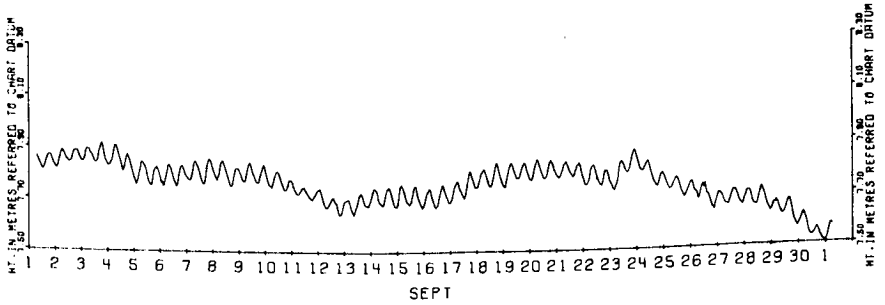

FIGURE 10: Water Levels Recorded at the Western End of Baker Lake.

3.2 ADMITTANCE FUNCTION

A tidal analysis consists of the extraction of the values of amplitude and phase of tidal constituents from a record of tidal water level data. Tidal constituents are cosine terms which, when summed, represent the tidal effect in a geophysical time series. The frequencies of the tidal constituents are of astronomical origin.

The traditional method of tidal analysis is the harmonic method. A harmonic analysis is performed by obtaining a least squares fit for the amplitudes and phases of specified tidal constituents, the frequencies of which are already known.

A less commonly used technique makes use of an admittance function between two sets of water level data. This method had its origins in the work of Munk and Cartwright [25] who related a tidal water level time series

to a tidal potential time series. Later, Cartwright, Munk, and Zetler [8] obtained tidal constituents at a station by relating its tidal time series data to that of another station with well-resolved constituents.

The admittance function gives the relationship between two linearly-related time series. If a series of water level observations $z_1(t)$ at a particular station has associated with it an adequately resolved set of tidal constituents, then one may obtain tidal constituents from a second set of water level observations $z_2(t)$ at a nearby station through the use of the admittance function. The admittance between the water levels at the two stations may be computed by means of the following formulae:

$$|H_{12}(\sigma)| = \frac{\sqrt{C_{12}^2(\sigma) + Q_{12}^2(\sigma)}}{G_2(\sigma)} = \gamma_{12}(\sigma)\sqrt{\frac{G_1(\sigma)}{G_2(\sigma)}} \tag{3.1}$$

$$\phi_{12}(\sigma) = \arctan \frac{Q_{12}(\sigma)}{C_{12}(\sigma)} \tag{3.2}$$

where: σ = frequency;

$|H_{12}(\sigma)|$ = gain between z_1 and z_2;

$\phi_{12}(\sigma)$ = phase shift between z_1 and z_2;

$C_{12}(\sigma)$ = co-spectrum between z_1 and z_2;

$Q_{12}(\sigma)$ = quadrature spectrum between z_1 and z_2;

$G_1(\sigma)$ = power spectrum of z_1;

$G_2(\sigma)$ = power spectrum of z_2;

$\gamma_{12}(\sigma)$ = coherence between z_1 and z_2; and

$H_{12}(\sigma)$, the admittance, is a complex function such that: (3.3)

$$H_{12}(\sigma) = |H_{12}(\sigma)|e^{i\phi(\sigma)_{12}}, \quad i = \sqrt{-1}$$

The coherence, γ_{12}, measures the degree to which the output series is linearly correlated to the input series, and it may have values between zero and one. A value of zero indicates that the two series are completely unrelated, while a value of one indicates that the output series is exactly linearly related to the input series.

Hence, for each individual constituent, j, we have:

$$A_{2j} = |H_{12}(\sigma_j)|A_{1j} \tag{3.4}$$

$$\phi_{2j} = \phi_{12}(\sigma_j) + \phi_1 \tag{3.5}$$

where: j denotes the j^{th} constituent in a standard list,

and A_{1j} = amplitude of the j^{th} constituent in the input series;

A_{2j} = amplitude of the j^{th} constituent in the output series;

σ_j = frequency of the j^{th} constituent;

$|H_{12}(\sigma_j)|$ = amplitude of the admittance in the frequency band in which the j^{th} constituent is found;

ϕ_{1j} = phase of the j^{th} constituent in the input series;

ϕ_{2j} = phase of the j^{th} constituent in the output series;

$\phi_{12}(\sigma_j)$ = phase shift of the admittance between the input and output series in the frequency band in which the j^{th} constituent is found;

and, the water levels at the output station may be written as:

$$z_2(t) = z_o + \sum_j A_{2j} \cos(\sigma_j t - \phi_{2j}) \qquad (3.6)$$

where: z_o is the mean water level and j ranges over all the constituents.

Godin [19] has found that the admittance calculation permits better resolution of the major constituent than the harmonic analysis and reveals more clearly the physics of the processes involved.

CONSTITUENT ANALYSIS

Godin et al [20] performed a tidal analysis of the Chesterfield Inlet tidal records. The constituents obtained at each water level station are shown in Table 3. For a background description of these constituents and their origins, the reader is referred to Dronkers [13] or Godin [19].

Tidal constituents were extracted from the water level records through a combination of the admittance and harmonic methods. The reference station used for the admittance calculations was Churchill, Manitoba, since it was the nearest station possessing long period, good quality records.

Constituents were derived from the admittance function at each station, and these constituents were used to generate tidal predictions over the period of record for which observations were available. A direct harmonic analysis was then applied to the residues (obtained by subtracting the predicted from the observed levels) in order to obtain the higher frequency constituents. Each of the higher frequency, shallow-water constituents extracted in this manner was then vectorially added to

Constituent	Frequency (cycles/hr)	Sandpiper Island		Severn Harbour		Deer Island		Barbour Bay		Promise Point		Primrose Island		Baleen Island		Norton Island	
		Amp. (m)	Phase (deg)	Amp. (m)	Phase (deg)	Amp. (m)	Phase (deg)	Amp. (m)	Phase (deg)	Amp. (m)	Phase (deg)	Amp. (m)	Phase (deg)	Amp. (m)	Phase (deg)	Amp. (m)	Phase (deg)
O_1	.0387	.037	126.7	.042	138.4	.048	147.4	.028	156.0	.037	178.0	.023	198.7	.022	193.6	.017	185.7
K_1	.0418	.077	168.1	.088	178.4	.116	180.9	.072	195.2	.072	217.2	.057	240.2	.050	237.0	.041	229.1
P_1	.0416	.024	174.1	.028	184.9	.036	186.9	.023	201.2	.023	223.2	.018	246.2	.016	243.0	.013	235.1
N_2	.0790	.284	66.2	.303	74.8	.324	82.4	.220	108.4	.215	124.9	.154	177.8	.208	198.2	.152	197.8
ν_2	.0792	.072	72.4	.076	81.0	.082	89.1	.055	115.0	.054	131.4	.038	183.8	.052	204.4	.038	204.0
OP_2	.0803	.050	66.3	.055	74.8	.057	85.9	.041	109.2	.038	126.3	.027	176.9	.036	198.7	.027	198.3
M_2	.0805	1.449	102.3	1.566	110.9	1.637	122.1	1.169	145.1	1.093	162.4	.763	213.1	1.046	234.9	.763	234.5
L_2	.0820	.067	158.1	.073	166.6	.073	177.0	.055	200.8	.049	218.5	.035	269.8	.048	292.6	.035	292.2
S_2	.0833	.444	160.0	.488	168.8	.472	179.0	.367	183.6	.335	219.8	.234	273.6	.315	296.6	.230	296.2
K_2	.0835	.121	159.6	.142	168.3	.136	178.6	.107	183.3	.097	219.4	.068	273.3	.091	296.4	.066	309.7
MK_3	.1223	.014	304.6														
MN_4	.1595	.010	128.2			.018	82.5			.014	133.9						
M_4	.1610	.019	158.9	.022	123.7	.031	95.5	.034	202.8	.037	193.0	.017	66.4	.050	46.4	.091	329.2
MS_4	.1638	.015	226.4	.012	191.2	.018	173.7	.028	290.1			.031	163.6				
SK_4	.1669					.012	175.5	.015	193.8	.030	260.5						
$2MO_5$	.1998													.016	346.0		
$2MN_6$	.2400	.026	286.1	.035	308.3	.048	328.6	.022	111.1	.023	136.0						
M_6	.2415	.031	330.8	.057	354.5	.074	10.7	.015	138.3	.032	188.9			.024	63.2	.077	18.3
$2MS_6$	.2444	.038	38.3	.078	57.9	.078	83.5	.037	202.1	.063	228.7						
NSK_6	.2459	.020	163.5	.019	200.9	.016	204.2			.015	52.7						
$2SM_6$	.2472			.018	119.2			.022	260.0	.028	284.2						
S_6	.2500					.010	73.1										
MKN_6	.2431							.014	113.9	.010	214.3						
M_8	.3220															.037	189.1
$3MS_8$	.3249			.010	192.9												
M_{12}	.4831															.018	270.5

TABLE 3: Chesterfield Inlet Tidal Constituents

the corresponding constituent determined previously from the admittance function. Godin et al [20] found that this technique reduced the variance of the residues significantly from that of either the harmonic method or the admittance function alone. In addition, they found that when the admittance-generated constituents fit the observed tide poorly, problems in the original data were indicated. Some of the anomalies they found in the Chesterfield Inlet tide gauge records are as follows:

1) There is a sharp drop in the datum on August 11, 1974 at Sandpiper Island;
2) A sharp rise in the level not observed in the records of any other stations occurs at Deer Island and is probably caused by a gauge malfunction;
3) The portion of Barbour Bay record between August 27th and September 6th appears to be of poor quality. Two hours were subtracted from the times for this section of the record in order to obtain consistent results; and
4) There is a discrepancy in the phases between Baleen Island and Norton Island. The results of the analyses have the tide reaching Norton before Baleen Island. This is not consistent with a predominantly progressive wave moving upstream. An error of one hour in the observations at Norton Island was suspected.

Because of the short periods of record at Baleen Island and Norton Island, the constituents computed from the records at these stations are not as well resolved as the constituents computed for stations which supplied longer time series. To ensure an adequate resolution of the major tidal constituents, the period of tidal record available for analysis must be at least 29 days.

The variation (throughout Chesterfield Inlet) of the amplitude and phase of the M_2 constituent, computed from field data, is shown in Figure 11. The M_2 is the largest tidal constituent in Chesterfield Inlet and is representative of the semi-diurnal band. The maximum amplitude occurs near Deer Island. As the tide moves upstream towards Primrose Island, the amplitude decreases. Near Baleen Island, the M_2 has a secondary

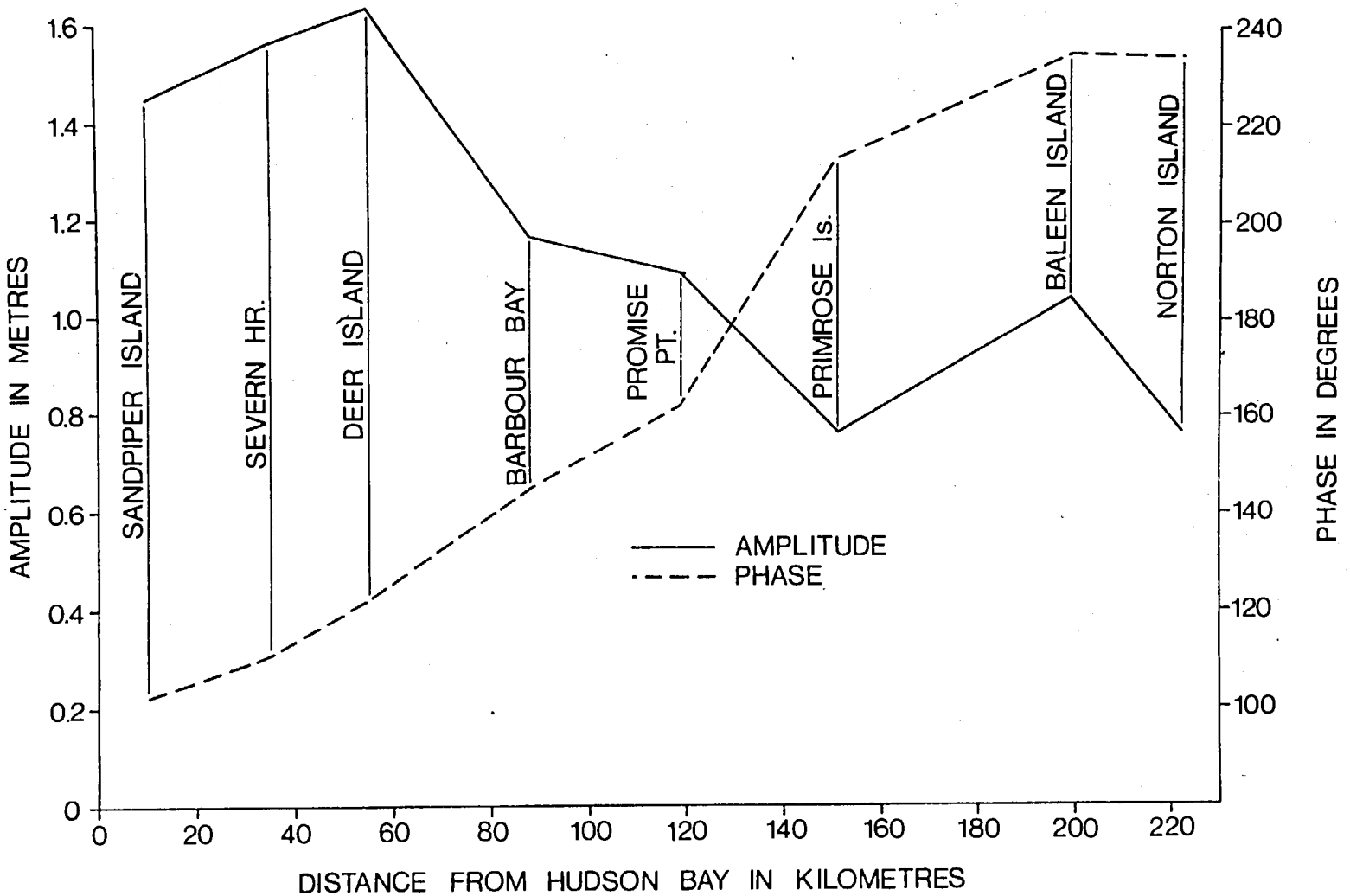

FIGURE 11: Phase and Amplitude of the M_2 Tidal Constituent as Obtained from Tidal Records in Chesterfield Inlet

maximum, probably due to the constriction in the channel at the Bowell Islands. From Baleen Island to Norton Island, the amplitude again decreases. The estimate of phase is probably less reliable than that of amplitude because of clock errors. The Ottboro tide gauges have mechanical clocks which drive the chart mechanisms. Time errors of 15 to 20 minutes, over a two-week period, are not unusual in these devices.

Figure 12 shows the variation in the K_1, the major diurnal constituent in the inlet. Past Primrose Island, the diurnal signal is too weak and the period of record is too short to ensure reliable values for amplitude and phase.

A harmonic analysis was performed on the Baker Lake water level record. The results are shown in Table 4. The fortnightly MS_f has the largest amplitude followed by the M_2. From the phase information, it may be deduced that the M_2 tide crosses the 90 kilometres of Baker Lake in roughly 3 1/2 hours.

3.4 CELERITIES

From the phase data of Table 3, the observed celerity of the M_2 tide between each pair of gauge stations has been computed. In addition, the frictionless shallow-water wave celerity ($C = \sqrt{gh^*}$, where h^* is the depth) has been calculated for the same reaches of the channel. Both sets of celerities are listed in Table 5. In a frictionless channel, the crest of high water should always travel at a speed in excess of $\sqrt{gh^*}$ when a mixture of standing and progressive waves exist. If the crest travels at a speed less than $\sqrt{gh^*}$, the wave is a damped progressive wave. The more damped the wave, the lower is its phase speed.

The M_2 tidal wave is definitely of a progressive nature up to Primrose Island. The observed celerity of 5.08 m/sec between Promise Point and Primrose Island seems much too low. The celerity there should be of the order of 11 m/sec since the depth is approximately equal to that between Deer Island and Barbour Bay. The celerity of -462.96 m/sec between Baleen Island and Norton Island is totally unreasonable for a progressive or partially-reflected wave. Total reflection, however, while possibly explaining a decrease in phase between Baleen Island and Norton Island, does not allow for the high current speeds of the order of 4 m/sec

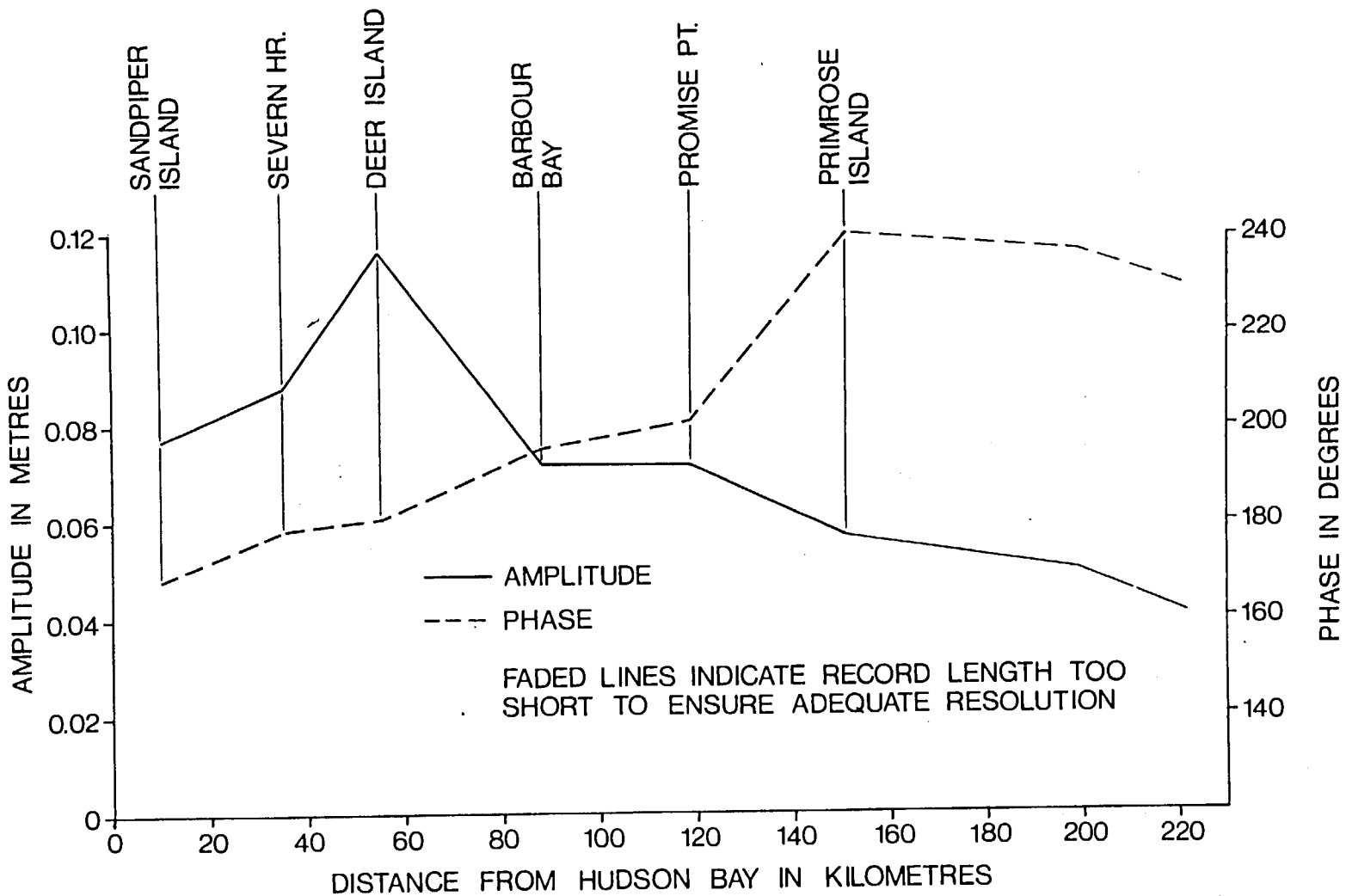

FIGURE 12: Phase and Amplitude of the K_1 Tidal Constituent as Obtained from Tidal Records in Chesterfield Inlet

Constituent	Frequency (cycles/hr)	Amplitude (m)	Phase (deg)
MM	0.0015	0.010	278.9
MS_f	0.0028	0.068	102.8
Q_1	0.0372	0.003	38.4
M_2	0.0805	0.032	333.1
S_2	0.0833	0.008	30.4
M_4	0.1610	0.003	233.1

TABLE 4: Baker Lake Tidal Constituents

Channel Reach	Length of Reach (km)	Mean Depth (m)	Observed Celerity (m/sec)	Adjusted Celerity (m/sec)	$\sqrt{gh^*}$
Sandpiper Island to Severn Harbour	25	55	23.4	23.4	23.8
Severn Harbour to Deer Island	20	45	14.4	14.4	21.0
Deer Island to Barbour Bay	33	35	11.6	11.6	18.5
Barbour Bay to Promise Point	31	35	14.4	14.4	18.5
Promise Point to Primrose Island	32	34	5.08	11.9	18.3
Primrose Island to Baleen Island	48	32	17.7	17.7	17.7
Baleen Island to Norton Island	23	19	-462.96	6.5	13.7

TABLE 5: Celerities in Chesterfield Inlet

observed in Chesterfield Narrows.

If one hour is subtracted from the times at Primrose Island, a celerity of 11.9 m/sec is obtained, which appears much more reasonable. If this change is made, then the celerity between Primrose Island and Baleen Island becomes 7.61 m/sec. Again this appears too low. If one hour is subtracted from the times at Baleen Island, the celerity between Primrose Island and Baleen Island becomes 17.7 m/sec, and the celerity between Baleen Island and Norton Island becomes 6.5 m/sec. A relatively high celerity could be expected in the vicinity of the Bowell Islands because of partial reflection from the islands themselves from Cross Bay and from the Quoich River. Thus a celerity of 17.7 m/sec does not appear unreasonable. The low celerity from Baleen Island to Norton Island would be expected because of the reduced depth in that portion of the channel. Frictional influences are greater here as can be seen from the larger amplitudes of the shallow-water constituents. Hence, it appears that recorded times at Primrose Island and Baleen Island are advanced one hour. After one hour had been subtracted from these times, the celerities were recomputed. These adjusted celerities are shown in Table 5 as well.

A second possibility would be that the times at Norton Island are in error by one hour. If one hour is added to the times there, a celerity of 6.5 m/sec is obtained through the Bowell Islands, the same value that was obtained through the previous hypothesis. However, this still leaves a celerity of 5 m/sec between Promise Point and Primrose Island.

The model results tend to agree with the first hypothesis.

CHAPTER 4

1.0 ONE-DIMENSIONAL NUMERICAL MODEL

The tidal propagation in Chesterfield Inlet was computed through the use of a one-dimensional, numerical model originally developed by Muir [24] with an equation solver developed by Budgell. The model utilizes a four-point, weighted, implicit, finite difference scheme to approximate the nonlinear de St. Venant, or shallow water, equations. Sparse matrix techniques are used to reduce computer time and memory requirements, and the equations are solved through Gaussian Elimination.

The model is flexible enough to permit the inclusion of any number of branches. Furthermore, various types of boundary conditions may be applied to any location, subject only to the constraints of the physical system.

The numerical model was designed to calculate open-channel flow under the following assumptions:

1) flow is one-dimensional;
2) geostrophic and wind-driven circulations are negligible;
3) a quadratic resistance law such as Manning's or Chezy is appropriate;
4) the geometry of the open channel network is constant with time; that is, no deposition or scouring occurs;
5) hydrostatic pressure prevails;
6) the section geometry can be schematized as regular in cross-section;
7) flow is entirely sub-critical; and
8) the fluid is homogeneous in density.

4.1 EQUATIONS OF MOTION

These equations consist of the continuity and momentum equations for unsteady, non-uniform flow in non-prismatic open channels. A schematic diagram of such a channel is given in Figure 13.

The continuity equation is given by:

$$(b + b_s)\frac{\partial z}{\partial t} + \frac{\partial Q}{\partial x} - q = 0 \qquad (4.1)$$

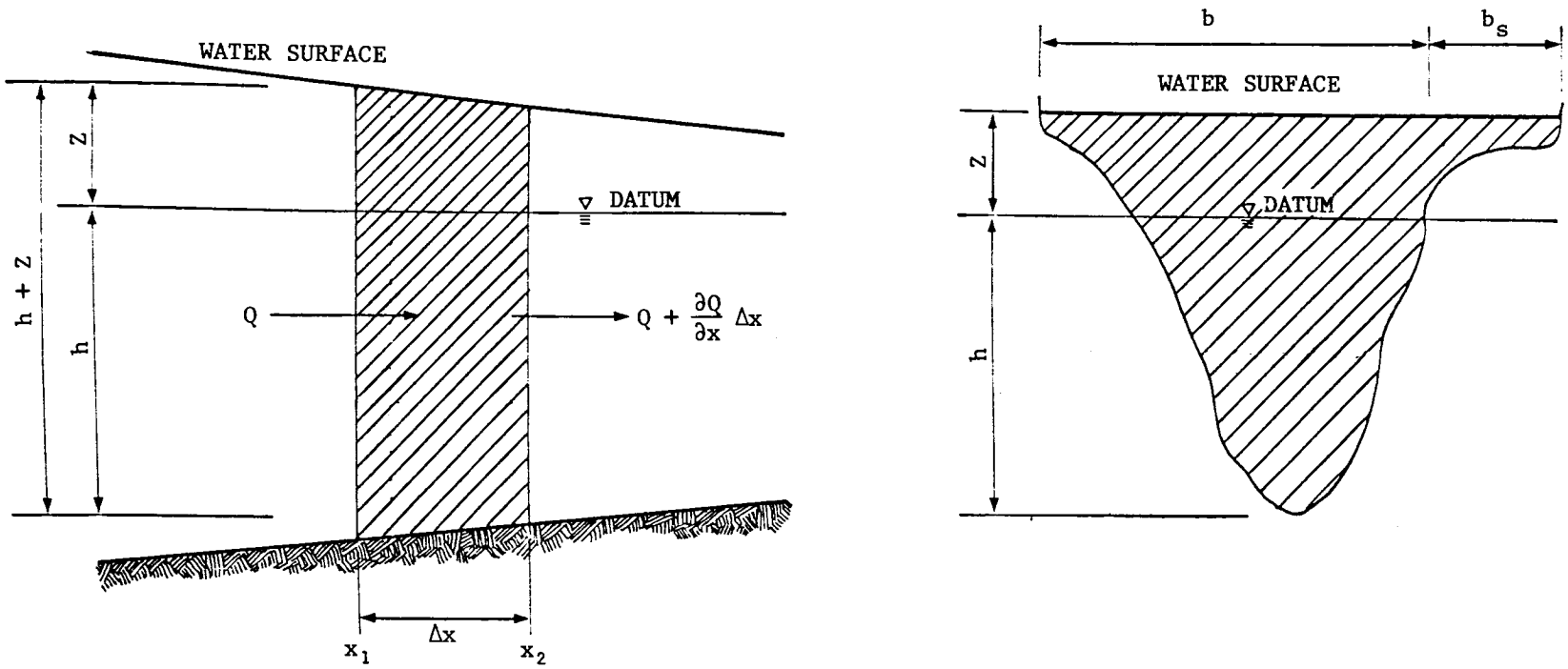

FIGURE 13: Definition Sketches for an Irregular Channel

where: b = topwidth of conveyance section;

b_s = topwidth of storage section;

z = elevation above model datum;

t = time;

Q = volume discharge;

x = distance; and

q = lateral inflow; positive for inflow, negative for outflow.

The momentum equation is of the form:

$$\frac{\partial Q}{\partial t} + u \frac{\partial Q}{\partial x} + Q \frac{\partial u}{\partial x} + gA \frac{\partial z}{\partial x} + \frac{g \cdot k \cdot Q|Q|}{Ah^*} = 0 \qquad (4.2)$$

where: $k = \frac{1}{C^2}$ (Chezy friction)

$k = \frac{n^2}{2.22(h^*)^{1/3}}$ (Manning's friction)

and u = average velocity at a cross-section (discharge per unit area);

g = gravitational acceleration;

A = cross-sectional area;

h^* = hydraulic mean depth;

C = Chezy friction coefficient; and

n = Manning's friction coefficient.

It is assumed that the rate of lateral inflow is very small compared to the flow in the main channel and acts at right angles to the main channel flow. It is further assumed that this inflow makes negligible contribution to the total momentum. In addition, it is assumed that the mass in the storage section contributes no momentum flux to the system.

4.2 JUNCTION EQUATIONS

Consider the generalized junction shown in Figure 14. The junction is assumed to be convergent, but the arguments apply equally well to divergent junctions. If the cross-sections are assumed to be very close together, then storage in the junction may be neglected, and the continuity equation may be written:

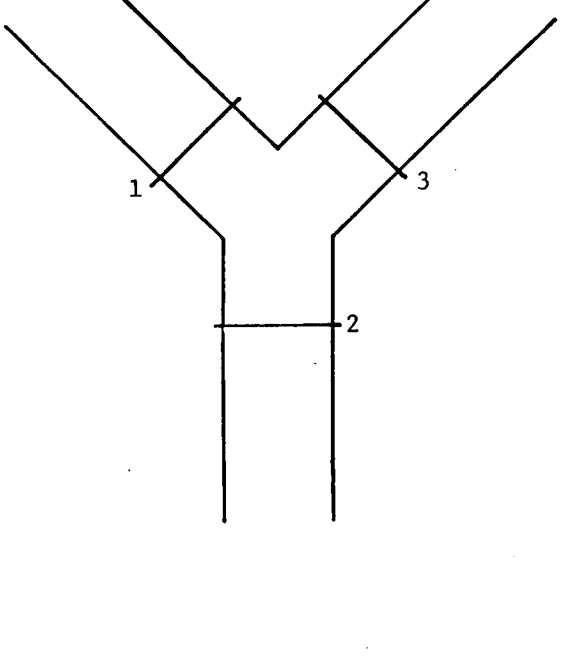

FIGURE 14: A Convergent Junction

$$Q_1 + Q_3 = Q_2$$

The momentum equation for the junction is developed from equation (4.2). If distances between the nodes, or cross-sections, are small, then the terms $\partial Q/\partial t$, $Q\ \partial u/\partial x$ and the resistance term may be neglected in the momentum equation. If the energy losses between node 1 and node 2, accruing from non-uniformity of flow and acceleration or deceleration, are taken into consideration by means of a factor, α, equation (4.2) becomes:

$$\alpha u \frac{\partial Q}{\partial x} + gA \frac{\partial z}{\partial x} = 0 \tag{4.4}$$

After dividing through by A and using a finite difference representation, we obtain:

$$z_1 - z_2 = \frac{\alpha}{2g} (u_2^2 - u_1^2) \tag{4.5}$$

Unfortunately, in an unsteady flow situation, as is the case in tidal waters, the value of α is probably a time-dependent function. In practice, its value may be unknown and extremely difficult to obtain. Thus, the development of a generalized momentum equation for all junctions is impractical at present.

If differences in velocity through a junction are small, and if centrifugal accelerations do not result in significant energy dissipation, then the momentum equations for the junction shown in Figure 14 become:

$$z_1 = z_2 \tag{4.6}$$

and

$$z_1 = z_3 \tag{4.7}$$

4.3 NETWORK REPRESENTATION

A network of open channels may be represented as a directed line graph composed of a number of branches intersecting at node points. Additional nodes are permitted on the boundaries of the graph or at arbitrary points on the graph. Nodes may be classified as follows:

1) bounding node;

2) interior node;

3) convergent node; and

4) divergent node.

Figure 15 shows the various types of nodes. A bounding node is connected to only one branch, an interior node is connected to exactly two branches, a convergent node has two branches entering and one branch leaving, and a divergent node has one branch entering and two branches leaving. The only difference between convergent and divergent nodes is in the direction chosen for the graph. Thus, the river system shown in Figure 16(a) may be schematized as the graph shown in 16(b). Distance relationships are not preserved in the graph representation since the relationships are purely topological. If more than three branches are connected to the same node, as shown in Figure 17(a), it is possible to split the node into two or more nodes, each having three branches attached to it as shown in Figure 17(b). The physical distance between the two nodes in this case (such as in a river network) would be considered to be zero.

At each node in the river network, we must solve for two unknowns, discharge and height. If there are N reaches in the network, there will be N + 1 nodes. Thus, it is necessary to solve 2(N + 1) simultaneous equations in 2(N + 1) unknowns when the implicit method is used.

If we consider a single-branched river which contains only bounding and interior nodes, then a continuity equation and a momentum equation may be written in finite difference form relating each pair of nodes. In this manner, 2N equations are obtained. The other two equations must be obtained from boundary conditions. The implicit method simplifies the handling of branches considerably. If the junction node shown in Figure 18(a) is split into three nodes as shown in Figure 18(b), three continuity equations and three momentum equations can be obtained between nodes 1 & 2, 3 & 4, and 5 & 6, giving a total of 6 equations. There are 3 boundary conditions required which brings the total to 9 equations. The junction continuity equation and the equating of water levels supply the remaining 3 equations for a total of 12 equations in 12 unknowns which may be solved.

4.4 FINITE DIFFERENCE SCHEME

A weighted, implicit, four-point, finite difference scheme has

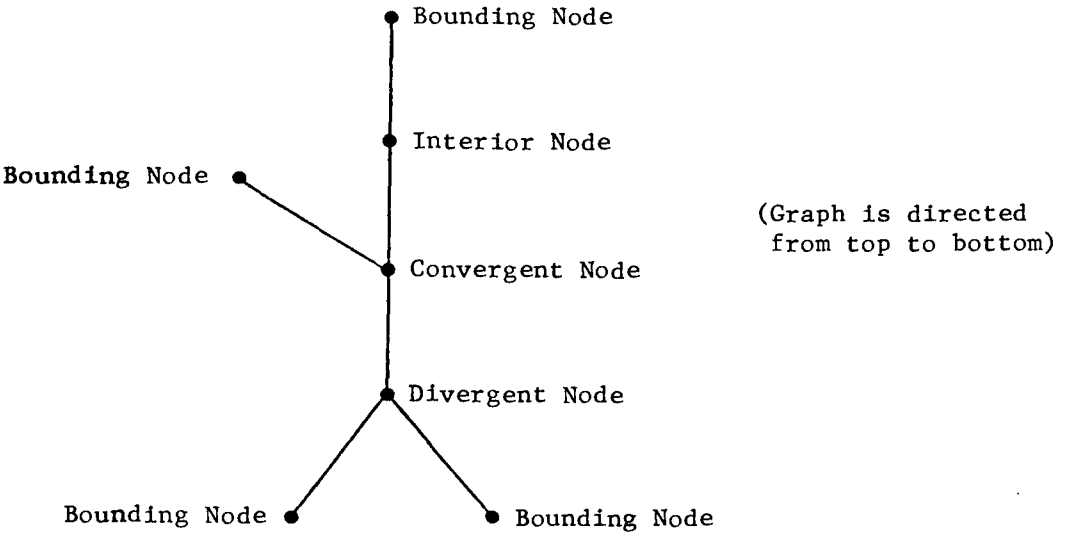

FIGURE 15: Node Types

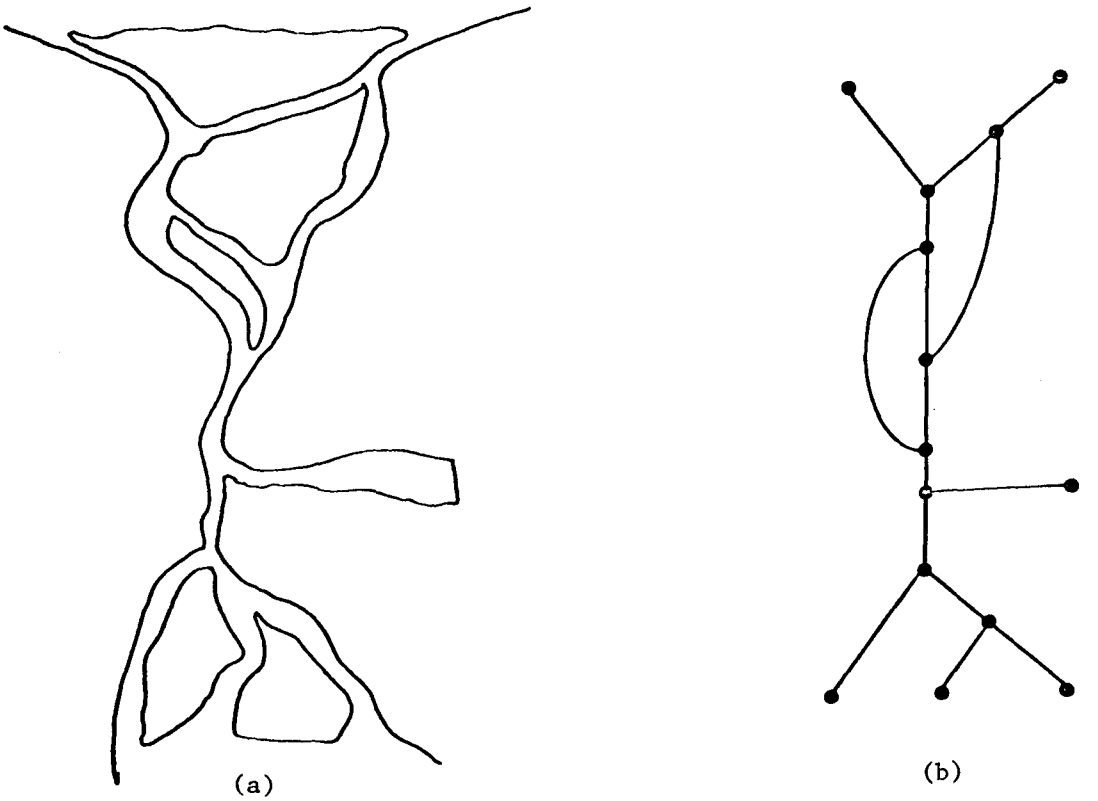

FIGURE 16: A River Network and Its Graph Representation

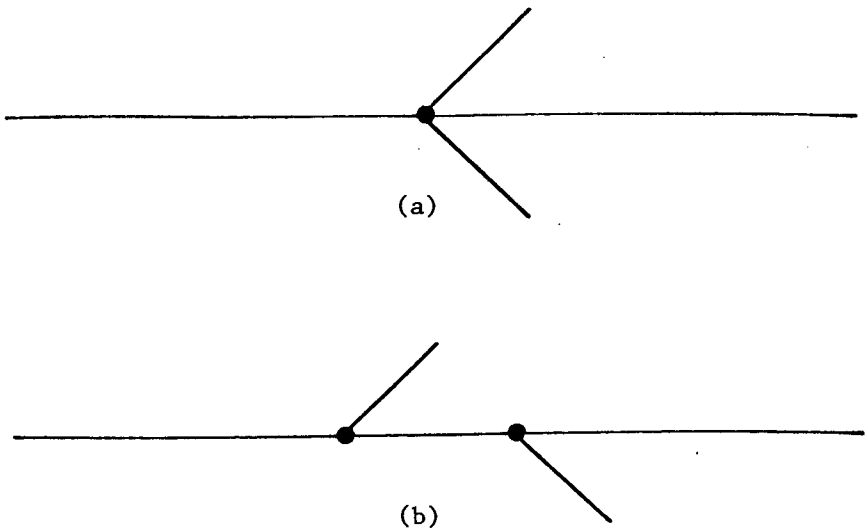

FIGURE 17: Splitting of a Junction Node

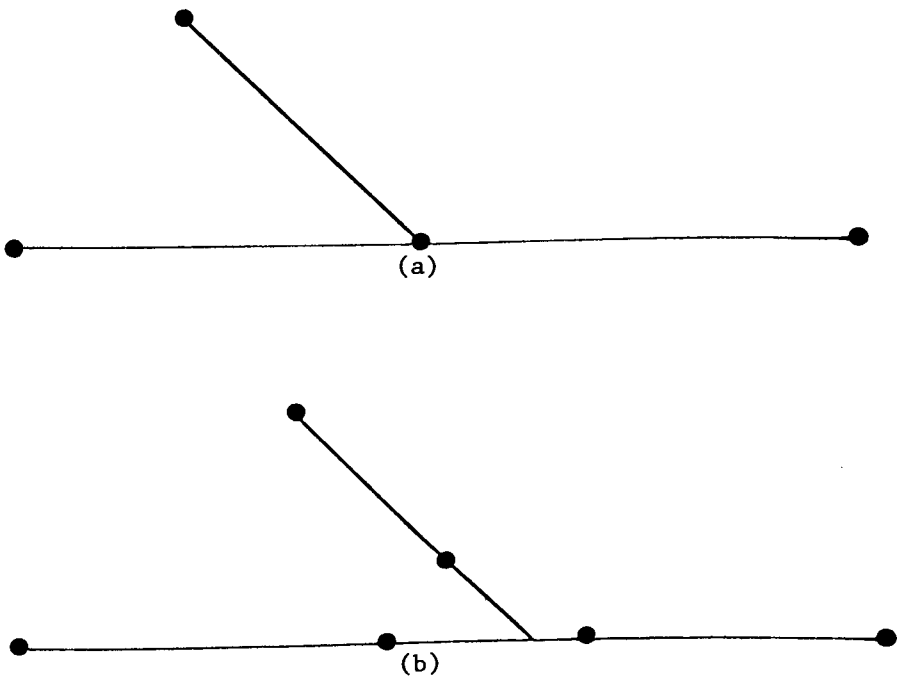

FIGURE 18: A Junction Node

been used to approximate the equations of motion described in section 4.1. The weighting factor can be used to control convergence and stability.

In the x - t plane shown in Figure 19, the abscissa represents the location in space and the ordinate represents the time. Lines drawn parallel to the t-axis represent the nodal points or cross-sections selected on the open channel and need not be a constant distance apart. Lines drawn parallel to the x-axis represent times at which solutions are generated. Thus, nodal points are locations in time and space at which solutions are to be obtained. Time steps need not be equal. In Figure 19, the function values and partial derivatives are to be evaluated at point R, which has the coordinates $(x_m + \Delta x_m/2,\ t_n + \theta\Delta t_n)$. "m" is the node number, "n" is the time step, and θ is a weighting factor $0 \leq \theta \leq 1.0$.

Thus, the function values and partial derivatives of any unknown junction, F, at a point, R, may be expressed in the following manner:

$$F \simeq \theta \frac{\left[F_m^{n+1} + F_{m+1}^{n+1}\right]}{2} + (1 - \theta) \frac{\left[F_m^{n} + F_{m+1}^{n}\right]}{2} \tag{4.8}$$

$$\frac{\partial F}{\partial t} \simeq \frac{1}{2\Delta t}\left[F_m^{n+1} + F_{m+1}^{n+1} - F_m^{n} - F_{m+1}^{n}\right] \tag{4.9}$$

$$\frac{\partial F}{\partial x} \simeq \theta \frac{\left[F_{m+1}^{n+1} - F_m^{n+1}\right]}{\Delta x} + (1 - \theta) \frac{\left[F_{m+1}^{n} - F_m^{n}\right]}{\Delta x} \tag{4.10}$$

In calculating the values of F at time t_{n+1}, it is assumed that the values of F are known at time t_n.

Substituting equations (4.8), (4.9), and (4.10) into equation (4.1), the continuity equation becomes:

$$\frac{\left[b_m + b_{m+1} + (b_s)_m + (b_s)_{m+1}\right]}{2}\left(\frac{1}{2\Delta t}\right)\left(z_m^{n+1} + z_{m+1}^{n+1} - z_m^{n} - z_{m+1}^{n}\right)$$
$$+ \theta \frac{\left[Q_{m+1}^{n+1} - Q_m^{n+1}\right]}{\Delta x} + (1-\theta) \frac{\left[Q_{m+1}^{n} - Q_m^{n}\right]}{\Delta x} - q_m = 0 \tag{4.11}$$

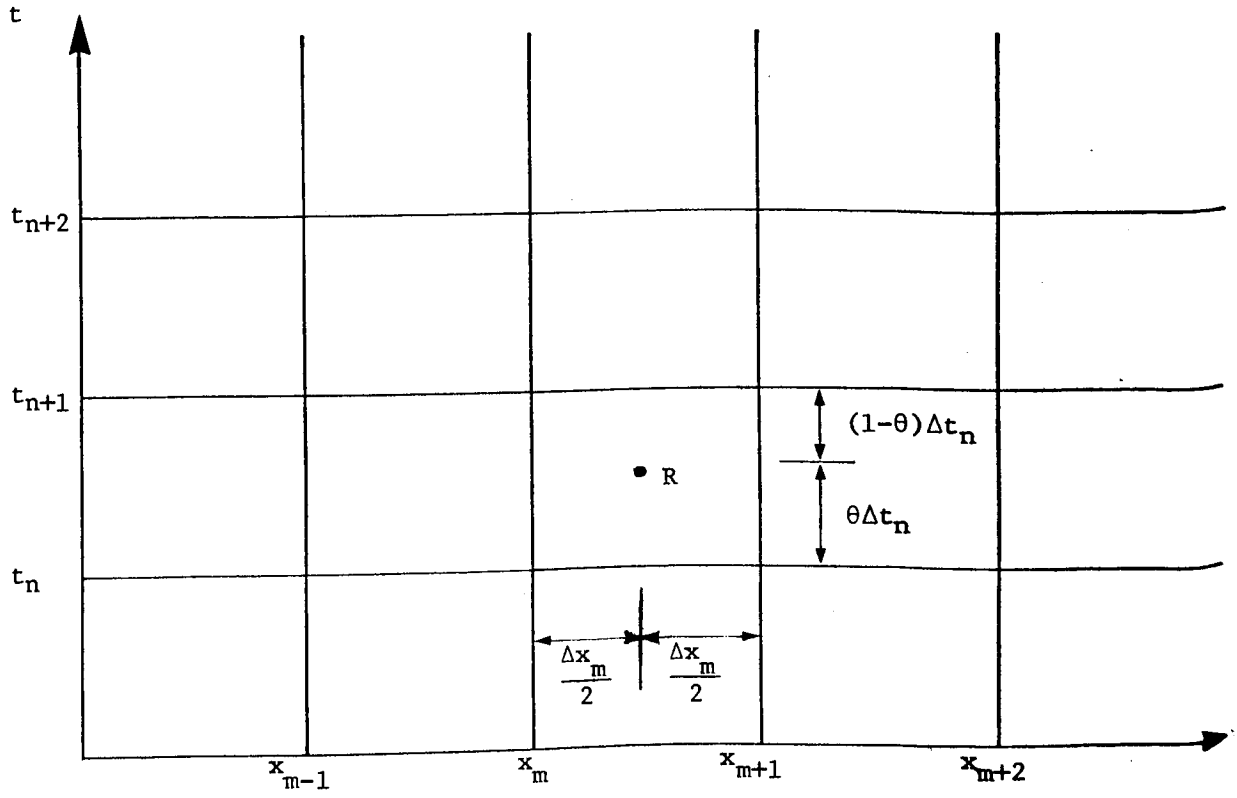

FIGURE 19: The x-t Solution Plane

Similarly, the finite difference form of the momentum equation is obtained by substituting equations (4.3), (4.4), and (4.5) into equation (4.2) to get:

$$\frac{1}{2\Delta t}\left[Q_m^{n+1} + Q_{m+1}^{n+1} - Q_m^n - Q_{m+1}^n\right] + \left(\theta\,\frac{u_m^{n+1} + u_{m+1}^{n+1}}{2} + (1-\theta)\,\frac{u_m^n + u_{m+1}^n}{2}\right) *$$

$$* \left(\theta\,\frac{Q_{m+1}^{n+1} - Q_m^{n+1}}{\Delta x} + (1-\theta)\,\frac{Q_{m+1}^n - Q_m^n}{\Delta x}\right) + \left(\theta\,\frac{Q_m^{n+1} + Q_{m+1}^{n+1}}{2} + (1-\theta)\,\frac{Q_m^n + Q_{m+1}^n}{2}\right) *$$

$$* \left(\theta\,\frac{u_{m+1}^{n+1} - u_m^{n+1}}{\Delta x} + (1-\theta)\,\frac{u_{m+1}^n - u_m^n}{\Delta x}\right) + g\left(\theta\frac{A_m^{n+1} + A_{m+1}^{n+1}}{2} + (1-\theta)\frac{A_m^n + A_{m+1}^n}{2}\right) *$$

$$* \left(\theta\,\frac{z_{m+1}^{n+1} - z_m^{n+1}}{\Delta x} + (1-\theta)\,\frac{z_{m+1}^n - z_m^n}{\Delta x}\right) +$$

$$+ \left(\frac{gk\left|\theta\left[\frac{Q_m^{n+1} + Q_{m+1}^{n+1}}{2}\right] + (1-\theta)\left[\frac{Q_m^n + Q_{m+1}^n}{2}\right]\right|}{\left[\theta\,\frac{A_m^{n+1} + A_{m+1}^{n+1}}{2} + (1-\theta)\,\frac{A_m^n + A_{m+1}^n}{2}\right]}\right) *$$

$$* \left(\frac{\theta\left[\frac{Q_m^{n+1} + Q_{m+1}^{n+1}}{2}\right] + (1-\theta)\left[\frac{Q_m^n + Q_{m+1}^n}{2}\right]}{\left[\frac{h_m + h_{m+1}}{2} + \theta\,\frac{z_m^{n+1} + z_{m+1}^{n+1}}{2} + (1-\theta)\,\frac{z_m^n + z_{m+1}^n}{2}\right]}\right)$$

$$= 0 \qquad (4.12)$$

where: $u_m^n = \dfrac{Q_m^n}{A_m^n}$;

$A_m^n = b_m(h_m^n)^*$;

$(h_m^n)^* = h_m + z_m^n$; and

h_m = depth of channel invert below datum at section m.

The variables Q and z are solved for directly. To determine the mean velocity, u, at a section, it is necessary to divide the discharge, Q, by the cross-sectioned area, A. The area is a function of the height, z, as shown above.

The weighting factor, θ, plays an important role in the above equations. If $\theta = 1$, an implicit scheme fully forward in time is obtained; if $\theta = 0.5$, the box scheme used by Amien [3] and Fread [16] is obtained, and if $\theta = 0$, an explicit finite difference is obtained. If $\theta = 0.5$, the system will conserve mass, but the farther θ departs from 0.5, the greater is this discrepancy. Bounded oscillations in numerical results will be obtained if $\theta = 0.5$, and the wave period is short relative to the time step. For $\theta \leq 0.5$, the Courant stability criterion must be applied. The numerical damping of a wave is proportional to θ. As θ approaches 1.0, waves are damped out rapidly. For unsteady flow situations, an optimum value for θ has been found to be 0.55. For steady state conditions, rapid convergence from inaccurate initial conditions will be achieved if $\theta = 1.00$. For a more complete discussion of the properties of the weighting factor, the reader is referred to Fread [15, 17].

4.5 CHOICE OF EQUATION SOLVER

In the original version of the one-dimensional numerical model, the nonlinear finite difference equations were solved using an algorithm developed by Brown [6]. Brown's algorithm is essentially a modified Newton's method based on Gaussian Elimination. The forward triangularization of the full Jacobian matrix is approximated by operating on one row at a time, eliminating one variable for each row treated.

In effect, then, the full $(2N + 2) \times (2N + 2)$ matrix is inverted for each iteration, even though there are, at most, four non-zero entries per row. Thus, for large networks, there is an enormous overhead of computer time and memory. Muir [24] has found that the execution time increases quadratically with the number of equations while using storage for the full matrix.

For the Chesterfield Inlet system (100 equations in 100 unknowns), Brown's algorithm was impractical. It was decided to use Muir's model with a more efficient equation solver. In this way, the inherent flexibility of Muir's model is retained while the demands on the computing facilities are

kept within reasonable bounds.

Significant reductions in computing requirements can be made by avoiding storing or operating on the zero coefficients of the network matrix. This method, known as a sparse matrix technique, can easily be combined with Gaussian elimination to produce a reasonably efficient equation solver. The method used in this study is based on that developed by Chandrashenkar, Muir, and Unny [9]. For a banded matrix, execution time increases linearly with the number of equations.

4.6 SOLUTION TECHNIQUE

The coefficients for Q and z at each of the nodes are determined from the finite difference equations for continuity and momentum (4.11) and (4.12) and from the junction equations and boundary conditions. The momentum equation is nonlinear. Therefore, the "constant" coefficients in the matrix will be a function of Q or z, or both.

Since the Matrix is of the form $[A] * [X] = [B]$ where $[X]$ is the solution vector, then the coefficients in $[A]$ and $[B]$ will not be constant but will be functions of Q or z, or both. For example, in the momentum equation, one of the nonlinear terms is $u \cdot \partial Q/\partial x$. In the solution technique, the term is quasi-linearized to $u^* \cdot \partial Q/\partial x$, where u^* is the velocity computed from the last iteration. For the first iteration at a given time step, u^* is the velocity computed at the last time step. For the first time step, the initial conditions are used for u^*.

Thus, the system of equations is now in a linear form. The matrix is reduced in three steps:

1) Zero diagonal entries initially in the matrix are filled. Any row, i, that has a zero diagonal entry has added to it a row, j, that has a non-zero entry in the i^{th} column, where $i < j$.
2) The matrix is upper-triangularized. Starting at the second row and working downwards, any non-zero entries to the left of the diagonal are eliminated through the use of the rows above.
3) Once the matrix has been upper-triangularized, back substitution is used to fill the solution vector.

Each time the matrix is reduced, the values for Q and z extracted from the solution vector are used to recompute the coefficients.

The matrix consisting of the new coefficients must now be solved. This process is repeated until convergence to a predetermined number of significant digits is achieved in the Q and z values. Convergence to four significant digits usually takes less than 10 iterations.

4.7 OPTIMAL ORDERING OF A MATRIX

For most networks, the method described in the previous section proves to be quite efficient. For large, complex networks, however, computer time increases rapidly with increased separation of non-zero entries in the bottom rows. This difficulty may be overcome by solving the equations in a different order.

Wing and Huang [27] have developed a technique for optimizing the order in which rows occur in a sparse matrix. Their technique selects diagonal pivots that will cause the minimum number of new non-zero entries to be generated in the Gaussian Elimination process. The department of Systems Design at the University of Waterloo has developed an algorithm based on this technique which can be used in conjunction with the numerical model. Unfortunately, because of time constraints, no attempt has been made herein to reorder the model equations, but this optimization process definitely appears to be promising, and should be investigated.

CHAPTER 5

5.0 APPLICATION OF THE MODEL TO CHESTERFIELD INLET

Once the available hydrologic and tidal data have been studied and interpreted, a modelling study can be undertaken. The hydrodynamics of Chesterfield Inlet were simulated through the use of the one-dimensional, numerical model described in the previous chapter. The intent of the modelling is not to develop a predictive capability but to provide insight into the nature of the tidal phenomena within the inlet. It should be noted that no attempt has been made to model non-tidal effects and that the hydraulic grade has been considered only when it affects the tide appreciably.

5.1 SCHEMATIZATION

In order to develop a one-dimensional network representation of the inlet, the inlet had to be broken down into a series of cross-sections connected by channel reaches. The cross-sections were selected such that the major changes in the cross-section geometry would be accounted for by the schematization. The cross-sections chosen are shown in Figure 20, and the network representation is shown in Figure 21. The channel width at a given section was divided into a conveyance width and a storage width, where the conveyance width is the effective width of the moving stream and the storage width is the width of that part of the channel assumed to possess no momentum. The conveyance widths and storage widths were determined through examination of hydrographic field sheets and aerial photographs of the area. The mean channel depth at the cross-sections were computed from bathymetric data extracted from hydrographic field sheets. The cross-section geometry was plotted; then the area obtained by planimeter was divided by the topwidth to obtain the mean depth. The variation in the computed conveyance width and depth of Chesterfield Inlet are shown in Figure 22. The depths are referred to the mean water level.

Since none of the gauge records were referred to mean sea level, it was assumed that the mean of the model-predicted tide was at the same elevation as the mean of the observed tide. At each of the gauge locations, a chart datum was selected by the Canadian Hydrographic Service.

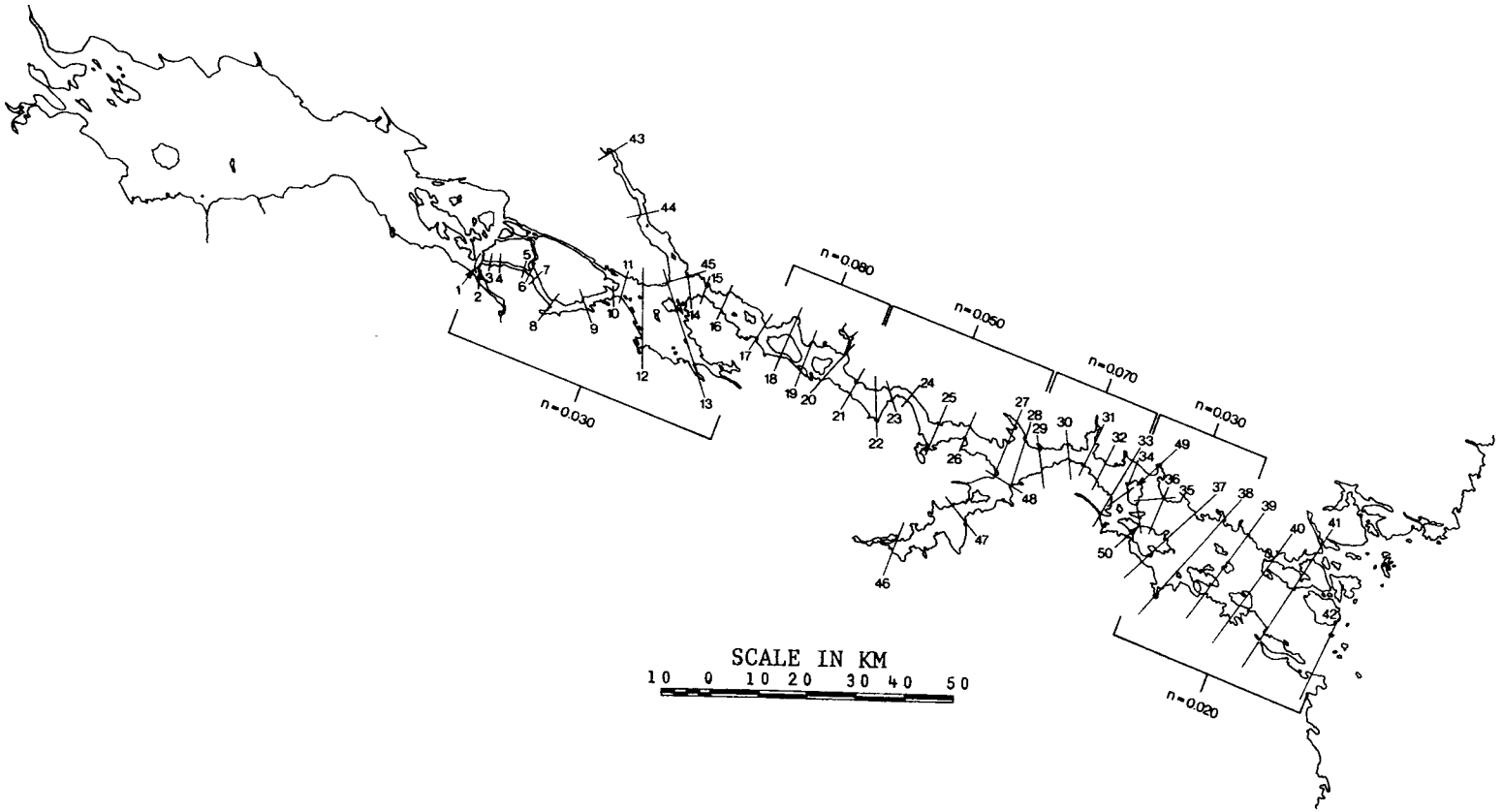

FIGURE 20: Cross-sections Selected for the Model Representation of the Inlet

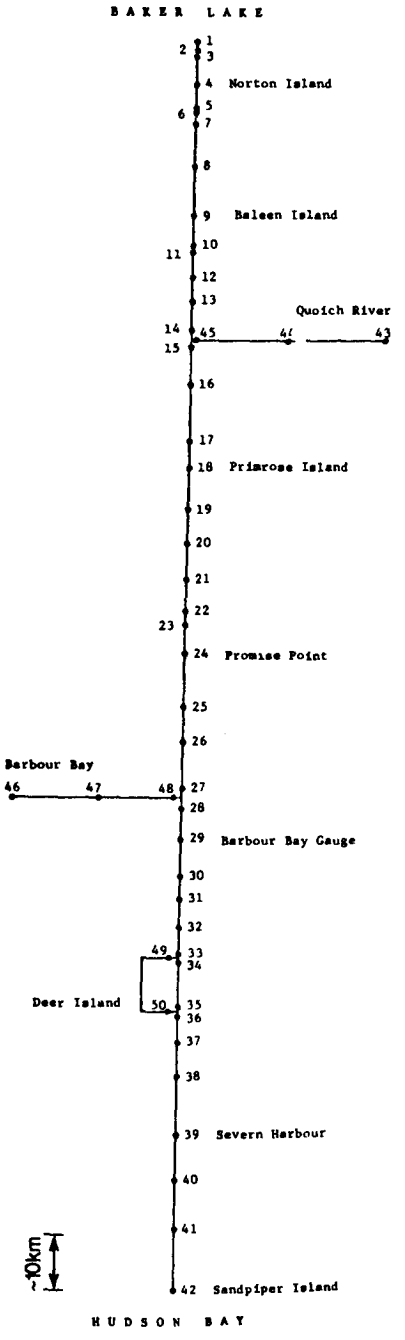

FIGURE 21: Line Graph Representation of the Chesterfield Inlet Network

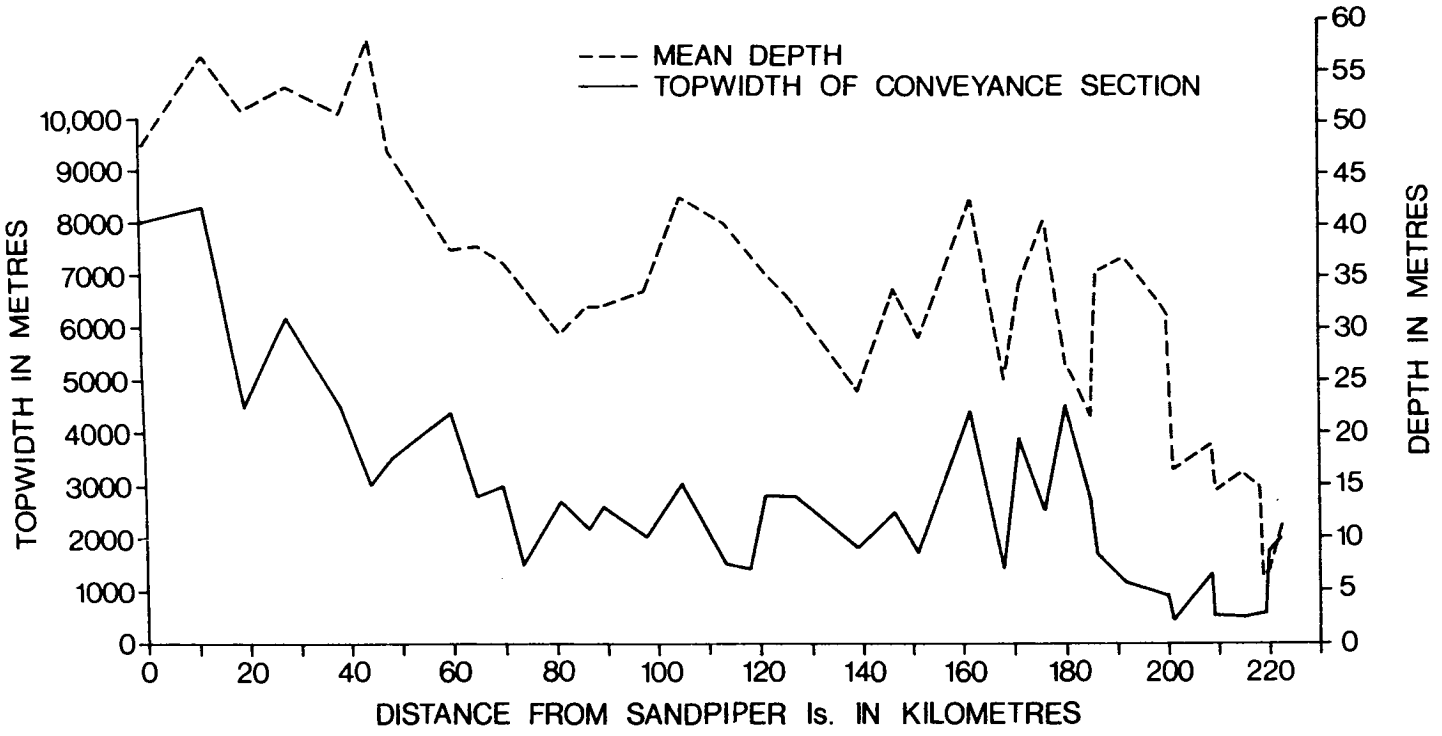

FIGURE 22: Mean Topwidth and Depth of Chesterfield Inlet

Water levels were referred to this level as were the soundings. Thus, to obtain the mean depth of flow at a station, it was merely necessary to add the depth below datum to the mean water level above the datum. Since the model datum was mean sea level at Hudson Bay, a new depth below datum, h, had to be determined. An initial value for h was assumed, then a model run was made. Since the value of the mean depth of flow at each station had to be preserved, the model-computed mean elevation above sea level, z_o, at each station was subtracted from the mean depth of flow to obtain a corrected value of h. The correction for h was assumed constant for each field sheet showing a tide gauge location. If a field sheet did not have any tide gauge locations, the correction for h was determined through a linear interpolation on the corrections of the two adjacent gauges. As parameters such as the Baker Lake elevation and the friction factors were changed in the various model runs, the computed values of z_o changed, and the values for h had to be altered. A model run would then have to be made to see if these changes resulted in differences in the computed values of z_o. If so, the process was repeated. Fortunately, the mean depth in Chesterfield Inlet is generally in excess of 30 metres, so that, over most of the inlet, small errors in the depth do not result in any appreciable error in the computed values of z_o. Only in the extreme upstream portion of the inlet, in the Bowell Islands, is the channel sufficiently shallow for this factor to be taken into consideration.

In addition to the lack of datum information, bathymetric data are scarce in some portions of the Chesterfield Inlet system. No bathymetry is available for Barbour Bay, the Quoich River, Cross Bay, the south channels at Primrose and Little Big Islands, and all but the south channel in the Bowell Islands. Bathymetric data are available for only a central corridor in Baker Lake. Often, depths in the shallow areas along the sides of the inlet were not recorded. Depths of 10 metres below mean sea level were assumed for Barbour Bay and the Quoich River; Cross Bay was assumed to be a storage area, so that the depth was unimportant. All flow was assumed to be in the south channel in the Bowell Islands and in the north channel at Primrose and Little Big Islands. The upstream boundary condition selected was the water level at the eastern end of Baker Lake.

Shallow areas in the channel were assumed to be storage areas. These assumptions obviated the necessity of assuming mean depths for many of the areas of the inlet where soundings were not taken.

Doubling the assumed depth at Barbour Bay and the Quoich River reduced the model-predicted tidal range by less than one per cent in the main channel. The section geometry at Cross Bay (section 12 in Figure 20) is shown in Figure 24. It was assumed that the ridge, which rises to within 5 metres of the surface, causes the momentum of the fluid to be concentrated in the main channel and that Cross Bay (south of the ridge) acts as a storage basin. Increasing the value for the storage width of Cross Bay, from 2,000 metres to 4,000 metres, decreased the amplitude of the model-predicted tide by less than 2 per cent at Baleen Island. Aerial photographs of the south channels at Primrose and Little Big Islands showed these channels to be much narrower than the north channels and to have many shoals. Thus, it was assumed that the flow in the south channels would have little effect on the tidal regime in that portion of the inlet.

Aerial photographs showed the north and central channels in the Bowell Islands to be approximately one-third as wide as the south channel. To assess the effects of the Bowell Islands on the computed tide, the north and central channels were included in the model schematization as shown in Figure 23. Dropping all but the south channel from the schematization increased the model-predicted tidal ranges at Baleen and Norton Islands as shown in Figures 25 and 26. A mean depth of 6 metres and a Manning's friction coefficient of 0.030 were assumed for the extra branches.

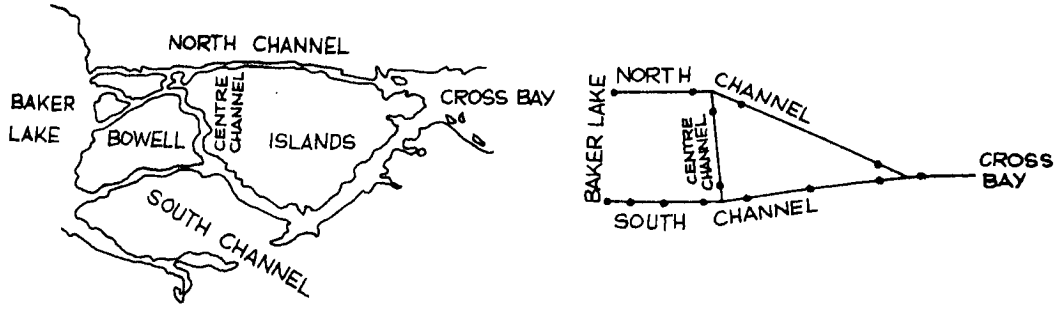

FIGURE 23: Schematization of the Bowell Islands

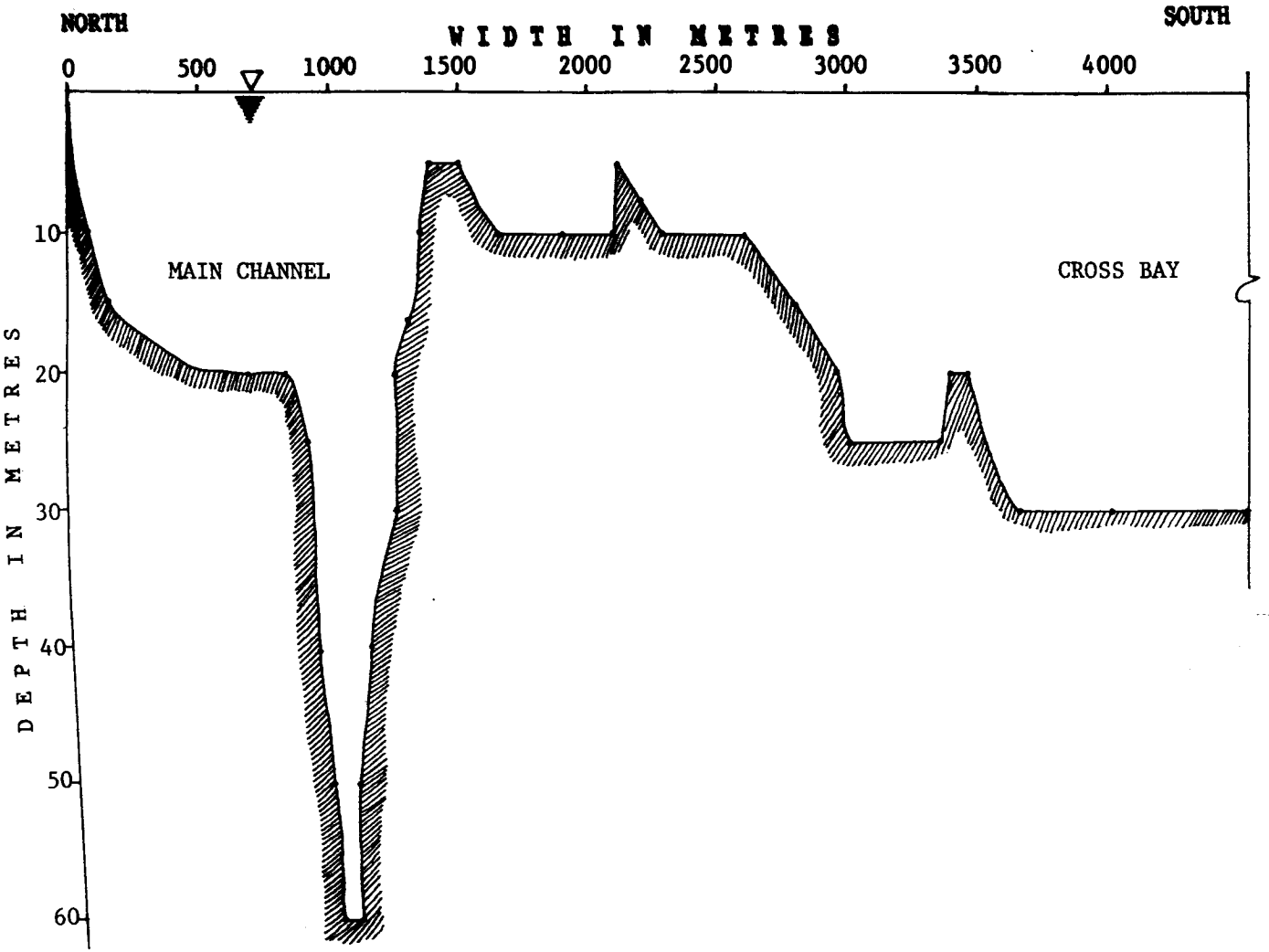

FIGURE 24: Cross-section Geometry at Cross Bay

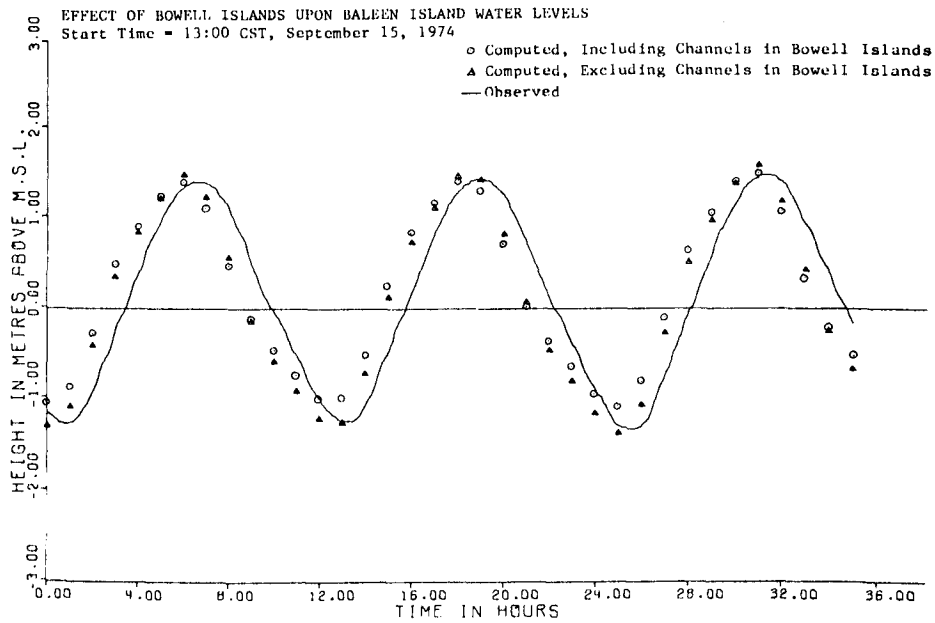

FIGURE 25: Effect of the Bowell Islands upon Computed Water Levels at Baleen Island

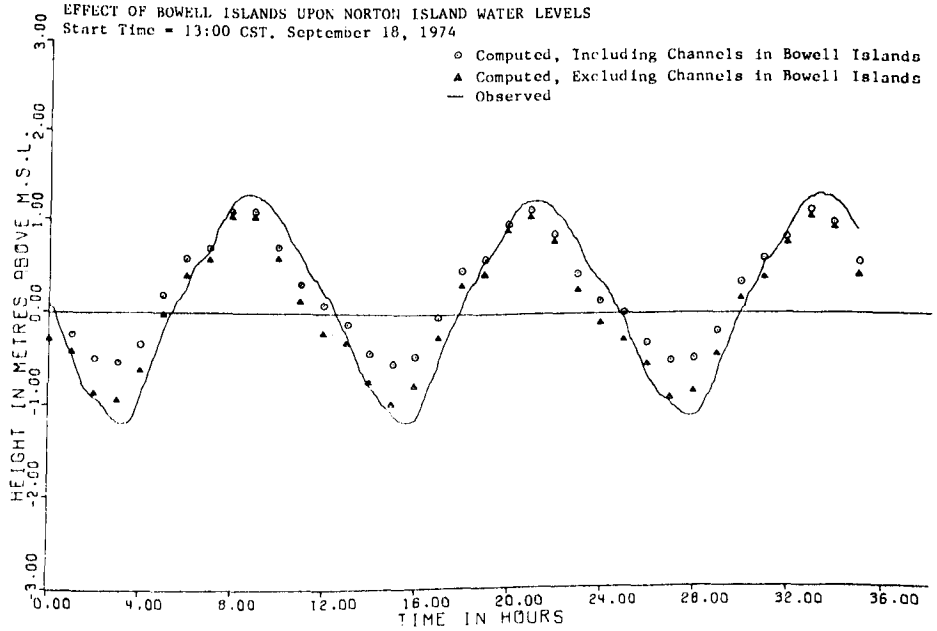

FIGURE 26: Effect of the Bowell Islands upon Computed Water Levels at Norton Island

From Figures 24 and 25, it would appear that the branches in the Bowell Islands influence the tidal properties at Norton Island more than they do at Baleen Island. This would suggest that the tidal regime at Norton Island is directly affected by flow in the north-south center channel. It is also significant that the tidal curve, computed at Norton Island with the extra channels included, is much flatter at low tide than is either the curve computed with the extra channels excluded on the observed tidal curve. This may indicate that the mean depths in the north and center channels are appreciably less than 6 metres or that the frictional effects there are much greater than those that would be obtained using a Manning's n of 0.030 in the numerical model.

Before the effects of flow in the north and central channels upon the tidal propagation in the south channel can be studied further, a hydrographic survey of the Bowell Islands network will have to be completed. The north and center channels in the Bowell Islands are probably relatively shallow. Thus, errors in depth at those locations are likely to have more impact upon model-computed tides and currents than at other places within the inlet.

5.2 BOUNDARY CONDITIONS

The boundary conditions for the model runs were taken to be the water level at the eastern end of Baker Lake and the water level at Sandpiper Island at the mouth of the inlet.

The water level at Baker Lake was assumed constant. Thus, Baker Lake was assumed to be an infinite reservoir with no tidal motion. From the water level record (shown in Figure 10) of the station situated at the western end of Baker Lake, it can be seen that this is not the case. Tidal effects, though small, are present in the record.

Although no water level records are available at the eastern end of Baker Lake, Wright [28] reported that sightings taken on a rod over a 6-hour period revealed no noticeable tide there. While there is undoubtedly tidal motion at the eastern end of the lake, high-frequency wave action probably masked the tidal effects at that time. Thus, the tidal range there is probably less than 0.5 metres. Strong tide rips, or turbulent areas, exist at the entrance to the eastern end of Baker Lake, and the lake is approximately 11 kilometres wide and 30 metres deep in that vicintiy. The combination of turbulent head losses and continuity

effects could combine to reduce the tidal range considerably.

On this basis, it was decided to assume a constant water level at eastern Baker Lake. It was felt that the tidal effect would be an order of magnitude less than at Norton Island, the nearest water level station. While it would be possible to run the model using the water levels at the western end of Baker Lake as a boundary condition, it was felt that too little was known about the bathymetry and frictional effects in the lake to justify the extra computer time caused by the increased number of cross-sections required. In addition, discussions with the inhabitants of the area indicated that the flow regime at the eastern entrance to the lake is too complex to be simulated with a one-dimensional model.

The problem of what elevation to use had to be dealt with. To date, no water levels at any location in Baker Lake have been tied to any standard datum or any useful reference elevation, such as mean sea level at the west coast of Hudson Bay. Discussion with various workers in the Geodetic Survey of Canada and the photogrammetry section of the Department of Energy, Mines and Resources led the author to conclude that the mean level at the eastern end of Baker Lake is between zero and 2.5 metres above mean sea level at Hudson Bay. Numerical experiments tended to indicate that mean level is very close to mean sea level at Hudson Bay. Thus, for most of the model runs, the level at Baker Lake was fixed at zero metres referenced to mean sea level at Hudson Bay. The effects of the Baker Lake elevation upon the model results are discussed in the next section.

The water levels used as the downstream boundary condition were the tidal predictions at Sandpiper Island. These predictions were obtained from the constituents inferred from the admittance function. Tidal predictions were used because the Sandpiper Island gauge was removed before most of the upstream gauges were installed. Thus, as shown in Figure 8, there is little overlap between the water level record at Sandpiper Island and the records from the rest of the gauges. Rather than use different stations for the downstream boundary conditions for different runs, it was decided to use the Sandpiper Island gauge for all the runs, since the increased accuracy obtained by following the former procedure would be offset by the greater number of computer runs required. Using tidal pre-

dictions also has the advantage of smoothing the water level record, such that fluctuations caused by local disturbances are removed.

Slightly more than one month of record was used in computing the Sandpiper Island tidal constituents. The residues obtained by subtracting the predicted from the observed levels are plotted in Figure 27. The effect of 10 per cent error in amplitude in the Sandpiper Island water levels upon the model results is shown in Figure 28.

Two other boundary conditions are required in order to obtain a solution. The upstream boundary conditions at Barbour Bay and the Quoich River must be defined. At Barbour Bay, the velocity was set to zero at the upstream end. It was assumed that non-tidal discharge in Barbour Bay is negligible. At the upstream end of the tidal portion of the Quoich River are the St. Clair Falls. Thus, a velocity of zero was set at that location, and a lateral discharge was added to supply a 300 m^3/sec mean discharge which is representative of the flow rates in that river during August and September. It was assumed that the discharge over the falls added no momentum to the flow in the channel.

5.3 CALIBRATION

The calibration of the numerical model of Chesterfield Inlet entailed two processes: the determination of the elevation at Baker Lake, and the selection of friction factors throughout the inlet. For the most part, these tasks could be tackled separately. The mean elevation at Baker Lake is, according to the available information, less than 2.5 metres above sea level. When the Manning's friction factor, n, was set to 0.030 everywhere in the inlet, it was found that varying the level of Baker Lake from zero to 2 metres had negligible effect on the tidal ranges downstream of Baleen Island. As a result, the friction factors downstream of the Bowell Islands could be determined assuming a fixed level of zero metres at Baker Lake.

The friction factors were obtained by forcing the model to reproduce as closely as possible the tidal curves obtained from water level gauges. The friction factors were obtained in blocks. Each block consisted of the sections between adjacent water level gauges. The friction factors were adjusted until the model-predicted tidal amplitudes matched the observed amplitudes to within 10 per cent. No attempt was made to match the modelled

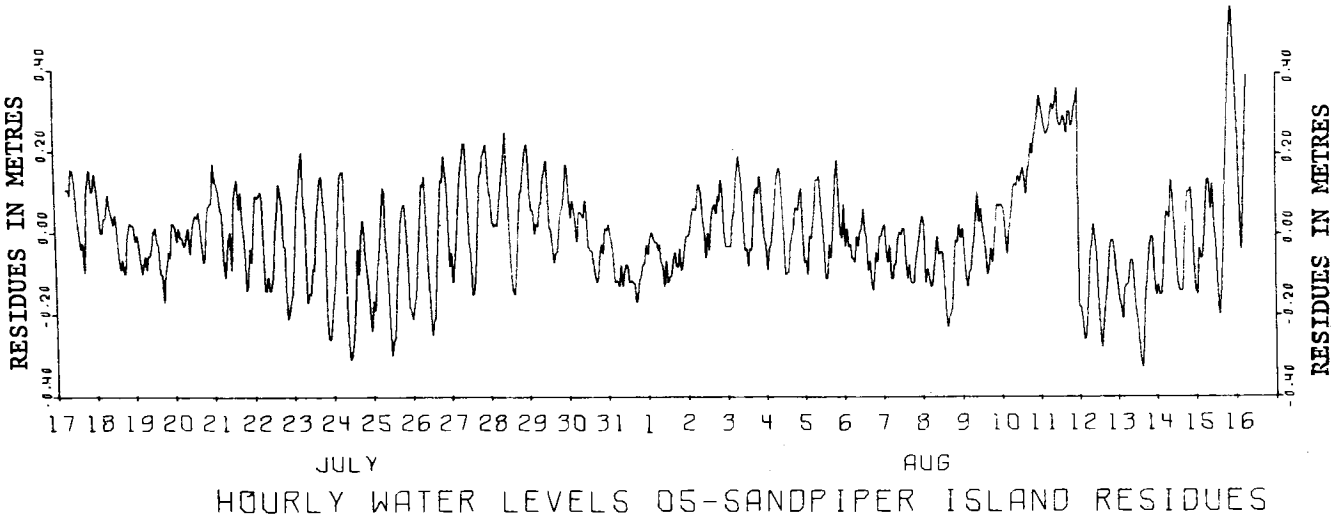

FIGURE 27: Residues at Sandpiper Island
(Observed Minus Predicted from Constituents)

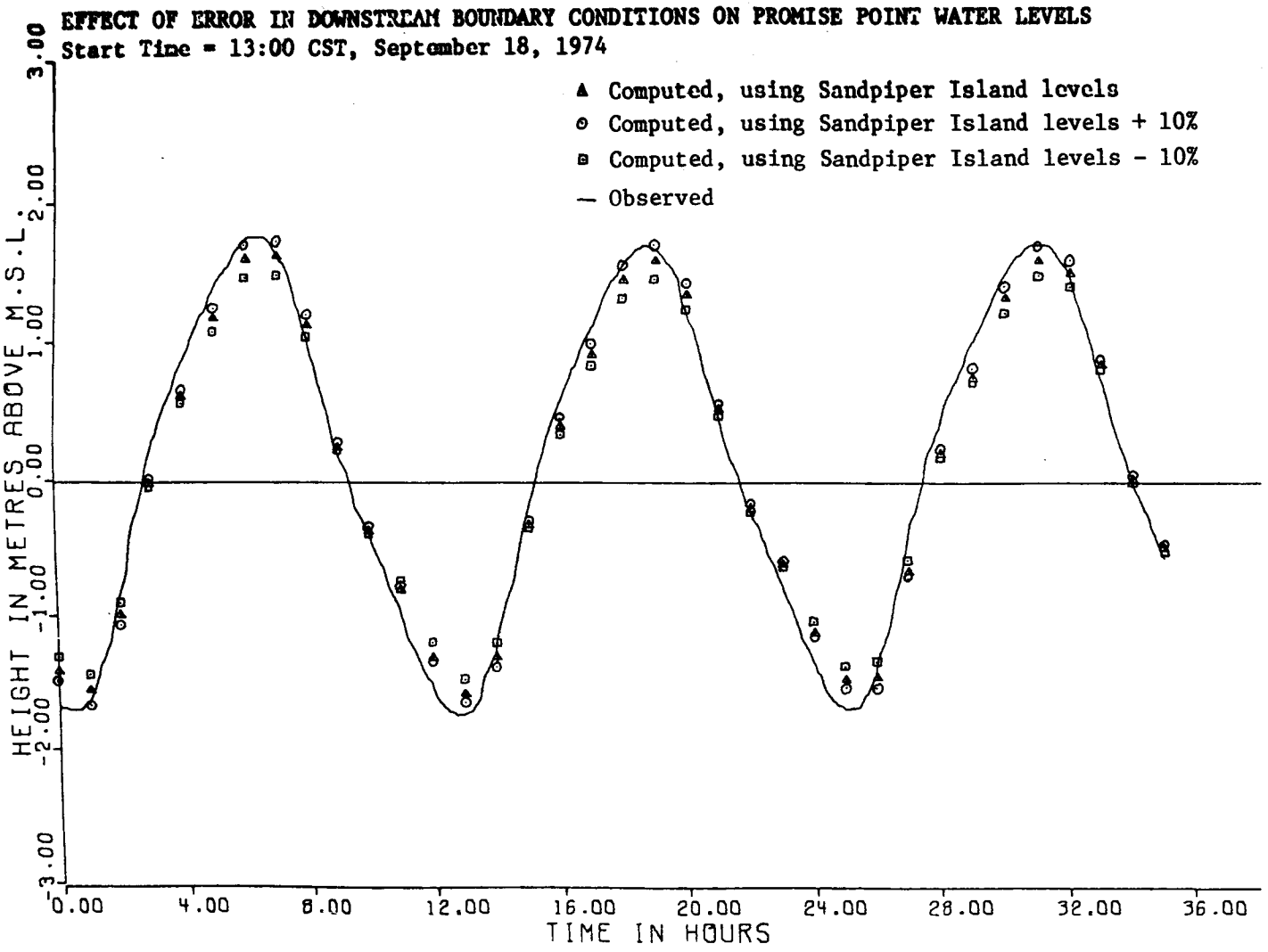

FIGURE 28: Effect of 10 Per Cent Error in the Downstream Boundary Condition upon the Computed Water Levels at Promise Point

phases with the observed phases. To reduce the number of computer runs required, the calibration was carried out for the period from September 17 to September 18, 1974. If a gauge was not recording at that time, tidal predictions for the station were used. The model was run for 48 hours. Only the last 36 hours were considered, the first 12 hours being required to let the model results "settle down". A time step of one hour and a weighting factor of 0.55 were used in the model runs. The model results are relatively sensitive to changes in these parameters. If the time step or weighting factor is changed significantly, the model may require recalibration. Fread [15,17] discusses the effects of variations in these parameters upon model-predicted transients.

Upstream of Cross Bay, the effect of the Baker Lake elevation had to be taken into consideration. The selection of the lake level and friction coefficients was essentailly a trial and error process. A Baker Lake elevation of zero metres and a Manning's n of 0.030 gave the best results. The effects of the Baker Lake elevation upon the model-predicted tide at Baleen and Norton Islands are shown in Figures 29 and 30. The water level in these plots are all referred to the mean tidal level so that the amplitude and shape of the curves could be compared more easily. A Manning's n of 0.030 in the channel upstream of Cross Bay was used in each case.

From Figure 29, we see that changing the elevation at Baker Lake has little effect upon the tidal curve at Baleen Island. At Norton Island, however, significant changes in the tidal curve take place as the level of Baker Lake is increased. Increasing the Baker Lake level from zero to one metre reduces the amplitude, smooths the low tide, and moves the distortions on the falling limb forwards in time. Increasing the Baker Lake level to 2 metres further reduces the amplitude and smooths the whole tidal curve. Overall, the tidal curve at Norton Island that was produced for a Baker Lake elevation of zero was considered to provide the best agreement with the observations.

As a rough check on the validity of this assumption, the mean discharge over 25 hours (approximately 2 M_2 cycles) on September 15 and 16, 1974 was computed from the model-predicted discharges at Big Point (cross-section 15 in Figure 20). Elevations of 0, 1 metre, and 2 metres at

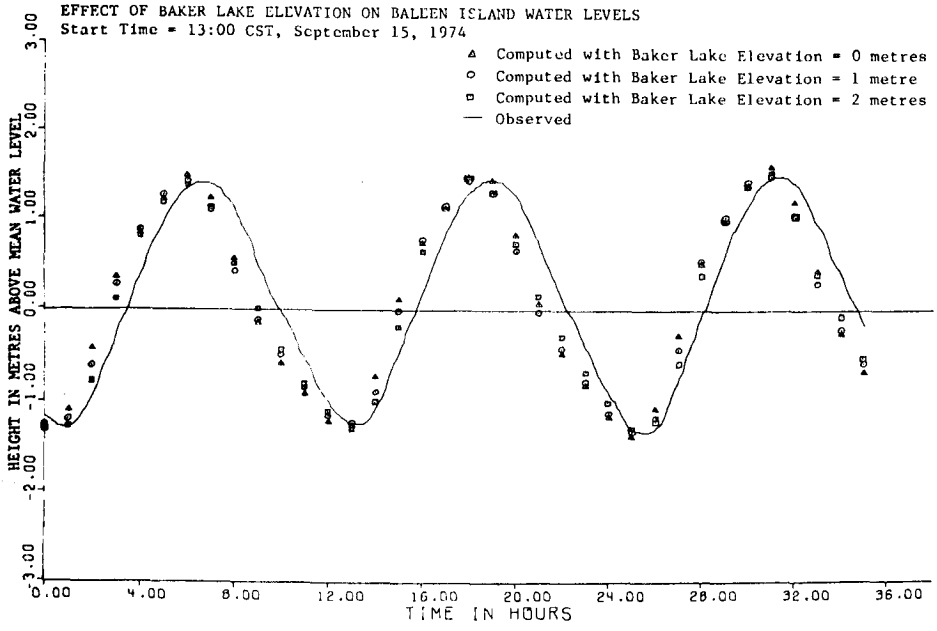

FIGURE 29: Effect of the Baker Lake Stage Upon Computed Water Levels at Baleen Island

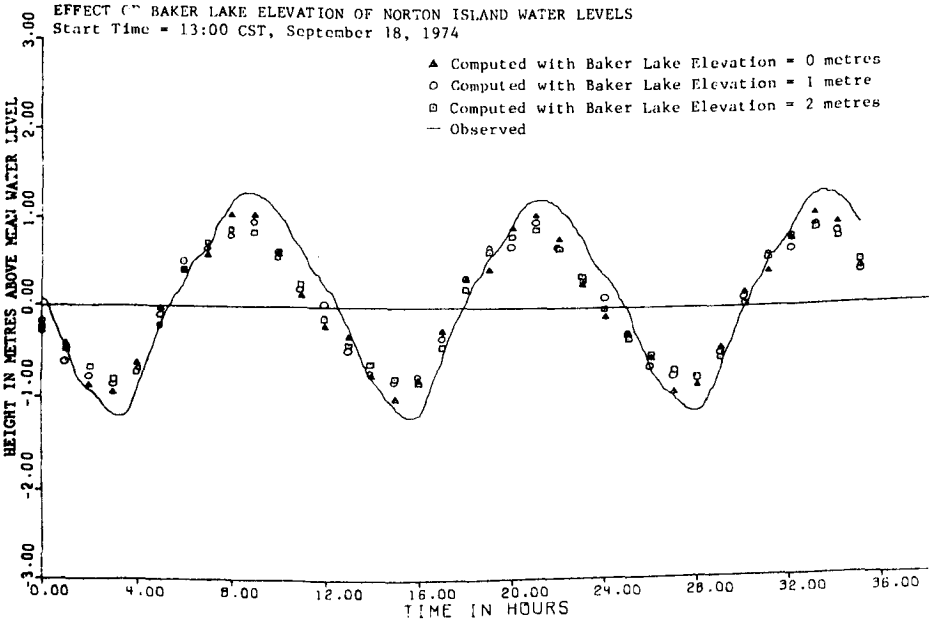

FIGURE 30: Effect of the Baker Lake Stage Upon Computed Water Levels at Norton Island

eastern Baker Lake yielded mean discharges of -260 m^3/sec, 5,950 m^3/sec, and 13,400 m^3/sec, respectively. Obviously the mean discharge resulting from zero elevation upstream, should be zero. The -260 m^3/sec is due to the truncation and discretization of the time series. The mean discharge for the months of August and September, as computed in Chapter 2, is approximately 2,300 m^3/sec. Thus, the elevation at the eastern end of Baker Lake is probably about 0.4 metres. Insofar as tidal propagation over the whole inlet is concerned, the elevation at Baker Lake may be considered to be zero, since a mean slope of 0.4 metres in 200 kilometres is relatively small.

Where possible, the model was tested for a spring tide and a neap tide at each of the calibration stations. Because of the lack of overlap in the records at these stations, five such runs were required. The calibration results are plotted in Figures 31 through 42. The observed tide was plotted from 5-minute water levels. The model values are plotted for 1-hour intervals.

Upstream of Barbour Bay, the tidal curves become noticeably distorted. The rising limb at each of the stations is steeper than the falling limb. This phenomenon is a nonlinear process caused by shallow water effects. It can be seen that the numerical model is successful in reproducing the shapes of the curves. Nonlinear, shallow water effects will be discussed in section 5.5.

Overall, the agreement between model-predicted and observed amplitudes and phases is generally good. The predicted tide tends to lead the observed tide, but usually by less than one-half hour. At Primrose Island (Figure 39 and 40), however, the predicted tide leads the observed tide by approximately one hour in phase, and the amplitudes of the predicted tide are roughly 70 per cent of that of the observed tide. At Baleen Island, Figure 41 shows that the predicted and observed tidal amplitudes match to within 10 per cent but, again, the predicted tide leads the observed tide by an hour. Finally, at Norton Island, as shown by Figure 42, the model underestimates the observed tide by 20 per cent, but the phase difference between the observed and predicted tides is negligible.

It seems rather unlikely that the model would predict the phase accurately over the first 110 kilometres; then, in the next 35 kilometres,

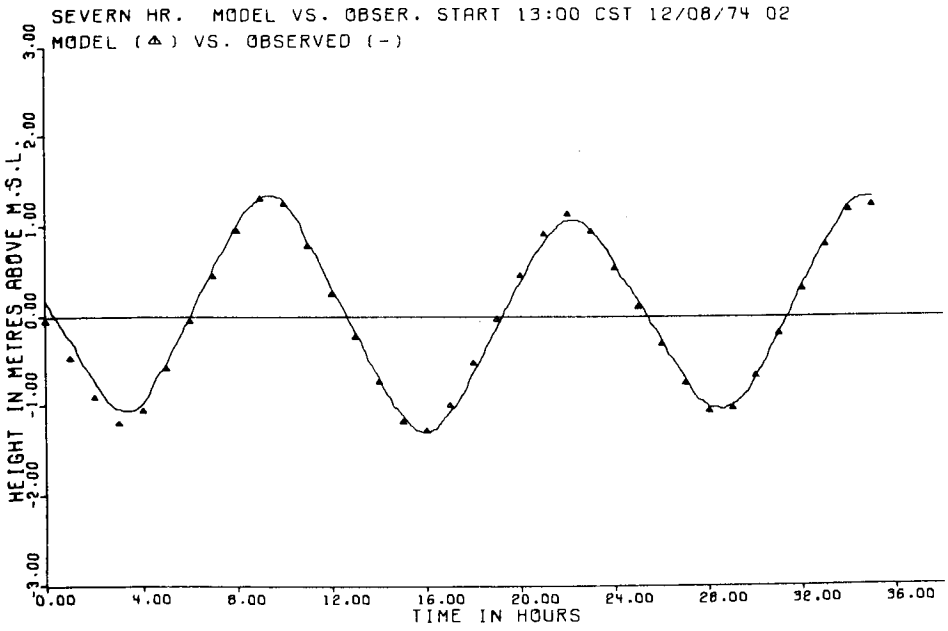

FIGURE 31: Computed and Observed Water Levels at Severn Harbour - Neap Tide

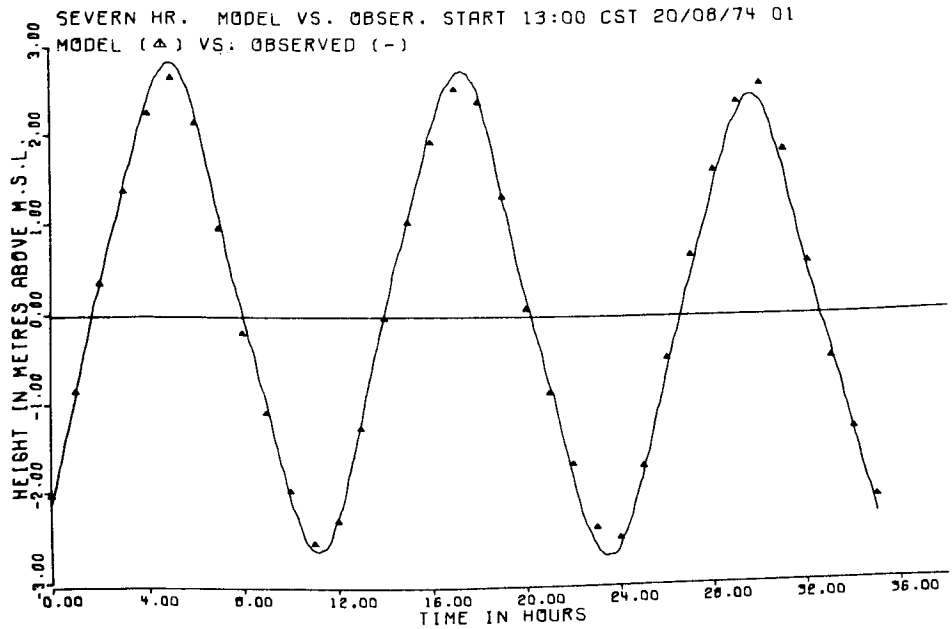

FIGURE 32: Computed and Observed Water Levels at Severn Harbour - Spring Tide

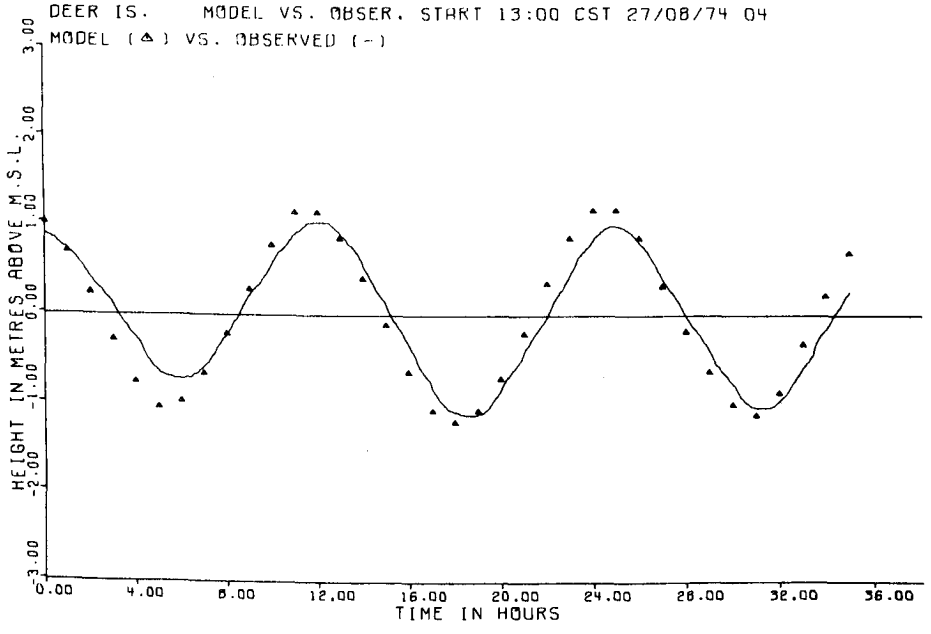

FIGURE 33: Computed and Observed Water Levels at Deer Island - Neap Tide

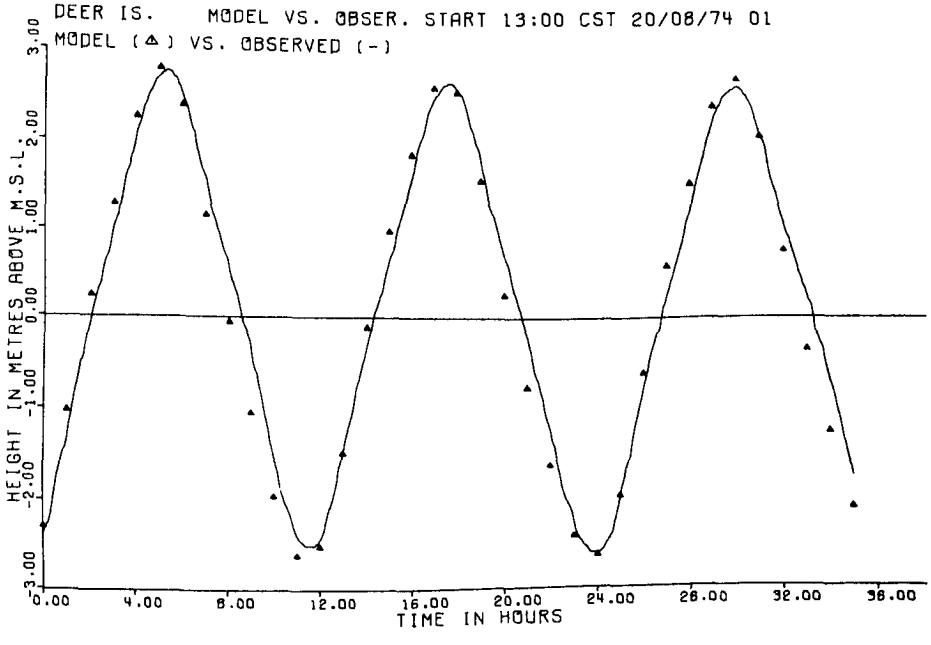

FIGURE 34: Computed and Observed Water Levels at Deer Island - Spring Tide

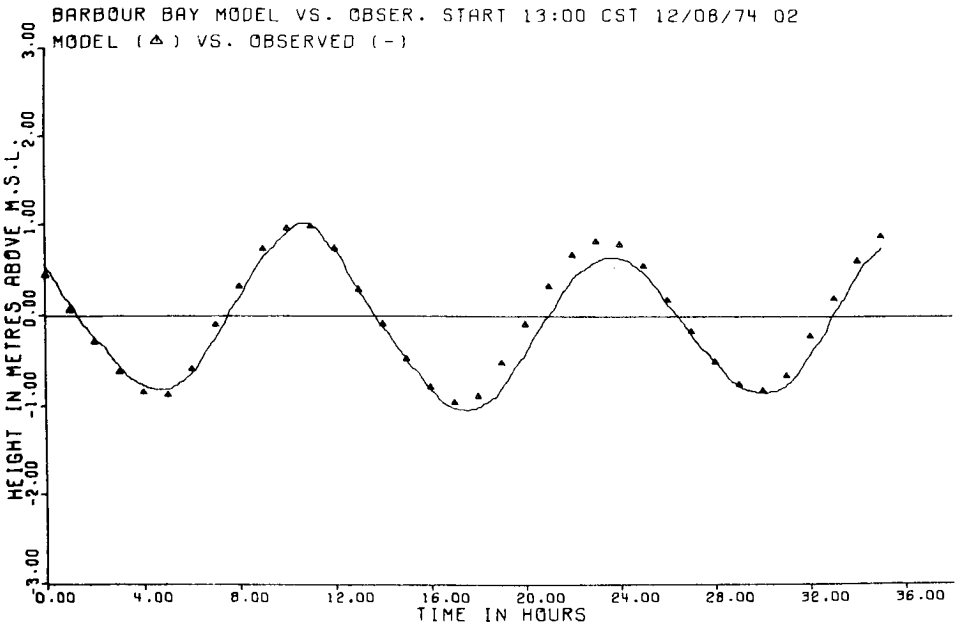

FIGURE 35: Computed and Observed Water Levels at Barbour Bay - Neap Tide

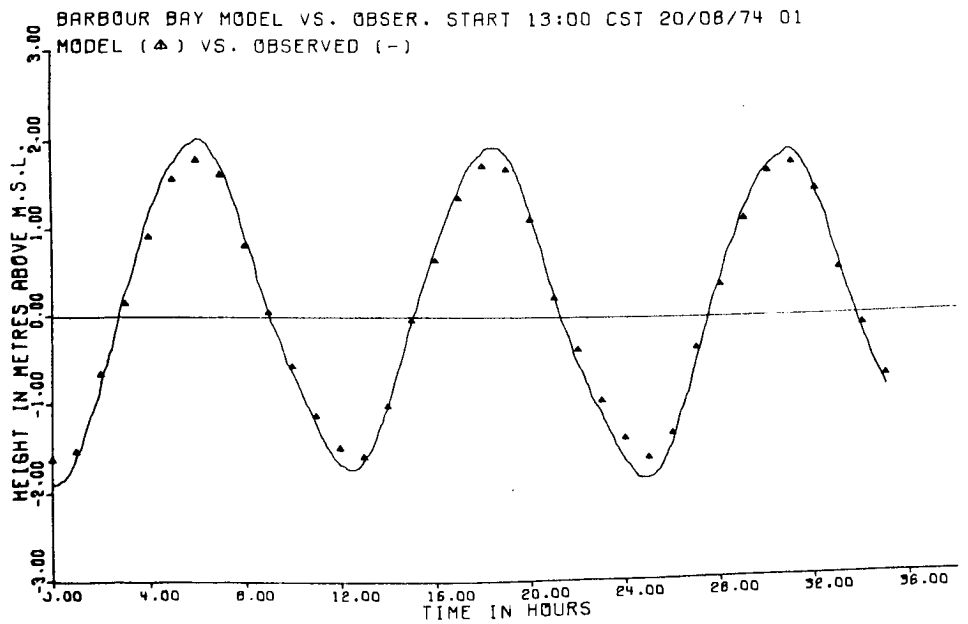

FIGURE 36: Computed and Observed Water Levels at Barbour Bay - Spring Tide

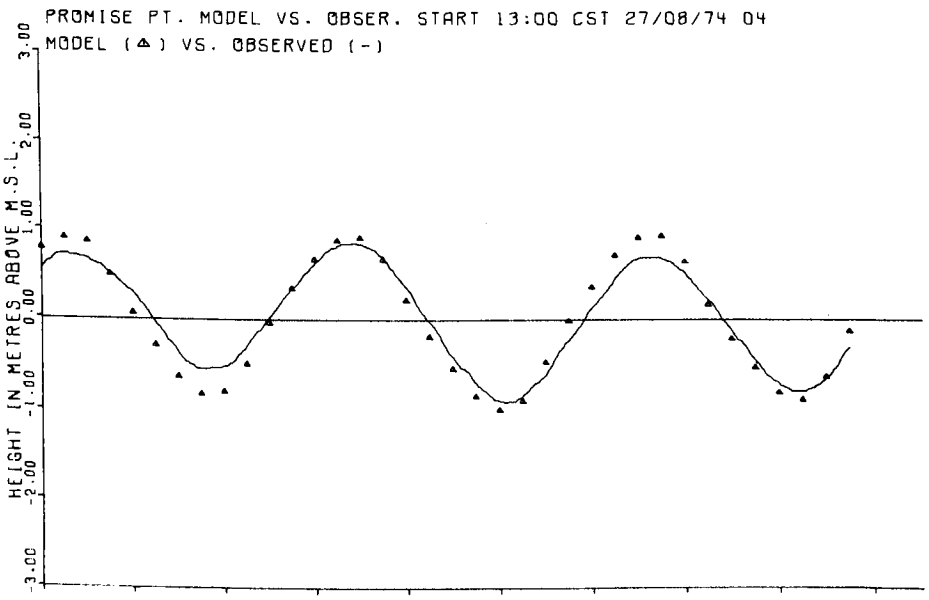

FIGURE 37: Computed and Observed Water Levels at Promise Point - Neap Tide

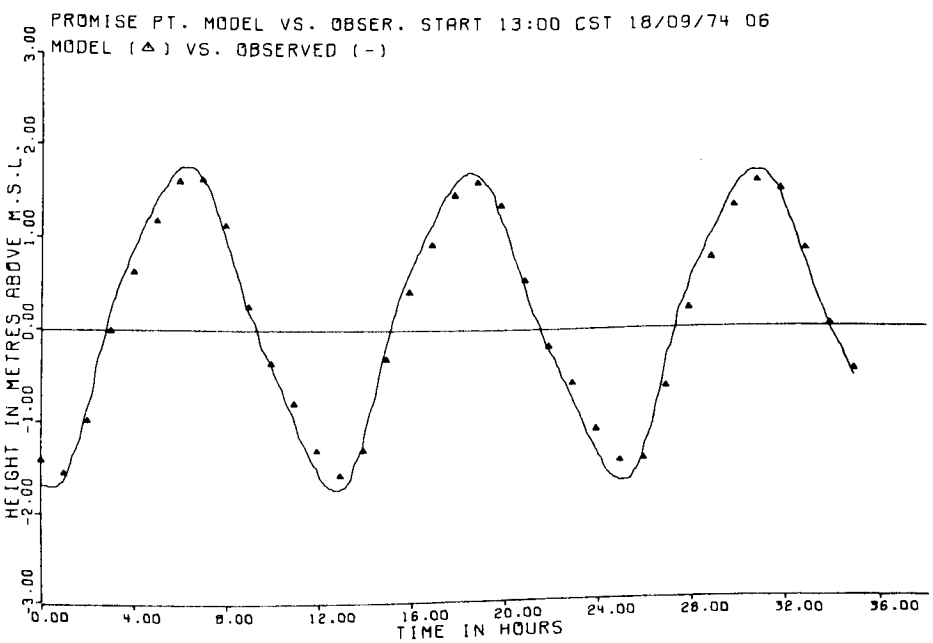

FIGURE 38: Computed and Observed Water Levels at Promise Point - Spring Tide

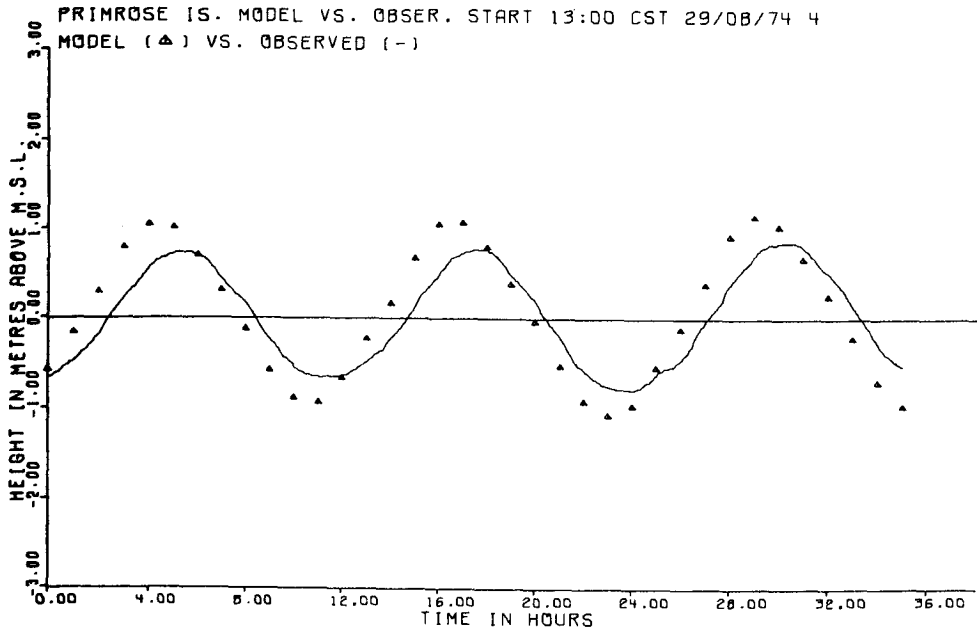

FIGURE 39: Computed and Observed Water Levels at Primrose Island - Neap Tide

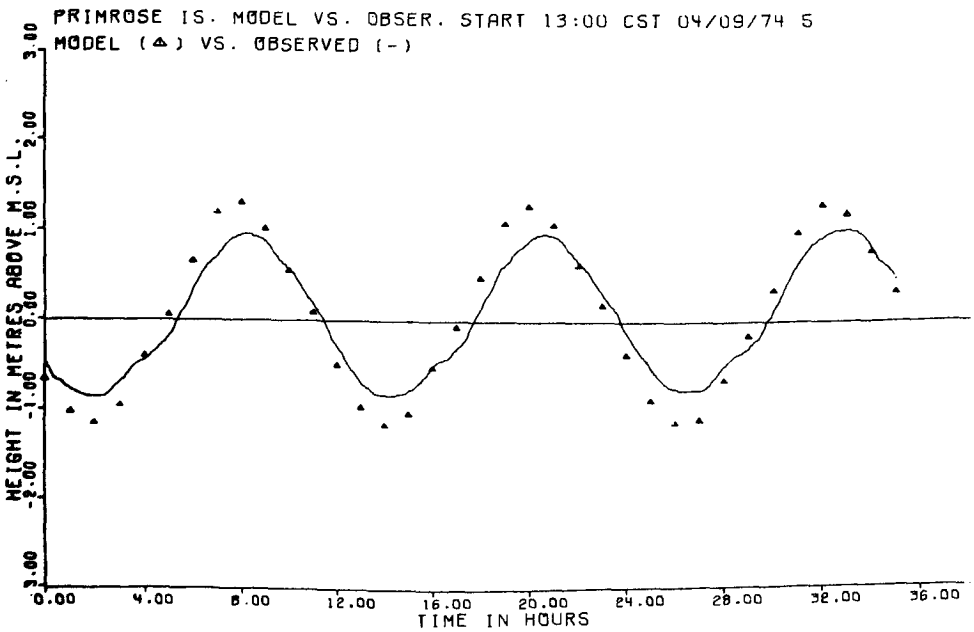

FIGURE 40: Computed and Observed Water Levels at Primrose Island - Spring Tide

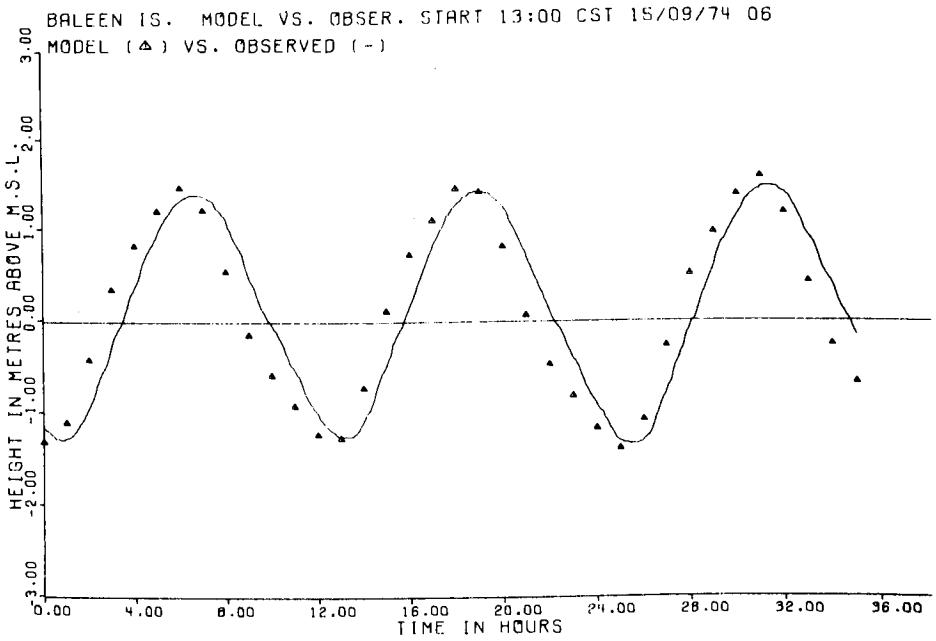

FIGURE 41: Computed and Observed Tide at Baleen Island

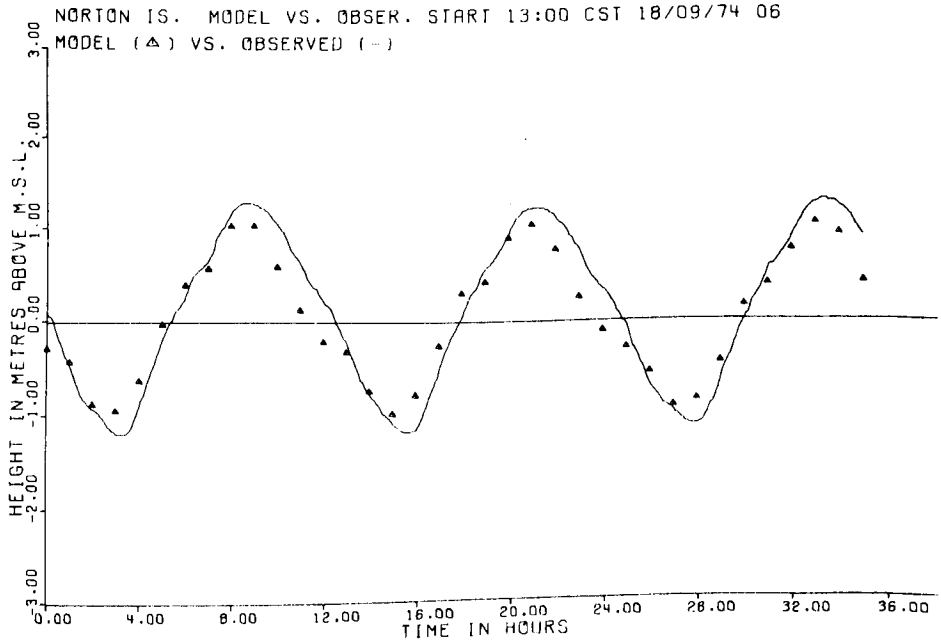

FIGURE 42: Computed and Observed Tide at Norton Island

develop an error of one hour in phase which persists over 45 kilometres; then lose the error in the next 25 kilometres. Phase errors in the model tend to be systematic, i.e. one would expect some sort of progressive error in phase increasing up the inlet if the model were inaccurate. When the celerities calculated in Chapter 3 are considered, the suspicion that something is amiss in the time records of these gauges is strengthened.

It should be noted that field workers checked the gauge-recorded times infrequently (often only two or three times over the period of record), and, when checks were made, a conversion from Central Standard Time to Greenwich Mean Time was required. Later, when the analogue gauge record was digitized and corrected for time, all the times were converted from Greenwich Mean Time to Central Standard Time. Under these circumstances, it is not difficult to gain or lose one hour in time.

A comparison of the original analogue record, taken from the Primrose Island gauge with the staff readings taken as a check, revealed that the gauge was underestimating the tidal range by roughly 20 per cent. In addition, it was discovered that the procedures used to correct the gauge record, based on the staff readings, correct only the mean water level; they do not correct the tidal range. An examination of the analogue traces taken from the other gauges did not reveal any further discrepancies. The other gauges appeared to reproduce the tidal ranges to within 5 per cent.

As described in section 5.1, the flow within the Bowell Islands network has been assumed negligible. This assumption cannot be verified without field measurements. From Figure 25, however, it would appear that the computed tide at Norton Island is sensitive to changes in the flow within the north and center channels of the Bowell Islands. Thus, it is likely that the neglect of the Bowell Islands network will incur errors in the model-predicted tides at Norton Island.

In addition, the dynamics of the tidal flow at the entrance to Baker Lake appear to be quite complex. It is possible that three modes of tidal motion exist there:

1) partial reflection (positive) from Chesterfield Narrows and from the Christopher Islands located 2 kilometres offshore in Baker Lake;

2) partial reflection (negative) from Baker Lake itself; and

3) partial transmission of the tidal wave through the Chesterfield Narrows and Baker Lake.

Unfortunately, only one of the above conditions could be selected as a boundary condition. Assuming full reflection from Baker Lake proved to give better results than assuming full reflection from Chesterfield Narrows and the Christopher Islands, or no reflection at all. Nonetheless, an incomplete representation of the flow regime at the upstream boundary undoubtedly has a deleterious effect upon the results at Norton Island.

Thus, it is the opinion of the author that the observed levels at Primrose and Baleen Islands are in error by one hour in time, that the Primrose Island gauge underestimated the tidal range by roughly 20 per cent, and that the model underestimated the tidal range at Norton Island because of the complexity of the flow regime near Baker Lake.

Because of the considerations described above, no attempt was made to reduce the discrepancy between the modelled and observed amplitude at Primrose and Norton Islands. No attempt would be made to reduce phase discrepancies in any event.

Some of the discrepancies between the observed and computed tides in the estuary are partially attributable to the one-dimensional representation of two- and three-dimensional flow regimes. For example, tidal motion in Cross Bay is undoubtedly two-dimensional, but insufficient soundings are available to permit the application of a two-dimensional model to the bay.

The Manning's friction coefficients chosen for the various portions of Chesterfield Inlet are shown in Figure 20. At the mouth, because of the great depth (50 metres), the friction coefficient is 0.020, which is quite low. Upstream of Severn Harbour, the coefficient increases to 0.030. From Centre Island to Barbour Bay, the coefficient becomes 0.070. This value is much higher than what would normally be expected from a natural open channel of this size.

If we examine the section geometry in the vicinity of Ekatuvik Point, we see that the channel becomes very constricted. The flow streamlines contract and then expand suddenly. This venturi effect results in a sudden energy conversion from potential to kinetic and back to potential

energy again. In the conversion from kinetic to potential energy, losses occur in the form of intense turbulence; in this case, tide rips. It is well known [11] that these eddy losses across a constriction are quadratic in velocity. Interestingly enough, the friction term included in the momentum equation is also quadratic in velocity. Hence, the friction term becomes a lumped parameter under these circumstances, since it reflects the turbulent losses due to the flow separation at a constriction as well as losses due to the frictional effects of the sides and bottom of the channel. The Manning's friction coefficient, n, which is essentially a weighting factor, then becomes unusually large. No attempt was made to separate the effects due to the constriction and the frictional losses.

Upstream of Barbour Bay, n drops to 0.050. This corresponds to the less frequent occurrence of tide rips in the stretch from Barbour Bay to Promise Point.

In the vicinity of Primrose Island, the value of n used was 0.080. Strong tide rips are prevalent in this region so that a factor of at least 0.070 is suggested, such as is the case near Ekatuvik Point. Because of the extreme channel roughness near Primrose and Big Islands, however, it was decided to use a friction factor of 0.080 for this area. Cubical blocks of granite, at least 2 metres thick, line portions of the shoreline in this stretch of channel. It was assumed that, if the bottom of the channel were at all similar to the sides, frictional effects would be pronounced. Even with such a high friction factor, the model predicts tidal amplitudes 30 per cent greater than those recorded at Primrose Island. If we consider that the recorded amplitudes are 20 per cent lower than the actual tide, as discussed previously, then the model would predict the actual amplitudes at Primrose Island to within 10 per cent.

From Primrose Island to Baker Lake, a friction factor of 0.030 was used. A lower friction factor in that region corresponds to the lack of tide rips there.

In areas for which no calibration data were available, such as in Barbour Bay, Cross Bay, and the Quoich River, a friction coefficient of 0.030 was assumed. The effects of a 10 per cent error in Manning's n, everywhere in the inlet, upon the model-predicted tides at Promise Point and Norton Island are shown in Figures 43 and 44.

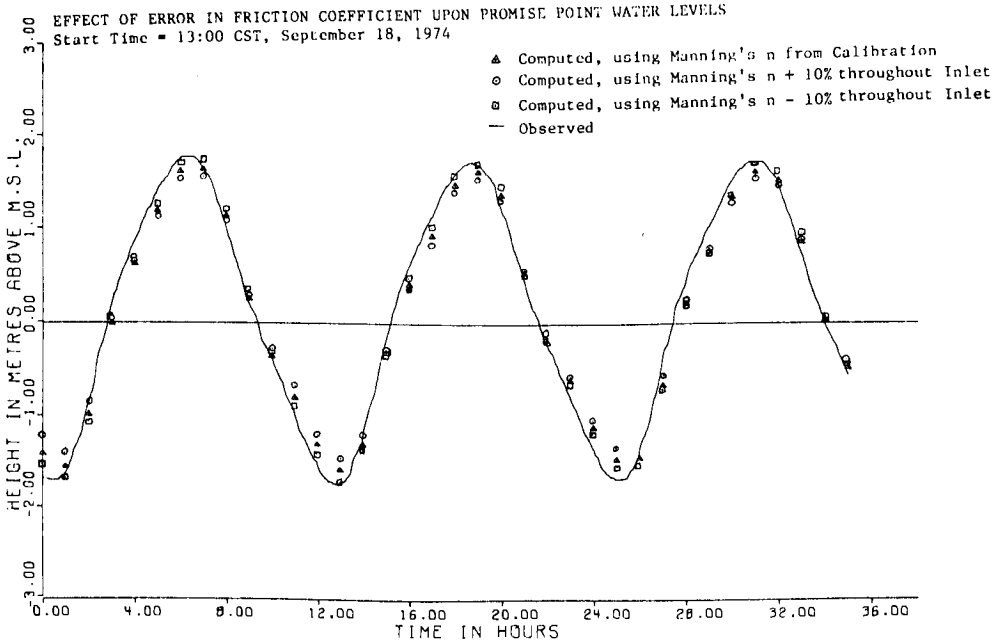

FIGURE 43: Effect of 10 Per Cent Change in Friction Coefficient on Computed Water Levels at Promise Point

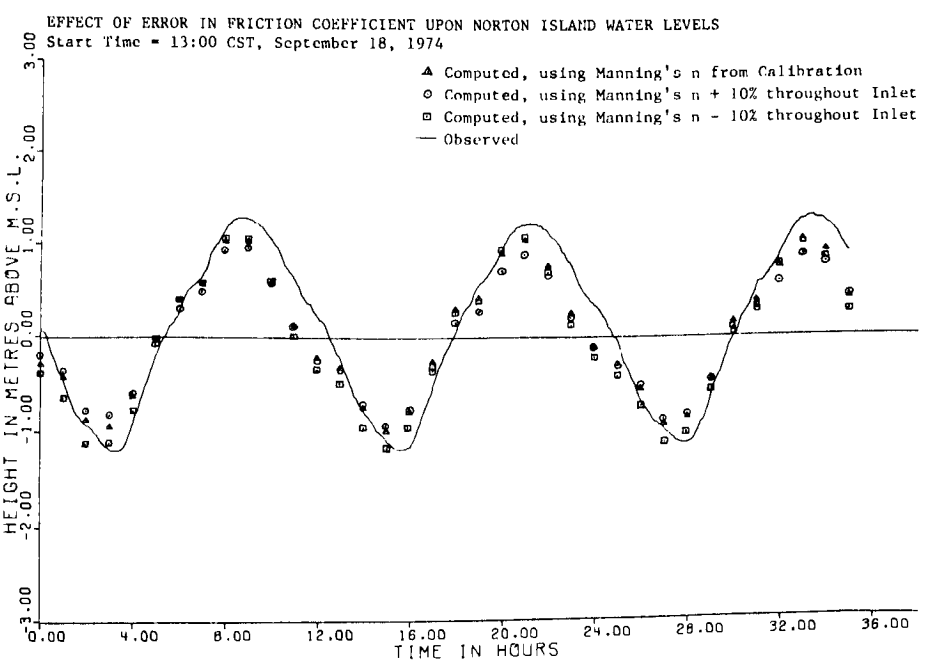

FIGURE 44: Effect of 10 Per Cent Change in Friction Coefficient on Computed Water Levels at Norton Island

5.4 MODEL-PREDICTED TIDES AND CURRENTS IN CHESTERFIELD INLET

As shown in Figure 45, the magnitudes of the model-predicted tides and currents within the inlet vary considerably. These plots were generated from model predictions for the 14th to the 19th of September. The reduction in tidal amplitudes across the channel constrictions at Ekatuvik Point, Promise Point, Big Point, and Chesterfield Narrows shows up in the current record as peaks. The large storage embayment at Cross Bay causes low velocity amplitudes there.

The time of high tide and the variation of spring and neap currents throughout the inlet, as computed by the model, are shown in Figure 46. The times of high tide were computed by using a 12.42 hour period cosine curve to interpolate between the hourly time steps. The velocity amplitudes which are plotted are cross-sectionally averaged. At the present time, insufficient current velocity data are available to verify the model-predicted currents.

If velocity measurements are to be taken in order to verify the model computations, they should be concentrated in the major channel constrictions. At these locations, the current velocities are a maximum, and the lateral variation in velocity should be minimized since the current direction tends to be parallel to the channel direction. It would still be necessary to obtain the vertical current profile, however, since salinity intrusion may negate the assumption of a homogeneous density structure and create a highly irregular vertical velocity distribution. Since the vertical velocity structure would vary over an M_2 tidal cycle, profiles should be measured over a period of at least 13 hours. If current phase information is desired, in-situ current measurements would have to be taken over a period of at least 29 days.

From the plots of the tidal ranges, we see that there is a pronounced difference in the ranges of spring and neap tides from Sandpiper Island (km 0) to Barbour Bay (km 80). In this portion of the inlet, the predicted neap ranges are less than half of those for the spring ranges. The magnitude of the spring tide drops sharply across Ekatuvik Point (km 75). This change is reflected in the predicted velocity plot where the average speeds of the maximum flood currents become 1.8 and 1.2 m/sec at spring and neap tides respectively. In the last 20 kilometres before Baker Lake

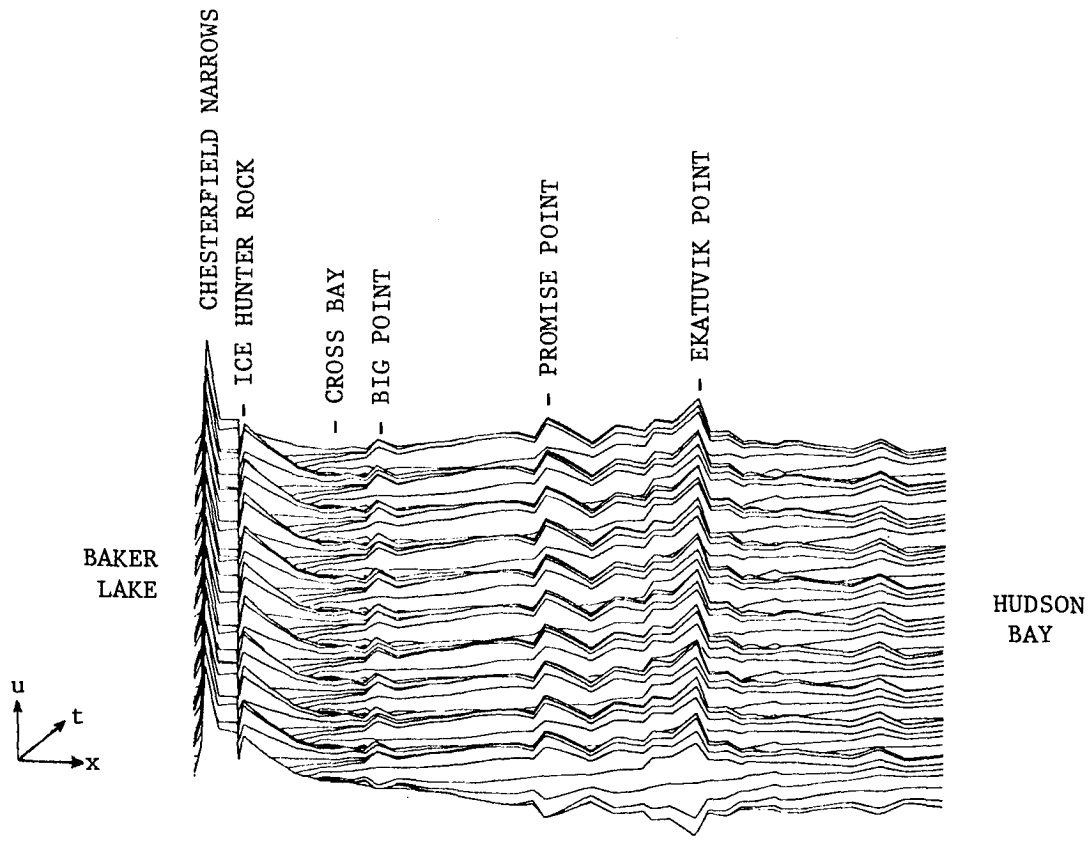

(a) Predicted Currents

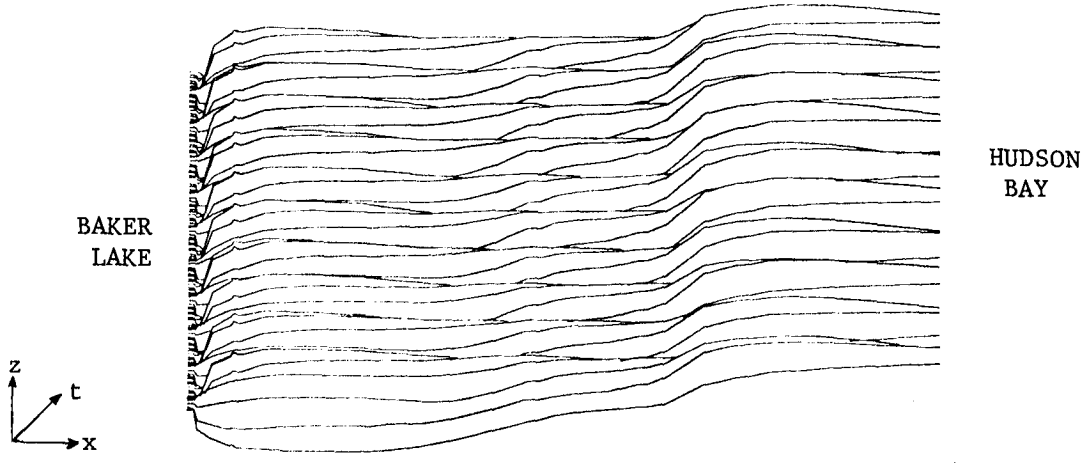

(b) Predicted Tides

FIGURE 45: Model-Predicted Tides and Currents in Chesterfield Inlet

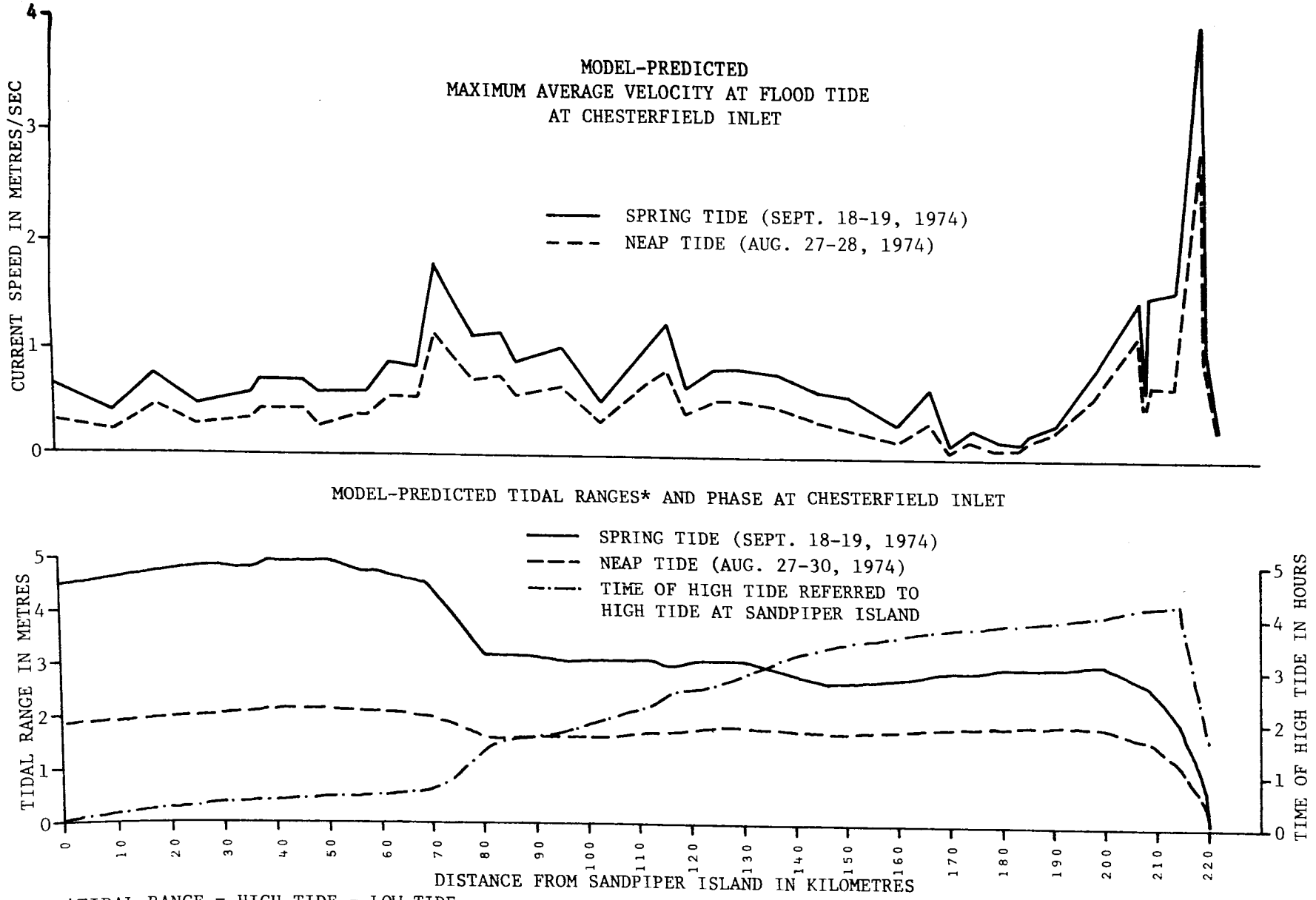

FIGURE 46: Model-Predicted Spring and Neap Tides and Currents in Chesterfield Inlet

(km 222), the model-predicted tidal range drops from 3.1 and 2.9 metres to zero during spring and neap tides. The predicted current amplitudes, on the other hand, increase from 0.3 m/sec to 4.0 m/sec in the stretch of channel from Cross Bay (km 180) to Baker Lake during spring tide. The sharp drop in the predicted velocity at km 208 corresponds to a channel expansion near Ice Hunter Rock. The times of high water were computed from the model-predicted spring tide of September 18th and 19th, 1974. The variation in the times of high water throughout the inlet tend to reflect the changes in tidal range and current described above. The upstream boundary condition has a pronounced effect upon the phase of the predicted tide in the immediate vicinity. The sudden decrease in the predicted time of high water is probably due to the negative reflection created by fixing the Baker Lake water level.

From these plots, then, Chesterfield Inlet may be divided into four distinct reaches, each with different tidal regimes:

1) Sandpiper Island to Ranger Seal Bay (km 0 to km 70);

2) Ranger Seal Bay to Barbour Bay (km 70 to km 80);

3) Barbour Bay to the Bowell Islands (km 80 to km 186); and

4) the Bowell Islands (km 186 to km 222).

From Sandpiper Island to Ranger Seal Bay, the channel is relatively deep (approximately 50 metres) and the tidal amplitudes, though quite large, are strongly modulated through spring and neap tides. The maximum tidal amplitudes in the inlet occur near Deer Island (km 50).

At Ekatuvik Point, which lies between Ranger Seal Bay and Barbour Bay, there is a reduction in the channel width from 7,700 metres to 3,800 metres. The high currents moving through this section reduce the spring tidal range from 5.0 metres to 3.2 metres through local turbulence (tide rips). Since the depth is approximately 35 metres in the stretch from Barbour Bay to the Bowell Islands, the spring tidal range remains relatively constant at approximately 3.0 metres, while the neap range remains at approximately 1.7 metres. A minimum of 2.5 metres at spring tide in this reach occurs near Primrose Island (km 147). Peaks in the velocity plot occur at constrictions such as Promise Point (km 113) and Big Point (km 168).

The flow regime in the Bowell Islands appears to be extremely

complex. Much more field data needs to be collected in this region before one could be assured of reliable model results. As we see from Figure 46, remarkable changes occur in the tide and current over very short distances. The model results indicate that the constricted passage in the Bowell Islands, particularly the shallow sill at Chesterfield Narrows, and reflection due to Baker Lake cause a sharp decrease in tidal amplitudes and increase the current speeds sharply.

To study the effect of the sill depth at Chesterfield Narrows on the water levels and currents there, a model run was made in which the channel depth from Baker Lake to Norton Island was increased to 16.0 metres, a change in depth of 10 metres. As shown in Figure 47, the model results indicate that this increase in the channel depth decreases the maximum currents by 50 per cent and the tidal range by 75 per cent during spring tide.

In order to determine the relative magnitudes of the tidal transport and the transport due to the mean discharge in Chesterfield Inlet, the tidal prism, or total volume of water moved by tidal forcing in one M_2 cycle, was computed at three locations: Big Point, Promise Point, and Severn Harbour. At Big Point, the tidal prism was computed to be approximately $7.71 \times 10^8 m^3$ from September 14th to September 15th, 1974. The volume of water moved by the mean discharge during the same period was approximately $1.02 \times 10^8 m^3$. Hence, from the model results, the mean discharge moved approximately 13 per cent as much water as the tide at Big Point for the period considered. At Promise Point and Severn Harbour, this figure is 6 per cent and 3 per cent, respectively. Thus, downstream of Big Point, the transport due to the mean discharge is small compared to that due to the tidal discharge. The relative importance of the mean discharge decreases with increasing distance from Baker Lake down the inlet.

5.5 CHESTERFIELD INLET AS A NONLINEAR SYSTEM

As the tide progresses up the channel, its propagation is influenced by changing channel depth and cross-sectional width. Distortion of the tidal wave takes place in shallow waters because the trough is retarded more than the crest.

This phenomenon may be described by the shallow water constituents which are generated by effects described by the nonlinear terms in

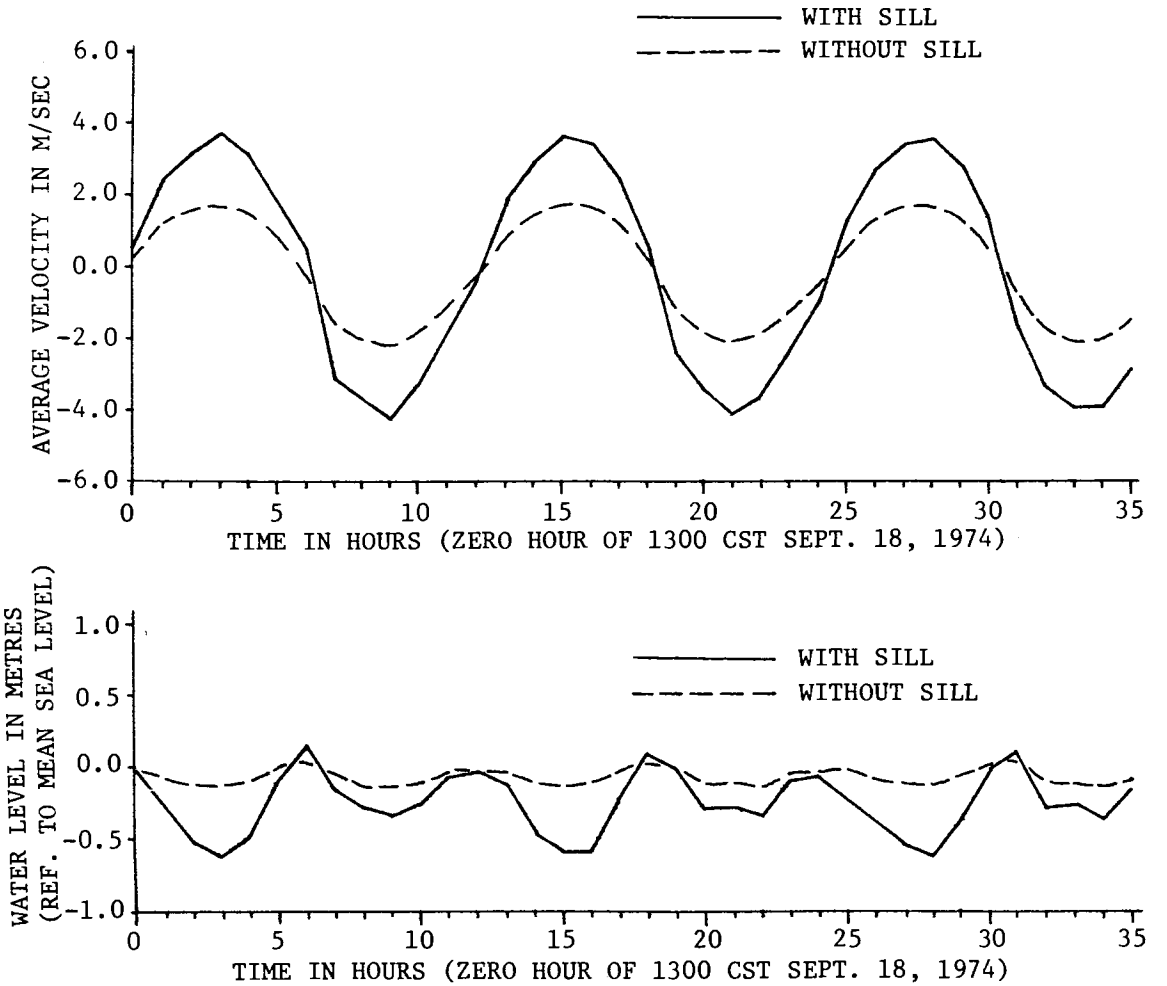

FIGURE 47: Effect of Deepening the Channel at Chesterfield Narrows upon the Computed Tides and Currents

the equations of motion. The continuity and momentum equations as stated in Chapter 4 are:

$$(b + b_s)\frac{\partial z}{\partial t} + \frac{\partial Q}{\partial x} - q = 0 \tag{4.1}$$

$$\frac{\partial Q}{\partial t} + u\frac{\partial Q}{\partial x} + Q\frac{\partial u}{\partial x} + gA\frac{\partial z}{\partial x} + \frac{gkQ|Q|}{Ah^*} = 0 \tag{4.2}$$

since: $Q = Au = bh^*u = b(h+z)u$

$$\frac{\partial b}{\partial t} = 0$$

$$\frac{\partial h}{\partial t} = 0$$

$$\frac{\partial h^*}{\partial t} = \frac{\partial z}{\partial t}$$

then, after some manipulation and use of the chain rule, equations (4.1) and (4.2) may be written:

$$(b + b_s)\frac{\partial z}{\partial t} + ub\frac{\partial h}{\partial x} + ub\frac{\partial z}{\partial x} + uh\frac{\partial b}{\partial x} + uz\frac{\partial b}{\partial x} + bh\frac{\partial u}{\partial x} + bz\frac{\partial u}{\partial x} - q = 0 \tag{5.1}$$

and

$$\frac{\partial u}{\partial t} + \frac{u}{h^*}\frac{\partial z}{\partial t} + 2u\frac{\partial u}{\partial x} + \frac{u^2}{b}\frac{\partial b}{\partial x} + \frac{u^2}{h^*}\frac{\partial h}{\partial x} + \frac{u^2}{h^*}\frac{\partial z}{\partial x} + g\frac{\partial z}{\partial x} + \frac{gku|u|}{h^*} = 0 \tag{5.2}$$

respectively.

The nonlinear terms in u and z are $ub\frac{\partial z}{\partial x}$, $uz\frac{\partial b}{\partial x}$, and $bz\frac{\partial u}{\partial x}$ from the continuity equation; and $\frac{u}{h^*}\frac{\partial z}{\partial t}$, $2u\frac{\partial u}{\partial x}$, $\frac{u^2}{b}\frac{\partial b}{\partial x}$, $\frac{u^2}{h^*}\frac{\partial h}{\partial x}$, $\frac{u^2}{h^*}\frac{\partial z}{\partial x}$, and $\frac{gku|u|}{h^*}$ from the momentum equation. These nonlinear terms can be used to describe the generation of shallow water tidal constituents.

If we consider the effect of one of the astronomical constituents, the contribution from this constituent to a one-dimensional current or the water level will be of the form:

$$\zeta_i = A_i \cos(\sigma_i t - \phi_i) \tag{5.3}$$

where: ζ_i = the contribution to the water level or rectilinear current from the i^{th} constituent;

A_i = the amplitude of the i^{th} constituent;

σ_i = the frequency of the i^{th} constituent; and

ϕ_i = the phase of the i^{th} constituent.

The quadratic terms, such as $2u \frac{\partial u}{\partial x}$, when applied to equation (5.3), will result in terms of the form:

$$\zeta_{ii} = K_1 \cos^2 (\sigma_i t - \phi_i) \tag{5.4}$$

where both u and z are functions of a single constituent, i, and K_1 is a proportionality constant.

Equation (5.4), through a trigonometric identity may be reduced to:

$$\zeta_{ii} = \frac{K_1}{2} (1 + \cos (2\sigma_i t - 2\phi_i)) \tag{5.5}$$

Thus, through the quadratic terms derived from the $\partial Q/\partial x$, $\partial Q/\partial t$, and the advection terms, higher order harmonics are generated. If the original constituent was the S_2 with a frequency of two cycles per day, then the process described above will result in the creation of the S_4 constituent with a frequency of four cycles per day.

If the effect of a second constituent, j, is considered, such that:

$$\zeta_j = A_j \cos (\sigma_j t - \phi_j) \tag{5.6}$$

then the quadratic terms will result in terms of the form:

$$\zeta_{ij} = K_2 \cos (\sigma_i t - \phi_i) \cos (\sigma_j t - \phi_j) \tag{5.7}$$

where: K_2 is constant of proportionality.

Using another trigonometric identity, equation (5.7) becomes:

$$\zeta_{ij} = \frac{K_2}{2} (\cos [(\sigma_i - \sigma_j)t - (\phi_i - \phi_j)] + \cos [(\sigma_i + \sigma_j)t - (\phi_i + \phi_j)]) \tag{5.8}$$

Hence, two new constituents are created with frequencies equal to the sum and difference of the two original constituents. If the two original constituents are M_2 and S_2, then the new harmonics generated will be MS_f and MS_4, where MS_f is a constituent with a fortnightly period created from the difference of the frequencies and MS_4 is a quarter diurnal constituent created from the sum of the frequencies.

The friction term will generate several constituents as well. Using Dronkers [13] technique, we may expand $u|u|$ through the use of Tschebyscheff polynomials such that:

$$u|u| \simeq \frac{(A_i + A_j)^2}{\pi} (1.07y + 2.13y^3) \tag{5.9}$$

where: i^{th} and j^{th} constituents are considered, and

$$y = \frac{A_i \cos(\sigma_i t - \phi_i) + A_j \cos(\sigma_j t - \phi_j)}{A_i + A_j} \tag{5.10}$$

Thus the new constituents M_6, S_6, $2MS_6$, $2SM_6$, $2MS_2$, and $2SM_2$ will be created from M_2 and S_2. M_6 and S_6 are sixth diurnal constituents, $2MS_6$ has twice the frequency of the M_2 plus the frequency of the S_2 and $2MS_2$ has twice the frequency of the M_2 minus the frequency of the S_2.

The constituents generated through equations (5.5), (5.8), and (5.10) are not of direct astronomical origin. These shallow-water constituents are classified as being either overtides or compound tides (Dronkers [13]). An overtide has a frequency which is an exact multipe of one of the astronomical constituents; the frequency of a compound tide equals the sum or the difference of the frequencies of two or more astronomical constituents. The most important overtides are those originating from the principle lunar constituent. Thus the major overtides are the M_4, M_6, and M_8 from the M_2. The compound tides originate from combinations of the principal astronomical constituents M_2, S_2, N_2, K_1, and O_1. The compound tides are too numerous to be listed here, but the major ones, such as the MS_4, $2MS_6$, $2SM_6$, MN_4, and $2MN_6$, are derived from the M_2 and S_2 or M_2 and N_2 constituents.

To determine whether the numerical model generated the higher order harmonics in the proper manner, two test cases were run. In the first case, a pure sinusoid with a period of 12 hours and an amplitude of

2.5 metres was used as a forcing function at Sandpiper Island. In the second case, the forcing function was the sum of two sine curves; the first had a period of 12.42 hours and an amplitude of 2.5 metres, and the second had a period of 12 hours and an amplitude of 0.5 metres. The periods 12.42 hours and 12 hours are the periods of the M_2 and S_2 constituents. The results of these two runs are shown in Figures 48, 49, and 50.

Figure 48 is a plot of the input spectra at Sandpiper Island for the two cases, while Figures 49 and 50 are plots of the spectra generated from the model results at Promise Point and Norton Island respectively. A time step of one hour was used for both cases. For the case using the 12-hour sine curve, the model was run for 348 hours (14.5 days). The first 12 hours were not used in computing the power spectrum, so that the spectral analysis was performed on 336 points. In the second case, the model was run for 144 hours (6 days), and the power spectrum was computed from 132 points. Twelve frequency bands were used for both cases.

From Figure 48, it can be seen that the leakage around the semi-diurnal band is greater for the double sinusoid case than for the single sinusoid. This is to be expected since each sinusoid will have leakage about it, and the two sinusoids are separated by 0.42 hours. In addition, a longer time record is available for the single sinusoid case, so that its truncation error is less. If an infinitely long record with continuous sampling were available, line spectra could be obtained as the representation of the downstream boundary condition. In practice, of course, such is not the case. Because of the foregoing considerations, one can expect that the leakage will not be any less at stations located further up the channel.

The output spectra at Promise Point and Norton Island, shown in Figures 49 and 50, indicate that the model is generating the proper frequencies in its predictions. When the single sinusoid is used as the boundary condition, the equivalent of overtides is generated, i.e. multiples of the forcing frequency 0.0833 cycles/hour are generated. Since the forcing frequency is in the semi-diurnal band, spectral peaks occur in the 4th, 6th, 8th, 10th, and 12th diurnal bands. Since 12 hours is the period of the S_2 tide, the new harmonics generated are analogous to the S_4, S_6, S_8, S_{10}, and S_{12} tides.

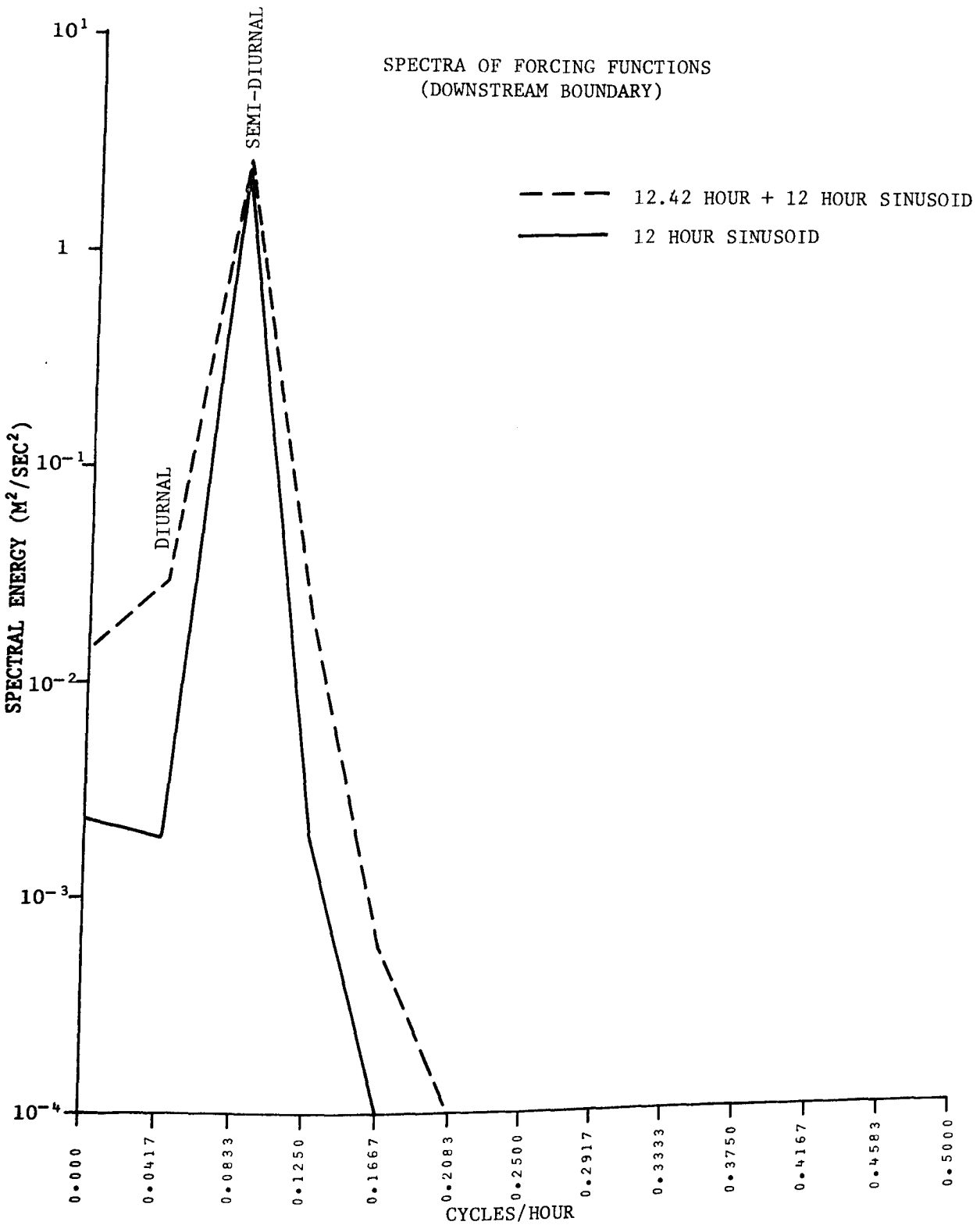

FIGURE 48: Power Spectra of Single and Double Sinusoids

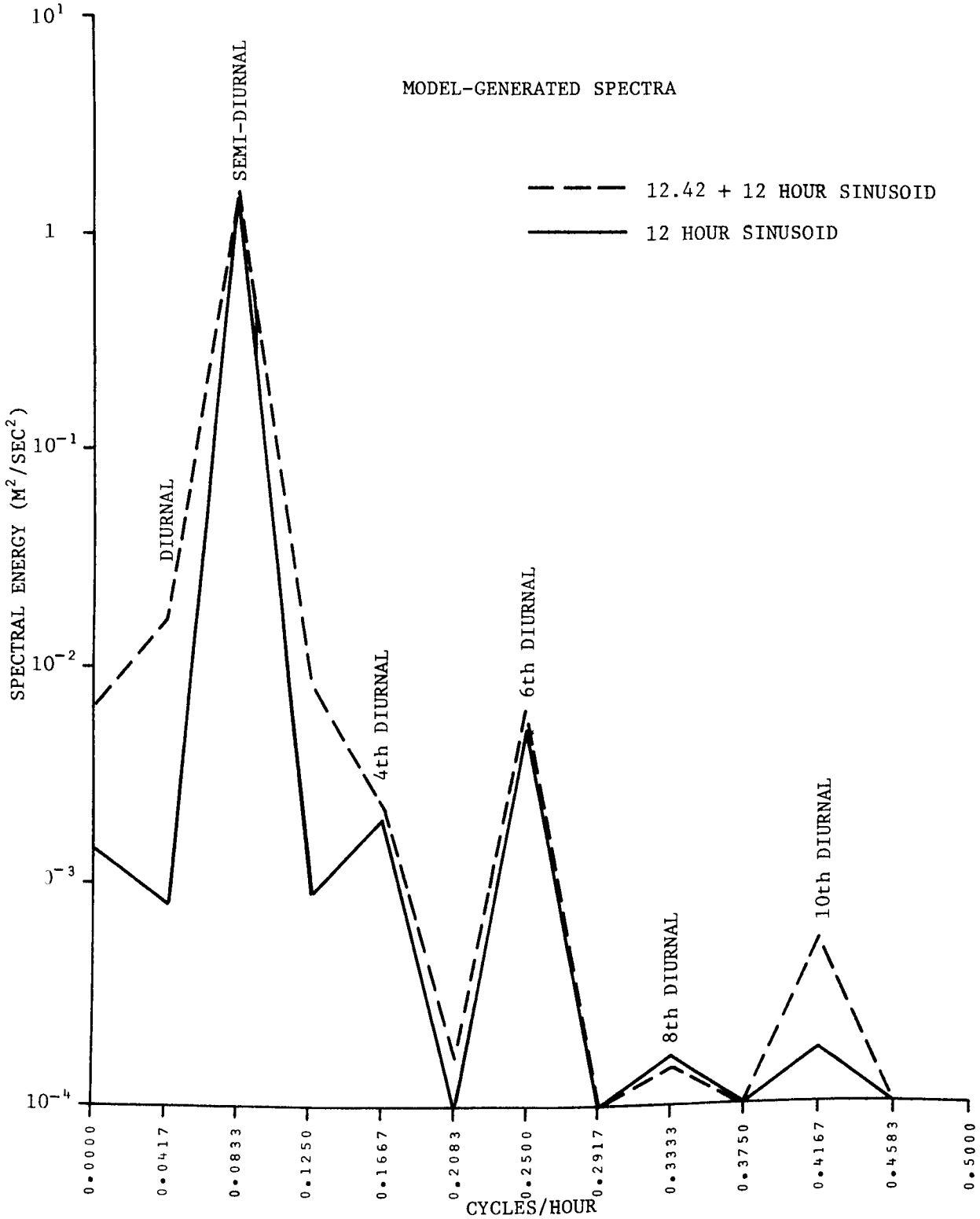

FIGURE 49: Power Spectra of Water Levels Computed at Promise Point with Single and Double Sinusoid Boundary Condition

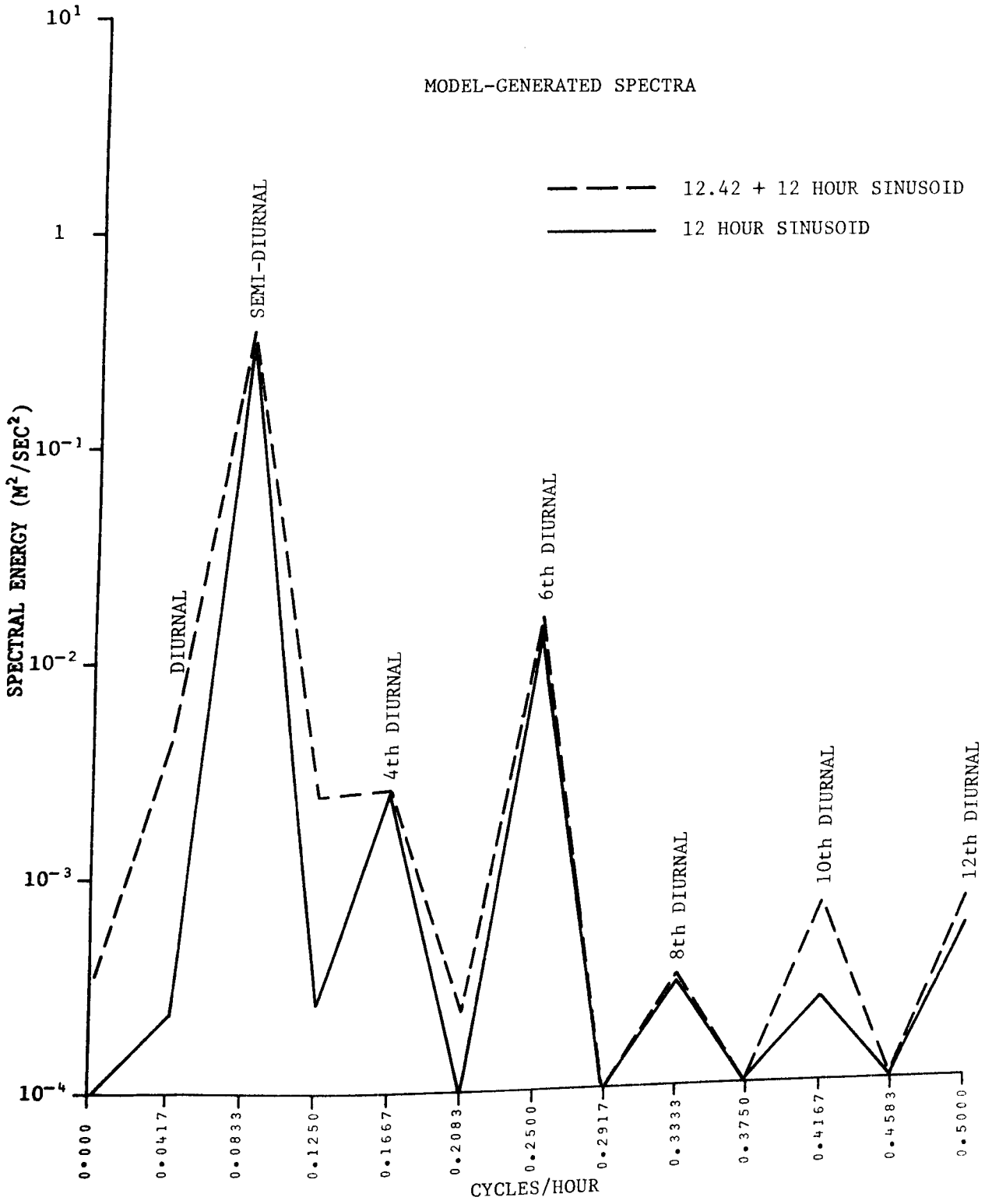

FIGURE 50: Power Spectra of Water Levels Computed at Norton Island with Single and Double Sinusoid Boundary Condition

The double sinusoid can be used to generate the analogue of compound tides as well as overtides. Since 12.42 hours and 12 hours are the periods of the M_2 and S_2 tides, respectively, we can expect overtides of the form M_4, M_6, M_8, S_4, S_6, and S_8 and compound tides such as $2MS_2$, $2SM_2$, MS_4, $2MS_6$, $2SM_6$, $3MS_8$, $3SM_8$, etc. The spectra, generated by the double sinusoid at Promise Point and Norton Island, are similar to those generated by the single sinusoid. However, the spectral energy generated by the double sinusoid in the 10th diurnal band is approximately 3.5 that generated by the single sinusoid in that frequency band. Thus, it may be inferred that the model-generated 10th diurnal harmonics existing as compound tides such as the $4MS_{10}$, $4SM_{10}$, $3SM_{10}$, $3MS_{10}$, etc., are likely to possess more combined energy than the M_{10} and S_{10} overtides. The differences between the two spectra in the lower frequency bands may be accounted for by the difference in the lengths of records, leakage effects, and the generation of the fortnightly MS_f by the double sinusoid.

Now the more complex case of the interaction of several sinusoids, the tidal constituents, may be considered. Figure 51 shows the spectra over 12 bands for the observed tide and the tide predicted from constituents at Sandpiper Island. The spectrum of the observed tide was computed from 720 hourly levels recorded between July 17 and August 15, 1974, while the spectrum for the predicted tide was calculated from the 132 hours of predictions between 1300 CST September 14 and 2400 CST September 19, 1974. Since the latter data set was used as the downstream boundary condition for a model run, the spectrum of these data may be considered to be the input spectrum. The differences between the two spectra may be attributed to the difference in record lengths and the fact that the lower frequency constituents, such as the MS_f and M_m, were not used in generating the tidal predictions.

Comparisons between the model-predicted and observed spectra at Promise Point and Norton Island are shown in Figures 52 and 53. The model-predicted spectra are based on 132 hourly values between September 14 and 19, 1974. The observed spectrum at Promise Point was computed from 696 hourly levels between August 26 and September 23, and the observed spectrum at Norton Island was calculated from 96 hourly values between September 18 and 21.

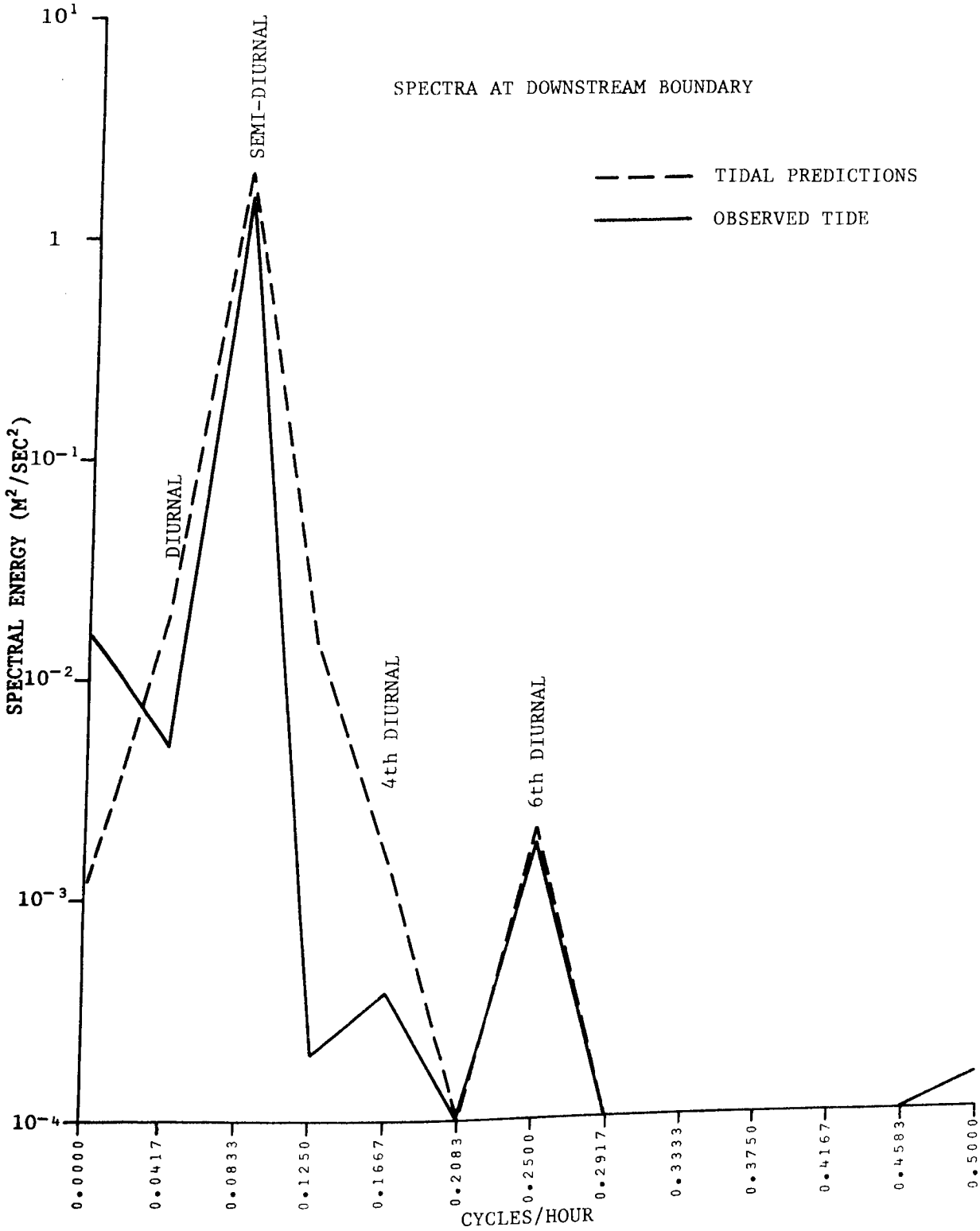

FIGURE 51: Power Spectra of Observed Water Levels and Tidal Predictions from Constituents at Sandpiper Island

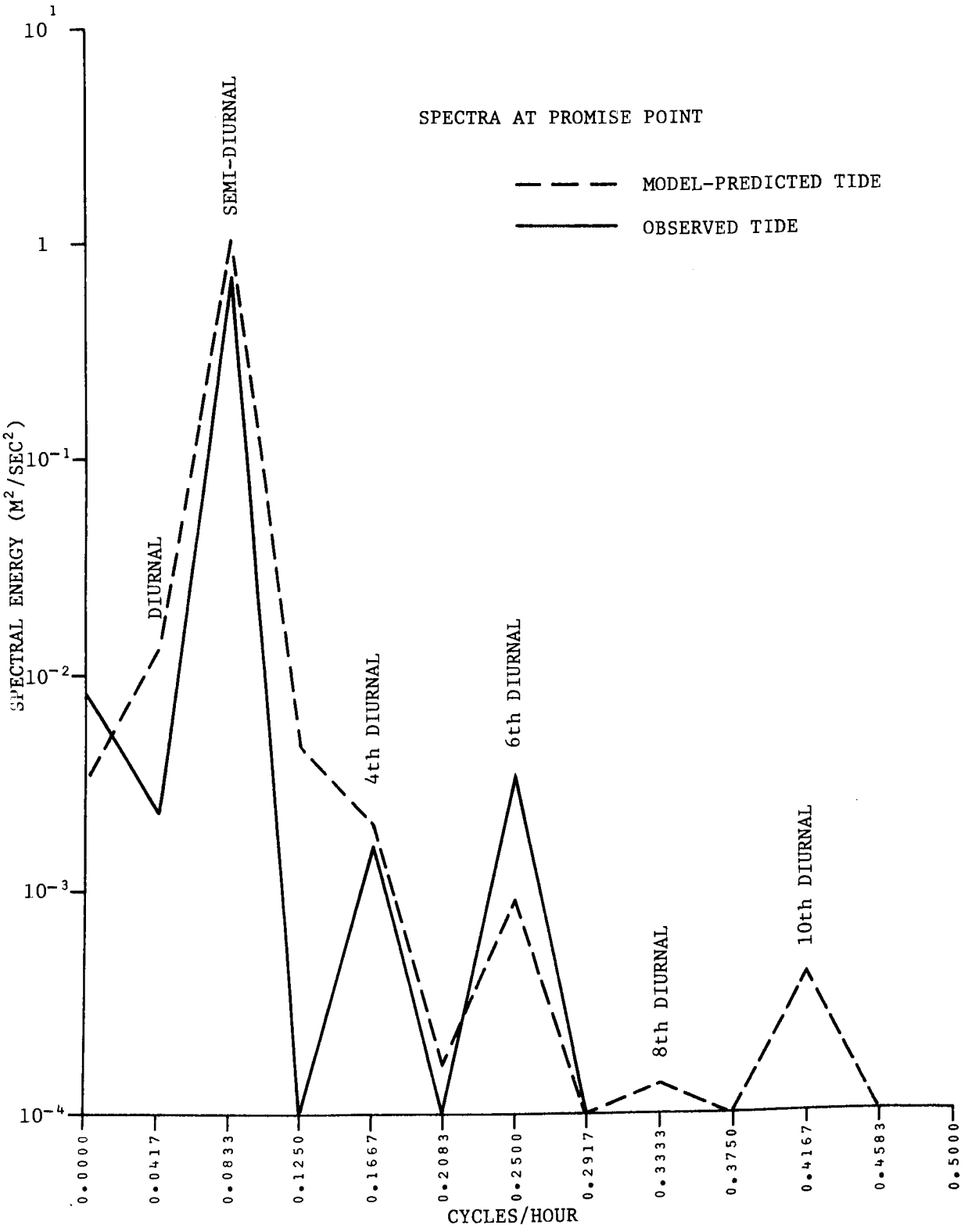

FIGURE 52: Power Spectra of Observed and Computed Water Levels at Promise Point

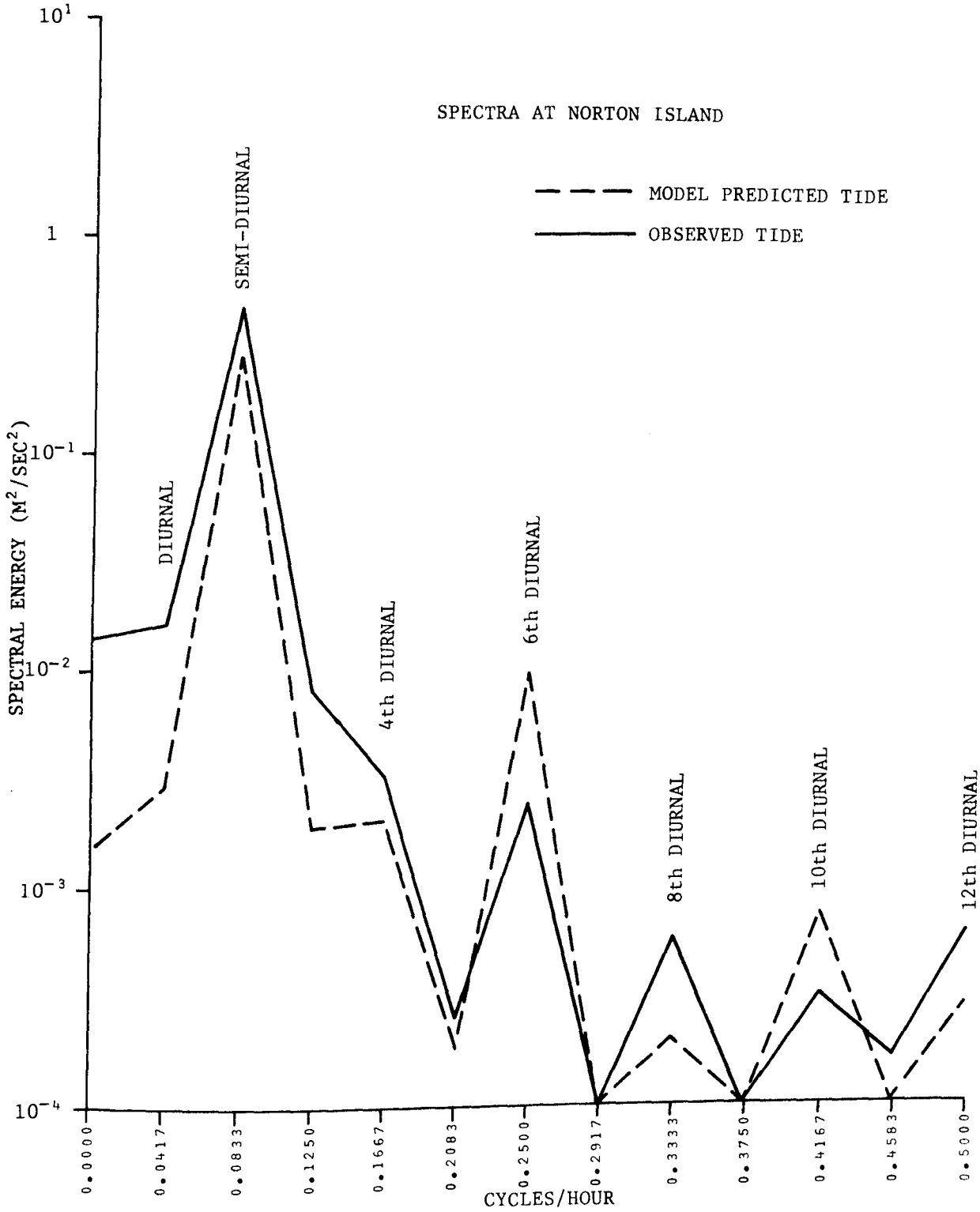

FIGURE 53: Power Spectra of Observed and Computed Water Levels at Norton Island

The agreement between the observed and model-predicted spectra is reasonably good at both locations, but there are some significant differences. At Promise Point, the model underestimates the spectral energy in the 6th diurnal band but overestimates the energy in the 10th diurnal band, while at Norton Island the model underestimates the energy in the 8th and 12th diurnal bands and overestimates the energy in the 6th and 10th diurnal bands. As discussed previously, the energy in the 10th diurnal band of the model-predicted spectra probably takes the form of compound tides. Since these 10th diurnal, model-generated, tidal harmonics are rarely observed in nature, we may assume they are attributable to distortions resulting from the numerical techniques used in the model.

Since over 90 per cent of the total spectral energy in the Chesterfield Inlet tidal records is located in the semi-diurnal band, the most important interactions will be between semi-diurnal constituents. The quadratic interactions (such as $u\,\partial u/\partial x$) in the equations of motion generate quarter-diurnal constituents directly, and cubic interactions (such as in the friction term) generate sixth-diurnal constitutuents directly when the interacting constituents are semi-diurnal. Although "second generation" sixth-diurnal harmonics may be created through the quadratic terms, it is assumed that the second generation of harmonics will possess considerably less energy than the harmonics created directly.

The friction term is the only term in the momentum equation which can be arbitrarily weighted. Thus, in Chesterfield Inlet, if the energy in the sixth-diurnal band of the model-predicted spectra is significantly higher than that in the observed spectra, it may be an indication that too much weight is being applied to the friction term (i.e. Manning's n) or that the actual energy dissipation mechanism present in the inlet is not adequately described by the friction law used in the model.

CHAPTER 6

6.0 CONCLUSIONS

Tidal forcing dominates the flow regime in Chesterfield Inlet. Only in the upper reaches of the channel does the steady current, due to freshwater discharge, have any significant effect on the tidal propagation. The tide in Chesterfield Inlet, which may be considered a progressive wave, reaches its maximum amplitude near Deer Island. The maximum currents occur in the Chesterfield Narrows and are in excess of 4.0 m/sec. Considerable energy losses are incurred at Ekatuvik Point resulting in a pronounced reduction in the tidal amplitude. Upstream of Barbour Bay, shallow-water constituents cause noticeable distortion of the tidal curve.

Chesterfield Inlet is well suited for the application of a one-dimensional nonlinear numerical model. Despite the serious lack of data, an implicit solution to the de Saint Venant equations provided results which are in reasonable agreement with the amplitude and phase of observed water levels over the lower 110 kilometres of the inlet. Good agreement in amplitude was achieved at all but two stations in the 220 kilometre-long inlet. At one of these, Norton Island, the results were influenced by an ill-defined upstream boundary and the neglect of flow through the Bowell Islands network, while at the other, Primrose Island, it was discovered that the water level recorder underestimated the actual tide range. The model-predicted phases are more susceptible to error; the model-predicted tide tends to lead the observed tide. Nonetheless, at only two stations, Primrose Island and Baleen Island, does the discrepancy in phase consistently exceed one-half hour. Moreover, calculations of the M_2 phase at these two stations revealed anomalies. Further field work would be required to determine whether the phase discrepancies are attributable to timing errors in the records or to some natural phenomena.

An examination of the power spectra of the model-predicted tides at Promise Point and Norton Island indicate that the nonlinear interactions described by the model equations generate higher order harmonics of the same order of magnitude as those observed in the inlet. The spectral energy in the tenth diurnal band, computed from the model results, is

higher than that computed from the observed data. This discrepancy is probably due to distorting effects of the finite-difference representation of the model equations.

6.1 RECOMMENDATIONS

The major difficulties encountered in conducting this study were caused by insufficient data in three areas: vertical control, bathymetry, and tides and currents. Before an adequate one-dimensional representation of the inlet can be achieved, these data requirements must be satisfied.

The most important requirement is for the establishment of vertical control from the western end of Baker Lake to the mouth of Chesterfield Inlet. The elevations of the channel inverts and chart datums, previously established by the Canadian Hydrographic Service and the Water Survey of Canada, should be tied into the Geodetic Survey of Canada network. Model results indicate that the tidal ranges and currents in the upper end of the inlet are more sensitive to changes in the mean water surface elevation at Baker Lake than are tidal ranges and currents at any other location in the inlet. Thus, the highest priority should be given to referencing water levels in Baker Lake and the Bowell Islands to mean sea level.

In only one area of the inlet, the Bowell Islands, did inadequate bathymetry hamper the modelling study. Before the impact of the flow through the Bowell Islands network upon the tides at Baleen and Norton Islands can be assessed, the bathymetry in the north and center channels must be measured.

Water level measurements should be taken at certain key locations within the inlet. These locations are the upper and lower boundaries of the inlet and areas at which the tidal properties change significantly. Thus, tide gauges should be located at Sandpiper Island and the eastern end of Baker Lake to define the system boundaries. Additional gauges should be placed at Ekatuvik Point, Promise Point, Primrose Island, Big Point, the eastern end of the Bowell Islands, and within the Bowell Islands network.

The tide gauges at Sandpiper Island and eastern Baker Lake should be left in place for the duration of the survey if possible, for these gauges would supply the information to be used in the boundary conditions

of future modelling studies. All of the gauges should be left in place for at least a month, since at least 29 days are necessary to resolve the major constituents in the tidal record. A longer tidal record will provide better resolution of the constituents, however, thus allowing more accurate predictions to be made.

If information on the tidal current regime in the inlet is desired, current speed and direction measurements should be taken at Ekatukik Point, Promise Point, Big Point, and as close as possible to Chesterfield Narrows. (Current velocities are generally too high within the Narrows to be measured with current meters.) The flow in the inlet at these locations should be following the channel boundaries, so that lateral variations in the current should be smaller than elsewhere within the inlet. Nonetheless, the currents will undoubtedly vary in the vertical and over the tidal cycle. Thus, it would be necessary to measure vertical current profiles over a 13-hour period. These measurements, besides helping to define the current regime in key areas, would help verify the model-computed velocities. For the amplitudes and phases of tidal current constituents to be computed, continuous sampling for at least 29 days with in-situ current meters would be required.

BIBLIOGRAPHY

1. Ages, A. and A. Woollard — "The Tides in the Fraser Estuary", unpublished manuscript, Pacific Marine Science Report 76-5, Institute of Ocean Sciences, Patricia Bay, Victoria, B.C., January, 1976.

2. Ambler, D.C. — "Runoff from a Small Arctic Watershed", Proceedings of Workshop Seminar, Permafrost Hydrology, Canadian National Committee for the International Hydrologic Decade, 1974, pp 45-50.

3. Amien, M. — "An Implicit Method for Numerical Flood Routing", Water Resources Research, Vol. 4, No. 4, 1968, pp 719-726.

4. Anderson, J.C. — "Permafrost-Hydrology Studies at Boot Creek and Peter Lake Watersheds, N.W.T.", Proceedings of Workshop Seminar, Permafrost Hydrology, Canadian National Committee for the International Hydrologic Decade, 1974, pp 39-44.

5. Bendat, J.S. and A.G. Piersol — Measurement and Analysis of Random Data, John Wiley and Sons Inc., New York, 1968.

6. Brown, K.M. — "A Quadratically Convergent Newton-Like Method Based on Gaussian Elimination", SIAM Journal of Numerical Analysis, Vol. 6, No. 4, December, 1969, pp 560-569.

7. Brown, R.J.E. — "Distribution and Environmental Relationships of Permafrost", Proceedings of Workshop Seminar, Permafrost Hydrology, Canadian National Committee for the International Hydrological Decade, 1974, pp 1-6.

8. Cartwright, D.E., W.H. Munk and B. Zetler — "A Suggested Procedure for the Analysis of Pelagic Tidal Measurements", EOS, Vol. 50, No. 7, July, 1969, pp 472-477.

9. Chandrashenkar, M., L.R. Muir and T.E. Unny — "A Numerical Two-Dimensional Flow Model for River Systems", Proceedings of Modelling 75 Symposium, ASCE Specialty Conference, San Franscisco, U.S.A., September, 1975

10. Church, M. "Hydrology and Permafrost with Reference to Northern North America", Proceedings of Workshop Seminar, Permafrost Hydrology, Canadian National Committee for the International Hydrological Decade, 1974, pp 7-20.

11. Chow, V.T. Open Channel Hydraulics, McGraw-Hill Book Co., Inc., New York, N.Y., 1959.

12. Dingman, S.W. "Characteristics of Summer Runoff from a Small Watershed in Central Alaska", Water Resources Research, Vol. 2, No. 4, 1966, pp 751-754.

13. Dronkers, J.J. Tidal Computations in Rivers and Coastal Waters, North-Holland Publishing Co., Amsterdam, 1964.

14. Findlay, B.F. "The Water Budget of the Knob Lake Area" in "Hydrologic Studies in Labrador-Ungava", McGill Subarctic Research Papers No. 22, 1966, pp 1-95.

15. Fread, D.L. "Effects of Time Step Size in Implicit Dynamic Routing", Water Resources Bulletin, Vol. 9, No. 2, April, 1973, pp 338-351.

16. Fread, D.L. "Technique for Implicit Dynamic Routing in Rivers with Tributaries", Water Resources Research, Vol. 9, No. 4, August, 1973, pp 918-926.

17. Fread, D.L. "Numerical Properties of Implicit Four-Point Finite Difference Equations of Unsteady Flow", NOAA Technical Memorandum NWS HYDRO-18, March, 1974.

18. Godin, G. Hydrodynamical Studies on the St. Lawrence River, Manuscript Report Series, No. 18, Marine Sciences Branch, Department of Energy, Mines, and Resources, Ottawa, 1971.

19. Godin, G. The Analysis of Tides, University of Toronto Press, Toronto, 1972.

20. Godin, G., S. Eldring, and R. Pinard — "The Reduction of the Tidal Observations in Chesterfield Inlet with the Help of the Admittance Function", MEDS Technical Note No. 9, Fisheries and Marine Service, Environment Canada, Ottawa, August, 1975.

21. Godin, G. — "The Reduction of Current Observations With the Help of the Admittance Function", MEDS Technical Note No. 14, Fisheries and Marine Service, Environment Canada, Ottawa, June, 1976.

22. Ingledow, T. and Associates Ltd. — Power Survey of the Kazan, Dubawnt, Thelon, and Hanbury River Basins, Northwest Territories, Department of Indian and Northern Affairs, Ref. No. HD1696 C3 N62, Ottawa, March, 1970.

23. Kane, D.C. and R.F. Carlson — "Hydrology of the Central Arctic River Basins of Alaska", University of Alaska, Inst. of Water Resources, Rpt. No. IWR-41, 1973.

24. Muir, L.R. — "Unsteady Flow in Networks of Open Channels", Manuscript Report Series No. 1, Ocean and Aquatic Sciences, Central Region, Environment Canada, Burlington, 1975.

25. Munk, W.H. and D.E. Cartwright — "Tidal Spectroscopy and Prediction", Royal Society of London Philosophical Transactions, Series A, V. 259, 1966, pp 533-581.

26. Nebiker, W.A. and S. Owig — "Evaporation and Transpiration from an Open Lichen Woodland Surface", Intl. Union Geodesy and Geophysics, Comptes rendus, Assemblee Generale de Toronto, 1957, III, pp 379-384.

27. Wing and Huang — "SCAP - A Sparse Matrix Circuit Analysis Program", IEEE Intl. Symposium on Circuits and Systems, Boston, 1975.

28. Wright, B.M. — Report on the Tide Gauge Program of Chesterfield Inlet, Marine Sciences, Ocean and Aquatic Affairs, Fisheries and Marine Service, Environment Canada, Burlington, 1974.

29. Wright, G.M. "Geological Notes on Central District of Keewatin, Northwest Territories", Paper 55-17, Geological Survey of Canada, Department of Energy, Mines, and Resources, Ottawa, 1955.